AMERICAN UNIVERSITY OF BEIRUT

USE OF STEADY AND INTERMITTENT PERSONALIZED VENTILATION IN INDOOR ENVIRONMENTS: THERMAL COMFORT AND INDOOR AIR QUALITY

by
DOUAA KHODER AL ASSAAD

A thesis
submitted in partial fulfillment of the requirements
for the degree of Doctor of Philosophy
to the Department of Mechanical Engineering
of the Maroun Semaan Faculty of Engineering and Architecture
at the American University of Beirut

Beirut, Lebanon
February 2021

AMERICAN UNIVERSITY OF BEIRUT

USE OF STEADY AND INTERMITTENT PERSONALIZED VENTILATION IN INDOOR ENVIRONMENTS: THERMAL COMFORT AND INDOOR AIR QUALITY
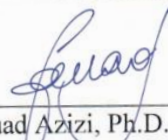
by
DOUAA KHODER AL ASSAAD

Approved by:

_____   _____
Prof. Kamel Ghali, Ph.D., Professor   Advisor
Department of Mechanical Engineering, AUB

_____   _____
Prof. Nesreene Ghaddar, Ph.D., Professor   Co-Advisor
Department of Mechanical Engineering, AUB

_____   _____
Prof. Fadl Moukalled, Ph.D., Professor   Member of Committee
Department of Mechanical Engineering, AUB

_____   _____
Prof. Fouad Azizi, Ph.D., Associate Professor   Member of Committee
Department of Chemical Engineering & Advanced Energy, AUB

_____   _____
Prof. Arsen Melikov, Ph.D., Professor   Member of Committee
Department of Civil Engineering, Technical University of Denmark

_____   _____
Prof. Walid Chakroun, Ph.D., Professor   Member of Committee
Department of Mechanical Engineering, Kuwait University

Date of thesis defense: 8 February, 2021

AMERICAN UNIVERSITY OF BEIRUT

THESIS RELEASE FORM

Student Name: <u>Al Assaad</u> <u>Douaa</u>   <u>Khoder</u>
       Last   First   Middle

I authorize the American University of Beirut, to: (a) reproduce hard or electronic copies of my thesis; (b) include such copies in the archives and digital repositories of the University; and (c) make freely available such copies to third parties for research or educational purposes:

☒ As of the date of submission

☐ One year from the date of submission of my thesis.

☐ Two years from the date of submission of my thesis.

☐ Three years from the date of submission of my thesis.

February 27, 2021

_____

Signature   Date

ACKNOWLEDGEMENTS

ABSTRACT
OF THE THESIS OF

Douaa Khoder Al Assaad   for   Doctor of Philosophy
                                              Major: Mechanical Engineering

Title: Use of Steady and Intermittent Personalized Ventilation in Indoor Environments: Thermal Comfort and Indoor Air Quality

The wellbeing and productivity of occupants in indoor spaces are correlated to their satisfaction with their thermal environment and their breathable air quality. This is highly dependent on the installation of carefully designed and energy-efficient air distribution systems such as personalized ventilation. These systems are individual devices consisting of a ducting network, which outlet delivers conditioned clean fresh air towards the occupant. As the issuing jet is adjustable in flow rate, direction and temperature, personalized ventilators respond to each occupant's thermal preferences while improving the inhaled air quality compared to standalone total volume ventilation. Research on personalized ventilation has investigated its performance under steady state conditions. In other words, its adjustable operating conditions were constant over prolonged periods of time.

The first part of this work integrates for the first time, the concept of personalized ventilation with dynamic cooling, known to enhance comfort in warm indoor conditions. This is done by supplying the personalized flow rate in a time-dependent sinusoidal profile that fluctuates between a minimum and a maximum at frequencies of 0.3-1 Hz. The occupant is hence given additional freedom to adjust the jet frequency to their liking or revert to steady supply. This device is denoted as intermittent personalized ventilation. This work studies through experimentally validated CFD models, the performance of intermittent personalized ventilation in a space equipped with typical mixing ventilation and another equipped with a chilled ceiling, in enhancing occupants' thermal comfort. Breathable air quality will also be assessed, and possible energy savings evaluated in comparison with a steady system. It was found that intermittent personalized ventilators enhanced thermal comfort especially in warm indoor conditions (26 °C) with increasing frequency. It did not perform well in neutral conditions (24 °C). Moreover, due to increased jet turbulence, it provided lower, but nonetheless satisfactory breathable air quality compared to steady personalized

ventilation. Energy savings of 16% and 8% were achieved in the case of mixing ventilation and chilled ceiling.

Personalized ventilation has always been viewed as a means to improve indoor quality for the person using it by reducing exposure to gaseous or particulate matter pollutants. However, in the presence of particle emissions, personalized ventilation can contribute to particle deposition on occupants' clothing, which can act as subsequent sources if triggered by occupants' physical activities. Hence, personalized ventilation can contribute to second-hand clothing-mediated exposures. This work also investigates through experimentally validated CFD models the effect of different air terminal devices in reducing inhalation exposure while contributing to second-hand clothing exposure. Results showed that a computer mounted panel showed the best performance as it simultaneously decreased all types of exposure. Vertical desk grills decreased inhalation exposure while having negligible effect on second-hand exposure. Round movable panels decreased inhalation exposure but significantly increased clothing mediated exposures.

TABLE OF CONTENTS

ILLUSTRATIONS

Figure

TABLES

CHAPTER I

PERFORMANCE OF INTERMITTENT PERSONALIZED VENTILATION IN OFFICE SPACES

A. Introduction

1. Background and context

Assuring the wellbeing of occupants in indoor workspaces is a crucial issue since people spend the majority of their time in indoor environments (workspaces, commercial or residential buildings...) [1]. This is done through the control of their thermal environment or in other words their state of thermal comfort and through the adequate satisfaction of indoor air quality (IAQ) requirements. Occupant thermal comfort can be fulfilled by the adequate implementation of heating ventilation and air conditioning (HVAC) systems. The latter condition the indoor environment either through radiative heat exchange and/or through convection phenomena by supplying cooled fresh air. The latter mixes with the hot indoor air, lowering ambient room temperatures and satisfying the thermal preferences of occupants indoors. On the other hand, regulating IAQ in workspaces is crucial to protect workers from possible contamination due to indoor pollutants, as it directly affects their health and productivity [2]. IAQ is majorly affected by the presence of contaminants in the space. pollutants can be emitted by human respiration (carbon dioxide) or building furnishings (volatile organic compounds) [3]. Long-term exposure to these pollutants contribute to occupant dissatisfaction as well as sick building syndromes (nausea, dizziness, irritation...) [4]. Achieving good breathable air quality is also related to implementation and careful design of air distribution systems.

Conventional HVAC systems that have been investigated are total volume ventilation systems such as mixing ventilation (MV) system, or hydronic radiant systems such as the chilled ceiling (CC). MV systems maintain the space at a constant temperature and a homogenous air quality by a mixed fresh-return air distribution system supplied from higher levels in the space. In such design, the individual environmental preference is not accommodated since room temperature is controlled by single thermostat. This may lead in an open space to the failure in satisfying the thermal comfort and indoor air quality needs of all occupants as well as increased energy consumption in an effort to fulfill these requirements [5, 6]. The CC is a popular system easily integrated within office spaces [7]. It is characterized by a metal panel installed at the ceiling level and cooled by chilled water pipes [8]. CC systems assure comfort mainly through radiative heat transfer cooling between the cold ceiling and different hot surfaces in the space such as occupants, walls and computers. This allows for a higher cooling efficiency than conventional systems and better thermal comfort [9]. In addition, CC systems reduce air motion and produce a more thermally uniform environment, which minimizes draught discomfort ([10, 11]). Moreover, CCs are characterized by their quiet operation, which decreases noise discomfort; unlike conventional systems where higher noise levels can cause disturbance to some occupants [12]. Even though the CC system is a superior system, it has two main drawbacks. Standalone CC systems are not efficient when high heat loads are present in the space [13, 14]. Additionally, CC systems compromise IAQ since they only condition the space without a fresh air supply to dilute pollutants unlike MV and DV systems. In CC systems, the lack of air renewal can lead to contaminants' build up and deteriorate IAQ [15-17]. Due to the shortcomings and limitations of MV and CC

systems, they cannot be operated as standalone systems in indoor spaces and need to be assisted by an additional system that is able to bridge the air quality and thermal comfort gap and to do so at minimal energy costs.

2. *Personalized ventilation*

A promising HVAC system is the personalized ventilation (PV) system. This system is an individual device that delivers cool fresh clean air directly towards the occupants [18-22]. Therefore, it can improve the quality of the inhaled air. Moreover, by allowing adjustment of its different supply parameters such as flow rate, temperature and direction, PV can respond to different thermal preferences and thus; enhance comfort [23]. In addition, PV is a cheap system that can assist other HVAC systems and reduce energy costs [24]. Success of personalized ventilation depends on the ability of the jet in penetrating the human respiratory flows as well as the free convective flow. Therefore, the design of the PV air terminal device (ATD) and issuing flow rate determines its efficiency. There are many PV ATDs that have been thoroughly studied in literature (computer mounted panels, desk fans, ceiling integrated, chair fans) [25-27] in conjunction with MV and CC systems and have proven to enhance thermal comfort, breathable air quality and save energy. In an experimental study, Lipczynska et al. [28] investigated the performance of a standalone desk mounted PV system assisting CC; in terms of IAQ and comfort. Their results showed that the CC/PV system was able to enhance the inhaled air quality in the occupant BZ by 89.6% compared to MV systems and reduce cross contamination.

3. *Intermittent localized cooling*

Most studies on PV were concerned with assessing the effect of delivery of a constant flowrate of cool fresh air from the task ventilation on energy savings. Recently, few studies investigated the effect of varying airflow amplitude and frequency on occupant thermal comfort and energy saving [29-32]. In fact, intermittent airflow can also enhance comfort by mimicking natural outdoor conditions. Ghali et al. [32] performed outdoor experiments on human subjects and reported that the average thermal comfort improved with the change in wind frequency. Furthermore, providing airflow intermittently can help decrease PV energy costs even further by reducing the amount of fresh air to be cooled by the system and lowering the fans' power consumption as reported by Kabanshi et al. [31], who used ceiling mounted Air Jet Diffusers supplying dynamic airflow in an ON-OFF pattern. Uğursal et al. [29] and Tanabe et al. [30] conducted indoor human subject experiments to investigate the performance of localized dynamic airflow at two different periods of 30 s and 60 s. Both studies reported that a period of 30 s provided more perceived thermal comfort. Zhou et al. [33] performed measurements in offices under natural and mechanical ventilation where occupants were subjected to fluctuating airflow in cool conditions. They concluded that room airflow felt most uncomfortable when the frequency ranged between 0.2 Hz and 0.6 Hz. However, none of these studies considered the effect of different supply flow rates and frequencies on thermal comfort or the effect of the varying airflow pattern on the IAQ. Accelerating and decelerating airflow could create turbulence and enhance the mixing of the contaminants in the BZ. This would decrease the ventilation efficiency of the PV and therefore deteriorate the air quality in the microclimate of the occupant. On one side, intermittent PV succeeds in bringing

comfort [34] but on the other hand, it may compromise IAQ. No previous research has addressed the use of intermittent PV to aid background HVAC systems (MV and CC), its ability to enhance thermal comfort, its impact on air quality, energy savings and compared it to a steady PV flow.

4. Aims and research questions

The aim of PART I of this work is to study the performance of intermittent PV assisting MV and CC in an office space setting in terms of their ability to provide thermal comfort and breathable air quality and possible energy savings. The performance of these systems will be compared to their steady PV counterparts. To achieve these objectives, numerical CFD models were developed to predict the flow field variables (velocity, temperature, contaminants' distribution). The models' predictions were validated experimentally in a climatic chamber equipped with the corresponding systems and thermal manikin; representing an occupant in an office space.

B. Methodology

1. System description

This study considers two office spaces conditioned by the conventional MV and CC system respectively. **c** illustrates the considered office spaces conditioned by these systems and the intermittent PV. MV systems supply cool fresh air from high levels in the space, from either a ceiling or wall diffuser. The supplied air mixes with the warm polluted indoor, cools the space and dilutes contaminants. Therefore, the MV system assures well-mixed conditions in the space, with uniform temperature and concentration

of pollutants. In this work, the MV system is illustrated in Figure 1(**a**). The MV system has its own air-handling unit (AHU), which supplies cool recirculated air into the room at a CO_2 concentration of 450 ppm. The CC illustrated in Figure 1(**b**) is characterized by a metal panel cooled by chilled water indirectly. The chilled water cooled the ceiling, which exchanges radiant energy with the different office surfaces (computer, walls, occupant and floor).

Both MV and CC systems are assisted by a desk-integrated computer-mounted PV system (Figure 1). The PV supplies cool fresh air from a rounded outlet horizontally towards the occupant's face in a sinusoidal manner as seen in Figure 1(**c**). The airflow downstream from the PV fan can have a swirl component, which can increase turbulence and mixing effects. To straighten the flow, a honeycomb flow straightener was sandwiched between two screens in front of the fan [35]. This technique was used previously to reduce the swirl effect. Note that the PV fresh air is withdrawn from an adjacent fresh air source and is filtered from all active particles. In addition, it has typical CO_2 fresh air concentration of 450 ppm. The transient PV airflow is characterized by an average flow rate $\bar{m}_{PV,upp}$ and a supply frequency f and amplitude A.
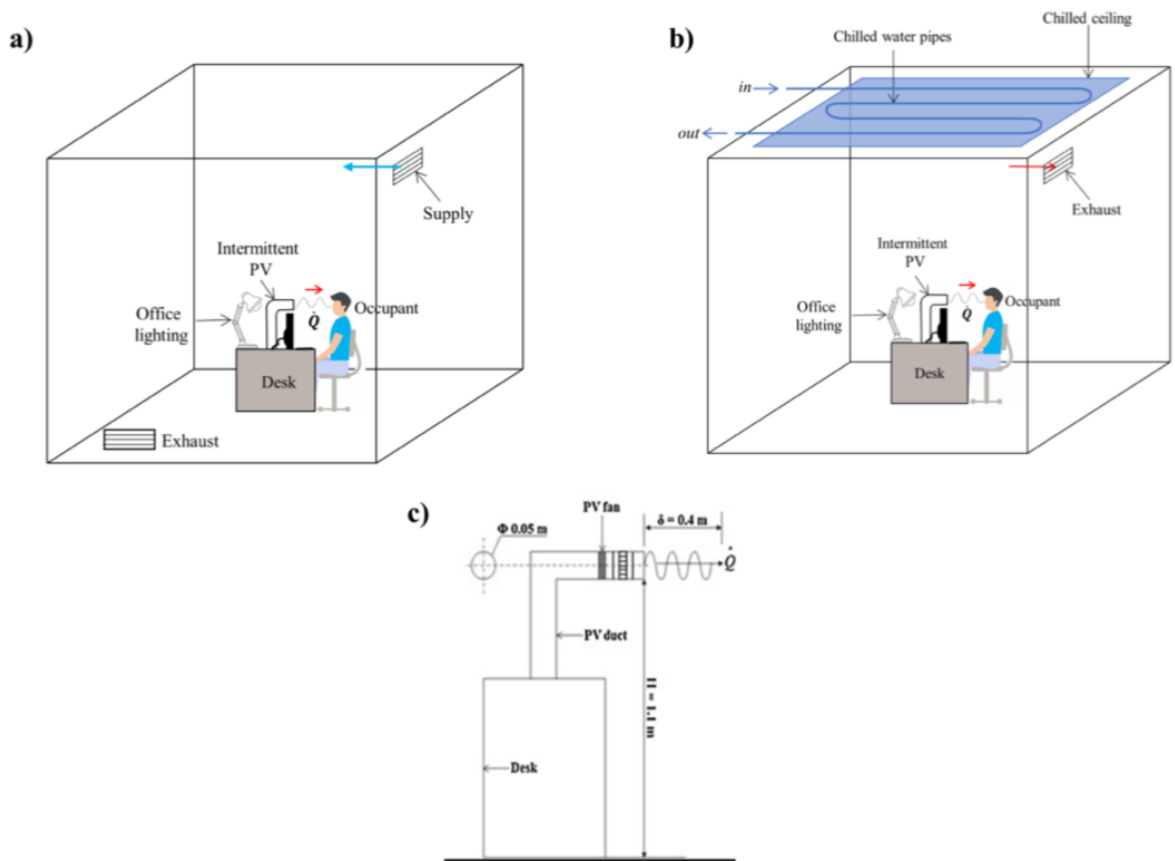
Figure 1 Illustration of the office spaces equipped with: a) the intermittent PV+MV system, b) the intermittent PV+CC system and c) the intermittent PV setup

a. Choice of PV frequency, average flow rate and supply temperature

A dynamic airflow is characterized by its perceptible range of fluctuation frequency, the range of associated amplitudes and mean velocities determined by a given minimum and maximum jet flow. Therefore, it is important to determine the dynamic jet airflow characteristics and their ranges for both the experimental work and the simulations where the jet should be able to reach the BZ and penetrate the occupant thermal plume. In addition, acceptable ranges should be established for the temperature of the surrounding air and the cooling jet within which thermal comfort is maintained. There has been a number of studies on human thermal comfort at several frequencies of

15

dynamic airflow in both outdoor and indoor spaces. In indoor environments, the study of the effect of flow frequency on comfort was carried out in neutral to cool and in warm thermal environments. According to Zhu et al. [36], the fluctuating airflow is defined by the range of perceptible frequency felt by the occupant, which lies between a lower limit of 0.1 Hz and an upper limit of 1 Hz. Several experiments were conducted in different ambient conditions to find the comfort range between these two limits. Fanger et al. [37] reported that under cool indoor conditions, discomfort reached a maximum at frequencies ranging between 0.3 Hz and 0.5 Hz. Zhou et al. [33] reported a range of frequencies between 0.2 Hz and 0.6 Hz; broader than the range found by Fanger et al. [37]. However, both studies show that under cool to neutral conditions, higher frequencies can cause discomfort and feelings of draft. On the contrary, in warm indoor conditions, such an airflow may induce feelings of comfort. In fact, Huang et al. [38] studied thermal comfort in warm indoor conditions (28 and 30°C), and reported that a higher range of 0.5 – 1 Hz provided cooling and comfort.

Based on previous studies, it is well established that a fluctuating airflow triggered comfort conditions depending on the airflow temperature and the room background temperature. In this study, the conditions in the space are from neutral to warm while the PV jet temperature is cool. For these conditions, three frequencies of 0.3 Hz, 0.5 Hz and 1 Hz, were selected based on the values found by Fanger et al. [33] (0.3 – 0.5 Hz) and Huang et al. [38] (0.5 – 1 Hz) in order to evaluate thermal comfort. A dynamic airflow is characterized by the jet velocity, which is defined by an average, a minimum and a maximum. The average flowrate was varied according to typical average flowrates used in PV airflow applications, which range between 3 L/s and 10 L/s. For this study, three average flowrates were taken into consideration: 3.5 L/s, 5 L/s

and 7.5 L/s. As for the choice of minimum velocity, it should be selected such that the supply jet can still penetrate the thermal plume of the occupant to deliver cool fresh air and provide comfort. For the considered PV, the minimum flow rate was equal to 1 L/s corresponding to a supply velocity of 0.5 m/s approximately.

2. *CFD modeling*

In these studies, complex physics govern the airflow field in the space. In fact, the MV system establishes mixing in the space, reticulation zones and high turbulence. As for the CC system, complicated flow physics are present in the space due to significant temperature differences. In fact, the warm air next to the heat sources rises upwards; driven by natural convection and forms thermal plumes. The plumes spread in the upper part of the room and flow reversal occurs due to heat exchange with the cold ceiling. Therefore, circulation zones appear in the space, enhancing turbulence and promoting mixing of temperature and contaminants in the macroclimate. Moreover, complex radiative heat exchange exists between the cool ceiling and the heat sources (occupant, walls, equipment), which cannot be neglected. The flow physics becomes time dependent and more complex when the office is equipped with the intermittent PV directed towards the face and creating transient periodic conditions. The latter interacts with the macroclimate air through entrainment and turbulent diffusion. In addition, the flow field is affected by the rising thermal plumes from the different heat sources in the space (thermal manikin, the wall plumes, office equipment). It is noteworthy that the flow field can be even more complicated with the inclusion of breathing from the thermal manikin, however velocities of exhaled air decline quickly after they exit the mouth and are considered negligible in comparison to the PV jet momentum [39].

Consequently, this study does not include a breathing thermal manikin. Nevertheless, the flow field is still very complex and calls for the use of a 3-D CFD simulation tool to resolve for the distribution of different dependent variables.

The results of the CFD model are validated through experiments. Following the CFD model validation, it is used to simulate a parametric study in a regular office space where the above-mentioned parameters are varied in order to study the effectiveness of the intermittent PV + MV/CC systems in delivering good indoor air quality and enhancing thermal comfort at minimum energy costs compared to their steady PV counterparts. Note that IAQ was evaluated in the occupant BZ. The BZ is defined as a control volume taking the shape of a sphere having a diameter of 2 cm at 2.5 cm away from the occupant's nose

b. Airflow modeling

To solve for the different variables present in the space (temperature, velocity, species' concentration, turbulent kinetic energy and its dissipation rate), a building simulation tool is needed, such as the commercial software ANSYS Fluent (version 17.2) [40]. The office spaces and their different components can be seen in Figure 2. In order to properly understand the flow physics; (radiation, buoyancy fluxes, development of thermal and dynamic boundary layers next to the office surfaces, recirculation zones) the space needs to be accurately meshed in Fluent [40] as seen in Figure 3.

a)

b)
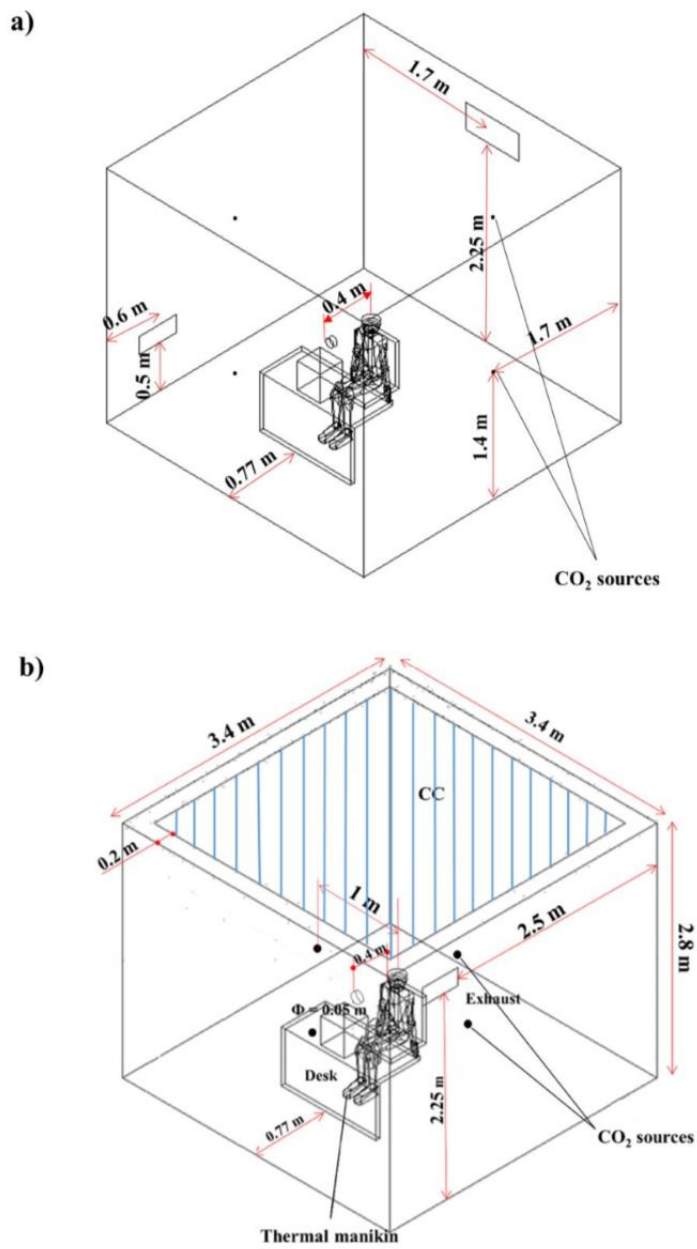
Figure 2 Illustration of the computational domain as seen on ANSYS of: a) the

intermittent PV+MV, b) the intermittent PV+CC

An unstructured grid with tetrahedral elements was chosen. In the case of CC only, due to the presence of radiation heat exchange, the size of the room air elements' faces were set to have a maximal size of 50 mm. In both cases, the wall and thermal manikin boundaries have specific face sizes of 2 cm and 1.5 cm respectively. Additionally, inflation layers were created next to the boundaries of interest (walls, thermal manikin) to capture the thermal and fluid boundary layers behavior. Inflation layers were chosen such that the dimensionless wall number y^+ varied between 0.8 and 4 [41]. This grid configuration guaranteed a mesh-independent solution with a maximum relative error reaching below 5%. The final meshes of the MV/CC space (Figure 3) were characterized by 303533/951942 nodes and 1,056,484/5119220 elements with a maximum relative error of 4.5% compared to a mesh characterized by face sizes of 1.5 cm and 2.5 cm for the manikin and walls respectively. Note that the room air corresponded to a fluid zone, while the manikin, chair, desk, computer and PV were considered as solid zones. The mesh independency tests can be seen in Table 1.

a)

b)

Thermal manikin

PV nozzle
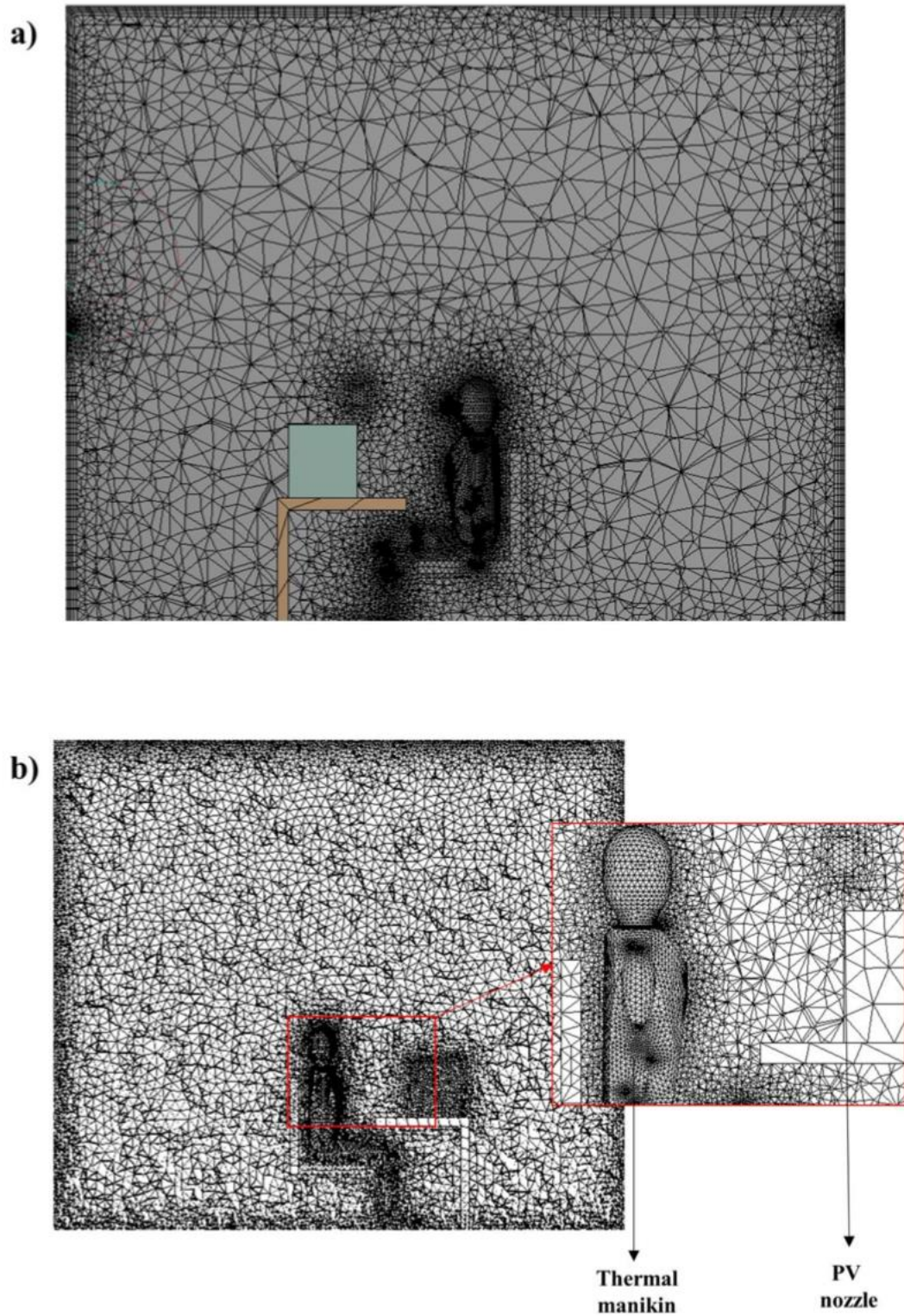
Figure 3 Illustration of the meshed computational domain for the case of: a) intermittent

PV+MV, b) intermittent PV+CC

Table 1 Grid independence tests

a) Intermittent PV+MV.			
	Face sizing (cm) Manikin/walls	Number of elements	Maximum relative difference in the predicted values of temperature and velocity values with previous mesh values (%)
Mesh 1	2/8	152395	-
Mesh 2	2/5	228592	44.62%
Mesh 3	1.5/3	480478	12.1%
Mesh 4	1.5/2.5	660302	5.3%
Mesh 5	1.5/2	1056484	4.2%
b) Intermittent PV+CC			
Mesh 1	2/8	738433	-
Mesh 2	2/5	1107648	45.72%
Mesh 3	1.5/3	2328168	13.5%
Mesh 4	1.5/2.5	3199510	6.2%
Mesh 5	1.5/2	5119220	4.5%

The flow field in the space is characterized by high turbulence intensities as well as recirculation zones due to the presence of the intermittent PV jet and the CC. Therefore, a proper turbulence model should be chosen as this could affect species' concentration and the assessment of the IAQ in the space. Hence, the RNG k-ε model with enhanced wall treatment and full buoyancy effects was selected to solve for the

turbulent kinetic energy k and its rate of dissipation ε. This model is adequate for use in highly turbulent flows [42]. As for the species' concentration, it is solved using the species' transport equation. Note that carbon dioxide (CO_2) is used to model the presence of passive contaminants in the space. The CO_2 sources are chosen at the middle of each wall (Figure 2). The Boussinesq approximation was employed to take into consideration natural convection phenomena. To account for radiation in the space in the case of CC, the surface-to-surface (S2S) radiation model was used. All equations (energy, moment, k, ε, species' transport) were discretized using a second order accurate method, which is the second order upwind scheme. The pressure equation was discretized using the "PRESTO!" scheme since this method considers pressure gradients near boundaries. In this time-dependent problem, the Fluent solver was set to transient conditions having a time step of 0.05 s, which is smaller than the intermittent PV fluctuation period. Moreover, a second order time stepping scheme was set for accurate predictions. To couple pressure and velocity, the "PISO" algorithm is used as it is compatible for time- dependent models. The solution was considered as convergent when: (i) the scaled residuals reach 10^{-7} for energy (the temperature is the easiest variable to converge) and 10^{-5} for all other variables; (ii) the total heat flux in the domain should be lower than 1% of the net heat gain.

c. CFD boundary conditions

In order to obtain a physical solution for the airflow field in the space, the boundary conditions concerning the different flow field variables should be accurately selected. The PV supply diffuser is chosen as a velocity inlet with an assigned user defined instantaneous velocity $V_{PV}(t)$ as seen in equation (1):

$$V_{PV}(t) = \frac{V_{min} + V_{max}}{2} + \left\{ \frac{V_{max} - V_{min}}{2} \times sin\,(2\pi ft) \right\} \qquad (1)$$

where V_{min} and V_{max} are the minimum and maximum flow velocities and t is time. For the PV nozzle, an inlet temperature was specified, as well as the turbulence intensity, hydraulic diameter and a constant species' concentration of 450 ppm. This corresponded to typical fresh air concentrations. The CO_2 sources (Figure 3) were assigned as a constant velocity inlet and a specific inlet species' concentration of pure CO_2 (10^6 ppm). The exhaust was assigned as a pressure outlet with zero-gauge pressure. The MV was assigned as a velocity inlet with constant velocity, temperature, turbulence intensity and length scale. The CC was assigned as a wall with a constant temperature and an emissivity of 0.9; while the walls, manikin, lighting and computer were assigned a constant heat flux. As for radiation in the case of CC, all heat sources in the spaces (walls, ceiling, occupant, computer, lighting and floor) have an emissivity of 0.95 [43]

3. *Thermal comfort assessment*

Due to the presence of the CC in the office space, the occupant body is subject to moderate velocities [28] and a surrounding environment, which is not radiantly uniform. In the office space equipped with MV, a quiescent environment with low velocities govern the space as well. Moreover, there is a high momentum intermittent PV jet delivered towards the occupant's face. The CC/MV macroclimates and the PV jet have two different cooling effects; the intermittent PV jet creates non-uniform and transient flow conditions near the face while the rest of the body remains at steady skin temperature.

This asymmetry and transient PV conditions affect the overall thermal comfort state of the occupant. In order to evaluate thermal comfort conditions, a model that mimics the human physiology and predicts the transient human thermal response is needed. Therefore, the transient bio-heat model of Othmani et al. [44] and the CFD model were coupled to output the skin temperatures of each body segment as a function of the environmental conditions and metabolic rate. These body segments were defined by the bio-heat model. They include the head, chest, abdomen, back, buttocks, upper arm, lower arm, thighs, calves, and feet. To obtain the desired output, the environmental conditions of each segment were taken as inputs into the bio-heat model.

In order to couple the CFD and bio-heat models, the thermal manikin was initiated with typical skin temperature. The ambient skin temperatures as well as convective heat transfer coefficients were used as input from the CFD model to the transient bio-heat model. For the face segment subject to the transient PV airflow, the ambient skin temperatures and convective heat transfer coefficients are transient while for the other segments, they remain constant. After obtaining the skin temperatures, they were taken as input boundary conditions to the thermal manikin in the CFD model. The latter was then simulated until convergence is reached once more. This coupling algorithm was iterated several times until the relative error between two iterations is smaller than 10^{-3}. After convergence, the output skin temperatures, core temperatures and their rate of change are taken as input into the sensation and comfort models of Zhang et al. (2010a, b, c). In these models, Zhang et al. [45-47] performed intensive human subjects' experiments to develop a sensation and comfort scales ranging from -4 (very cold, very uncomfortable respectively) to +4 (very hot, very comfortable, respectively).

4. Breathable air quality assessment

The objective of this study is to evaluate the performance of the intermittent PV+CC/MV systems in delivering high IAQ towards the occupant's BZ. For this reason, tracer gas method was used and carbon dioxide (CO_2) was selected. The ventilation effectiveness index ε_v that allows for analytic evaluation of IAQ was used as well. This index was suggested in [18] to assess the ability of a PV in providing fresh air. To evaluate the performance of the intermittent PV in assuring good breathable air quality to the BZ, Al-Assaad et al. [48, 49]adopted the average values of ε_v. The ventilation effectiveness index is given by:

$$\epsilon_v = \frac{C_{ex} - C_i}{C_{ex} - C_{fr}} \times 100 \qquad (2)$$

where C_{ex} is the species' concentration at the outlet, C_i is the CO_2 concentration at any location in the space, C_{fr} is the concentration of CO_2 in the PV fresh air supply and it is equal to a typical value of 450 ppm. Since ε_v was evaluated at the BZ (denoted by $\varepsilon_{v,BZ}$). When ε_v index is high, the contaminants' concentration is close to that supplied at the PV nozzle outlet indicating high IAQ. However, when ε_v is low, this means that the PV air is polluted and does not supply good quality of fresh air.

5. Experimental methodology

The ability of the CFD models in accurately predicting the temperature, velocity distributions in the room as well the CO_2 concentrations was validated by conducting experiments in a climatic chamber equipped with the intermittent PV+MV/CC systems.

26

The climatic chambers used were twin chambers, one equipped with the MV and the other with CC.

d. Obtaining the sinusoidal airflow

In both experiments, the intermittent PV was used in conjunction with MV and CC. For this reason, to create the sinusoidal airflow characteristic of the intermittent PV, a variable-speed fan having dimensions of 80 mm (length) $\times$ 80 mm (width) $\times$ 25.4 mm (height) was placed inside the PV duct. The fan has a maximum DC voltage of 12 V and maximum power of 6.25 W. The PV fan was controlled using LabVIEW software, which takes the time and frequency as inputs and supplies the fan with a sinusoidal voltage. Accordingly, the fan can generate sinusoidal airflow with different fluctuation frequencies and different average flowrates. The two latter parameters are chosen according to typical values used in indoor spaces. The PV fan was placed in the duct away from the nozzle outlet. The fan flow circulated through the PV duct and measures were taken to straighten the flow before being supplied. To reduce swirling effect, flow turbulence intensity and airflow mixing, a honeycomb flow straightener sandwiched between two screens was placed downstream inside the duct after the fan as shown in Figure 1(c). The honeycomb is 30 mm thick and has holes which diameter is equal to 4 mm such that the thickness over diameter ratio (t/D) is equal to 7.5, which gives optimal results [35].

e. Setup I: Intermittent PV + MV

The experimental setup consists of a chamber conditioned by a mixed air supply system that recirculates and conditions the room air. The chamber has inner dimensions of 2.5 $\times$ 2.75 $\times$ 2.8 m with two identical supply diffusers located at 2.0 m above floor

level. The supply diffusers have a cross sectional area of 0.57 m (width) $\times$ 0.37 m (height). The exhaust diffuser is located at the adjacent wall at 0.53 m above floor level, it has a cross sectional area of 0.524 m (width) $\times$ 0.52 m (height). In this chamber, the thermal manikin "Newton" manufactured by the Northwestern measured technology is used [50] (Figure 4). This manikin is characterized by high performance of ± 0.1 °C temperature measurement and set point control with a maximum power output range from 0 to 700 W/m^2. "Newton" is subdivided into twenty different control zones where each zone can report the segmental surface temperature based on assigned constant heat flux. "Newton" is controlled through "ThermDAC" control software that is user-friendly Windows-based application providing all possibilities of control. An internal load of 30 W/m^2 was generated in the room resulting in 135 W, and thermal manikin generating 100 W resulting totaling at 235 W. At a distance of 0.4 m from the manikin and at a 1.1 m height from the floor, a personalized ventilation nozzle of diameter 0.05 m is installed, the nozzle withdraws conditioned fresh air from a twin chamber and supplies it towards the occupant.
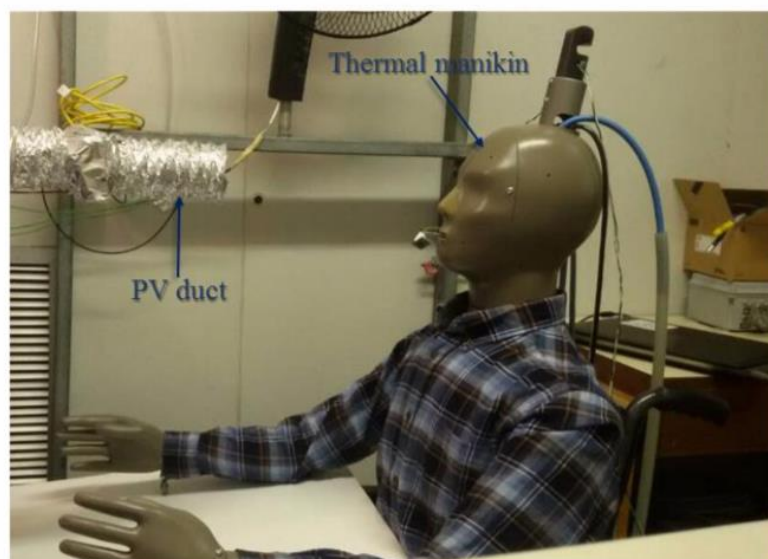
Figure 4 Illustration of the thermal manikin with its workstation equipped with the PV duct

To study the ability of PV in delivering fresh air to the occupant, a constant source of CO_2 was placed at each wall to create uniform conditions inside the room. Four sources of CO_2 deliver a constant flow rate of 2 L/min (each source delivering 0.5 L/min), the source of CO_2 represents passive contaminants generated in the room. CO_2 sensors were used to measure the concentration at different positions in the space. The sensors used were the FIGARO CDM7160 CO_2 sensor module having a detection range of 300 – 5000 ppm and having an accuracy of $\pm$ 50 ppm. They were placed at the PV and mixing supplies and exhaust diffusers and in the BZ at 2.5 cm away from the manikin's face; (See Figure 5 **(a)**, **(b)**)) and connected to OMEGA DacPro data logger to store the data and check stabilized residuals. The CFD model predicted instantaneous values of temperature (when coupled with the bio-heat model) and concentration. The latter were averaged (See equations 3 and 4 respectively) in order to compare with the average experimental output data on temperature and concentration and perform the validation:

$$\overline{T} = f \int_0^{1/f} T(t)dt \qquad (3)$$

$$\overline{C} = f \int_0^{1/f} C(t)dt \qquad (4)$$

where $\overline{T}$ and $\overline{C}$ are the average temperatures and concentrations, $T(t)$ and $C(t)$ are the instantaneous values of temperature and concentrations.
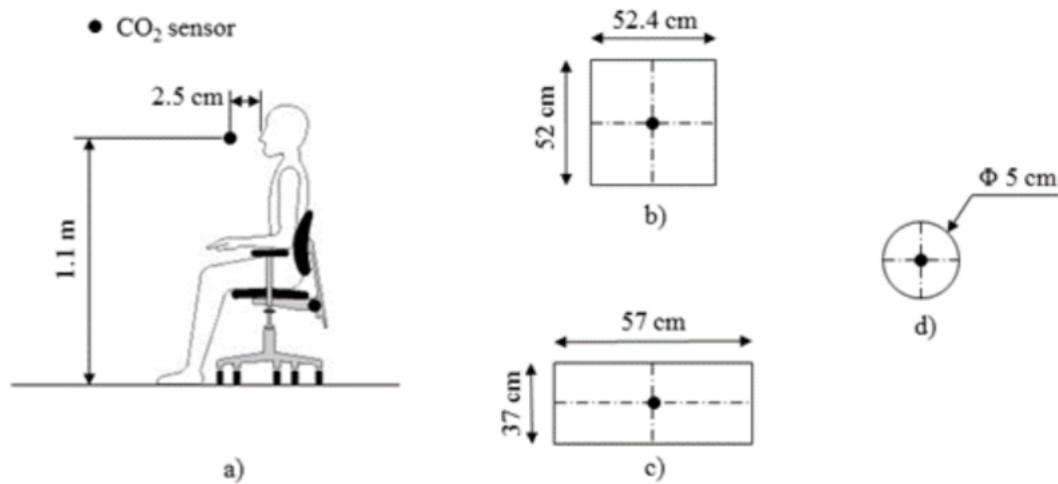
Figure 5 Schematic illustrating the different measuring locations of CO_2 concentrations: a) BZ, b) exhaust, c) supply, d) PV nozzle

i. Protocol

Initiating experiments begins by turning on the MV system and the lights in the chamber and setting the manikin to a constant heat flux representing sedentary activity of 39 W/m^2. The flow rate and temperatures are set to 80 L/s and 28±0.3°C respectively, then the CO_2 source is introduced into the room. Before turning on the personalized ventilation, the MV system, thermal manikin and CO_2 sources were operated for 3 hours until reaching steady state conditions and the segmental skin temperatures of the manikin reached stable values. After reaching steady state with the standalone mixing system, the PV system was turned on and it supplied cool fresh air intermittently at 24±0.2°C towards the thermal manikin at an average flowrate of 3.5±0.25 L/s. The CO_2 concentrations in the supplied fresh air were equal to ~449±10 ppm. The averaged skin temperatures and CO_2 concentrations were monitored until stabilization. The experiment was repeated several times for accuracy.

f. Setup II: Intermittent PV + CC

The experimental room had dimensions of 2.5 m × 2.75 m × 2.8 m as well. It was conditioned by the same intermittent PV system used in the previous MV experiment. The space was also equipped with a CC system as seen in Figure 6 and Figure 7. The CC covered 80 % of the ceiling surface area. It was made of a highly conductive copper panel with chilled water parallel pipes welded to it running through common header (Figure 7 **(b)**). Due to its high conductivity, the ceiling had a uniform temperature across its surface with a temperature difference less than 0.3°C. The room has a circular exhaust situated at 2.25 m above the ground and has a diameter of 5 cm. The PV nozzle is situated at a breathing height of 1.1 m, it has an outlet diameter of 5 cm and a distance of 40 cm separates it from the occupant. The intermittent PV jet delivers conditioned air from an adjacent fresh air source and supplies it horizontally towards a thermal manikin "Newton" manufactured by Northwestern measured technology [50] (Figure 7 **(a)**). The room had a load of 30 W/m^2 divided between the manikin (100 W) and lighting (100 W). The walls in the room are nearly adiabatic having a small U-value of 0.3 W/m^2.K.
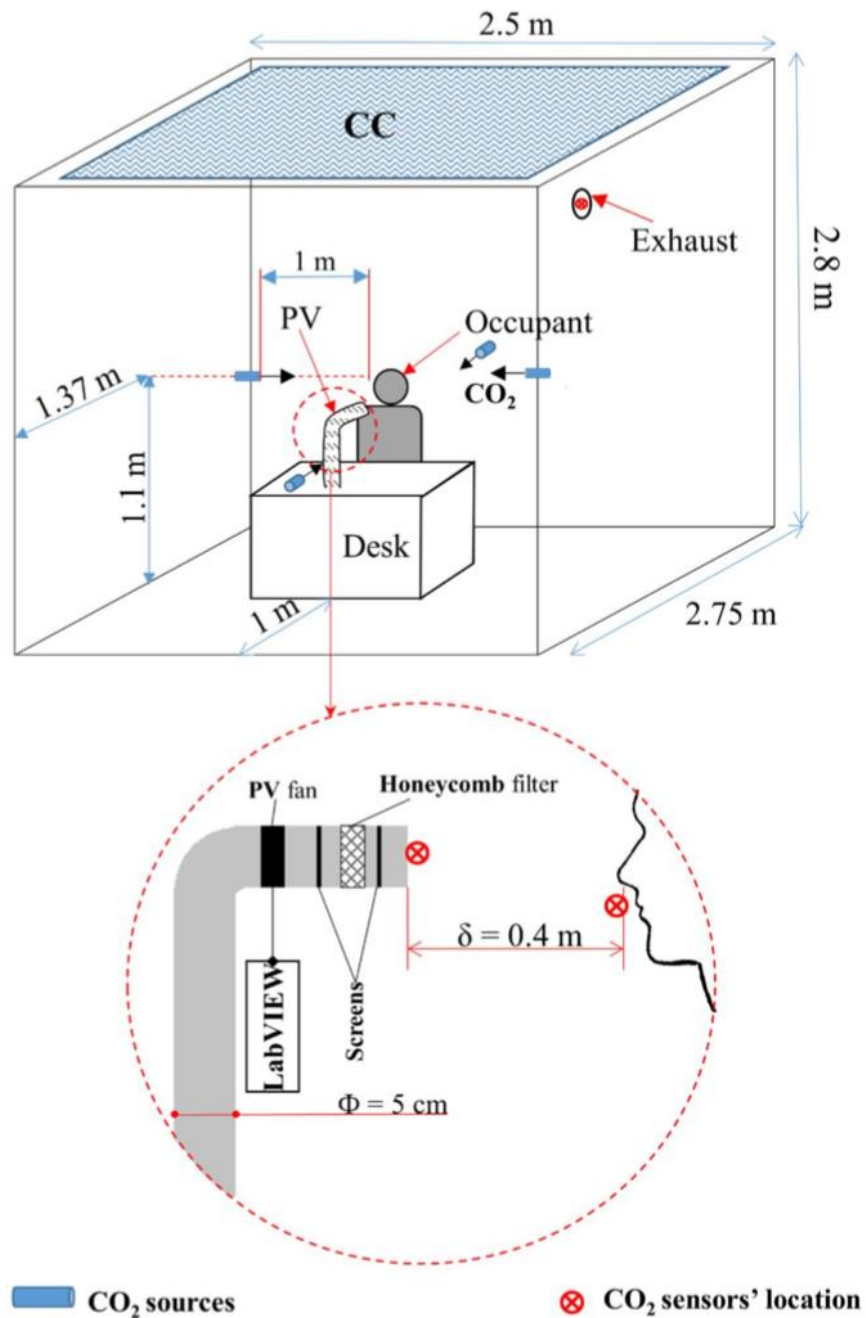
Figure 6 Illustration of the experimental chamber equipped with the intermittent PV, CC as well as temperature and CO2 concentration sensors

To understand the influence of intermittent PV coupled with CC on the quality of the air in the space and especially in the BZ, a constant source of CO_2 (representing passive contaminants) was introduced in the room by installing a CO_2 tank (See Figure 7(**a**)). A total flow rate of 2 L/min was set and distributed between four sources of CO_2 such that each source supplies 0.5 L/min. The sources were located at the breathing height at 1 m away from the BZ and directed towards it to simulate the critical contamination scenario (Figure 6). To measure CO_2 concentrations at different locations in the space, FIGARO CDM7160 CO_2 sensors were used. These sensors are characterized by a detection range of 300 ppm – 5000 ppm, a 2 min response time and an accuracy of ± 50 ppm. As seen in Figure 5, these sensors were placed at the exhaust to measure the CO_2 concentration at the return C_{ex}, at the PV nozzle outlet to measure the concentration in the fresh air supply C_{fr} which has typical values of 450±10 ppm. Sensors were also placed at the BZ to measure C_{BZ}. These sensors measure the average species concentration at each location and are connected to an OMEGA DaqPro data logger to collect the data. Note that the measured data was collected for a duration of three hours after reaching quasi steady state conditions. The CFD model predicted instantaneous values of temperature (when coupled with the bio-heat model) and concentration. The latter were averaged (See equations 3 and 4 respectively) in order to compare with the average experimental output data on temperature and concentration and perform the validation.
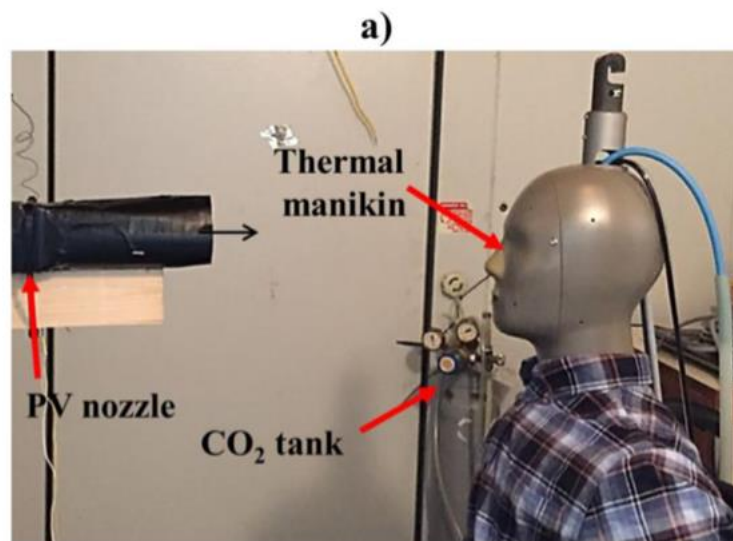
Figure 7 Illustration of the climatic chamber equipped with: a) the thermal manikin, PV nozzle, CO_2 source tank and b) CC system

i. Protocol

Before starting the experiment, the room was well ventilated by opening all the doors. To begin, the CC system was turned on by activating the chiller and fully opening the valve that delivers cold water from the chiller to the pipes at the ceiling level. This guaranteed an average CC temperature of 16°C. The lights (100 W) were turned on in the room and the manikin was set to emit a constant heat flux of 39 W/m²

corresponding to sedentary activity in office spaces (100 W). After four hours, steady state conditions were reached with the airflow field of the standalone CC system (the different segmental skin temperatures of the manikin reached steady state values). After that, the PV and CO_2 emission sources were turned on and reached quasi steady state conditions in three hours. The PV nozzle supplies air intermittently at an average flow rate of 3.5±0.25 L/s and an inlet temperature of 21±0.2 °C. The PV inlet temperature was 3°C lower than the ambient temperature (24°C) to minimize body temperature asymmetry [28]. Temperatures were measured using a hot wire anemometer system OMEGA HHF2005HW model characterized by an accuracy of ±0.5°C for temperature and ±10% of full scale velocity measurement, ranging between 0.2 m/s and 20 m/s).

The intermittent jet is characterized by its turbulence, which increases with the increase in frequency. To test the effect of PV operating frequency on IAQ, three frequencies were experimentally tested: 0.3 Hz, 0.5 Hz and 1 Hz. As for the CO_2 sources; they were set to emit 0.5 L/min each. After several hours of running the experiment, temperatures and concentrations in the room reached stable values. The average temperatures of the manikin were given by the "ThermDAC" software while the average concentrations were measured using the CO_2 sensors. Each experiment was repeated five times to ensure accurate and repeatable results. It is worthy to note that temperatures and concentration values and trends, were consistent between the repeated experiments with a maximum relative error of approximately 6%.

6. Parametric studies

The main parameters affecting comfort and IAQ of the studied case are the PV average flowrate and fluctuation frequency. For this reason, a parametric study was conducted on a typical office space to study their effect on thermal comfort, air quality and energy savings.

A typical office space with inner dimensions of 3.4 m × 3.4 m × 2.8 m with supply and exhaust grills having a cross sectional area of 0.7 m (width) × 0.3 m (length) and 0.5 m (width) × 0.2 m (length) respectively was considered as was shown in Figure 1(**a**). In the case of MV, the MV system supplies 63 L/s of air at 20°C assuring a set point temperature of 26°C inside the space. In the case of CC, two temperatures were chosen to study the effect of temperature gradients on comfort and IAQ. The chosen temperatures of the CC were 16°C and 20°C. In both cases, the PV outlet of diameter 0.05 m and was fixed at a distance of 0.4 m from the manikin. This is a typical separation distance between a PV device and an occupant in an office space. A load of 40 W/m^2 distributed between lighting, walls, and occupancy, is set in the room. In the case of MV, the temperature of the dynamic airflow exiting the PV was set 22°C. In the case of CC, the temperature of the dynamic flow was set to 21°C and 23°C for CC temperatures of 16°C and 20°C respectively. Four CO_2 sources are introduced into the room, each supplying 0.5 L/min through a tube to ensure a uniform distribution of passive contaminants within the room.

In order to optimize the frequency and the average flowrate of the PV jet, 3 sets of simulations were conducted. The PV fan was operated at three different frequencies (0.3 Hz, 0.5 Hz and 1 Hz), and average flowrates (3.5 L/s, 5 L/s and 7.5 L/s). It is

noteworthy that the velocities near the face for the maximum PV flowrate was nearly 1 m/s, 1.2 m/s and 2 m/s respectively. Velocities were further reduced at close proximity to the eye due to the presence of the rising thermal plume. Nevertheless, the transient pattern allows higher velocities to be reached at the face level [32], therefore, this reduces the risk of eye discomfort. Table 2 presents the set of simulations to be conducted for each study

Table 2 Different simulation cases

a) Different simulation cases at a background temperature of 26°C and PV jet temperature of 22°C for the MV case.		
	Average flowrate (L/s)	Frequency (Hz)
Set 1	3.5 L/s	0.3 Hz, 0.5 Hz, 1 Hz
Set 2	5 L/s	0.3 Hz, 0.5 Hz, 1 Hz
Set 3	7.5 L/s	0.3 Hz, 0.5 Hz, 1 Hz
b) Set of simulations to be conducted in the case study of CC case		
CC temperature (°C)	PV operation / temperature (°C)	
CC16	No PV (Standalone CC)	
	Steady PV/ PV21 (CC16PV21)	
	Intermittent PV/ PV21 (CC16PV21)	0.3 Hz
		0.5 Hz
		1 Hz

37

CC20	No PV (Standalone CC)	
	Steady PV/ PV23 (CC20PV23)	
	Intermittent PV/ PV23 (CC16PV23)	0.3 Hz
		0.5 Hz
		1 Hz

C. Results and discussion

1. *Validation of the CFD models*

a. Intermittent PV + MV

The CFD validation was performed for the conditions of the experiment at a room temperature of 28°C and a PV jet of 24°C supplying an intermittent flowrate of average 3.5 L/s. Three frequencies were tested experimentally: 0.3 Hz, 0.5 Hz and 1 Hz. The CFD validation is done based on comparison between predicted and measured values of segmental skin temperatures and ventilation efficiency ε_v.

The bio-heat and CFD models predict instantaneous values of segmental skin temperatures (Figure 8) and the CO_2 concentrations. However, the thermal manikin and CO_2 sensors cannot capture the instantaneous response at high frequencies due to the limitations of their response times. In fact, the CO_2 sensors have a long response time of 2 minutes whereas to capture a transient response from the thermal manikin, the operating period was lowered to 19 seconds corresponding to a frequency of 0.056 Hz. This frequency is outside the range of indoor frequencies, which is why it was not included in the validation. Therefore, the validation was based on the predicted and

measured values of the average segmental skin temperatures and average ventilation efficiencies.
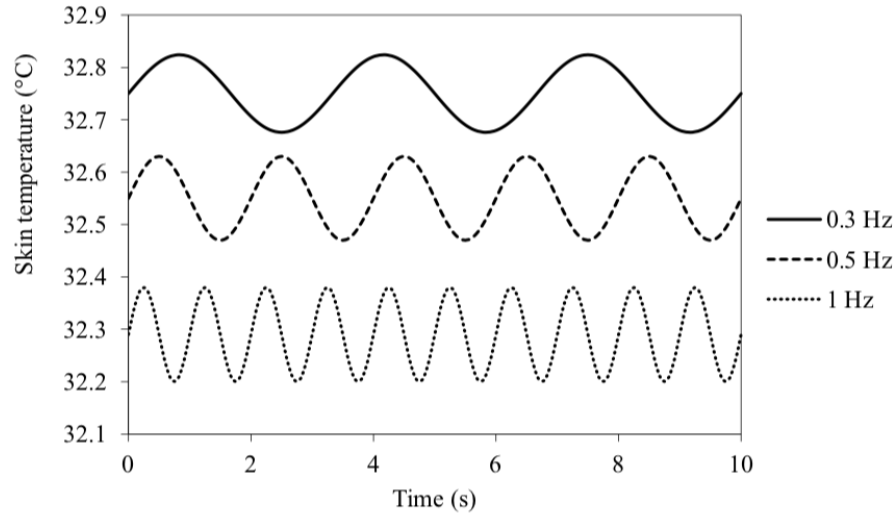
Figure 8 Variation of face temperature for an average flowrate of 3.5 L/s and with frequencies of 0.3 Hz, 0.5 Hz and 1 Hz

The average segmental skin temperatures for the considered experimental conditions are presented in. When the PV fan was turned on supplying an intermittent jet flow, it was able to reduce the average skin temperature of the face from 34.5°C to averages of 32.7°C, 32.5°C and 32.1°C for 0.3 Hz, 0.5 Hz and 1 Hz respectively (Figure 8). This is due to the increase of the convective currents at the head level and therefore heat loss from that segment. The results showed good agreement between predicted and measured segmental surface temperatures with relative errors ranging between 1.84% and 3.34% as can be seen in Figure 9.
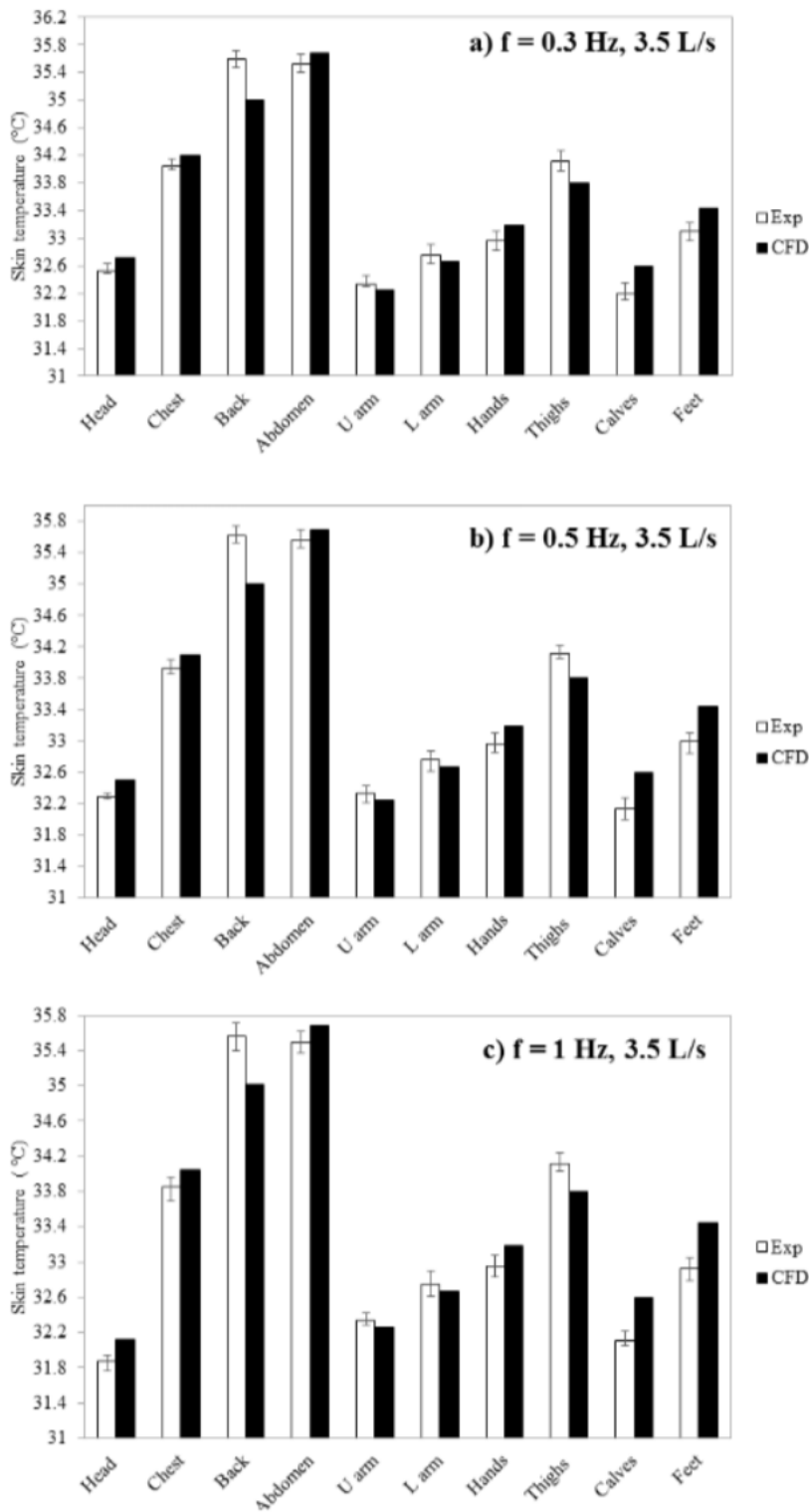
Figure 9 Segmental surface temperature validation for an average flowrate of 3.5 L/s
and 3 different frequencies

The air quality is assessed using the ventilation efficiency (ε_v) parameter. The results are shown in Figure 10 for 0.3 Hz, 0.5 Hz and 1 Hz. When increasing the frequency, there are two competing effects, the enhanced turbulence and the faster supply of fresh air to the BZ. For instance, with an increase in frequency from 0.3 Hz to 0.5 Hz, ventilation efficiency improved from 66.7% to 75.71%. However, when frequency further increased to 1 Hz, the efficiency degraded from 75.51% to 70.12% due to increased turbulence intensity at higher frequency, which overcame the faster supply of fresh air. In fact, turbulence increased in the BZ by 13.71% and 26.25% when increasing the frequency from 0.3 Hz to 0.5 Hz and from 0.5 Hz to 1 Hz respectively. Results showed good agreement between experimental and predicted values with relative errors ranging between 1.94% and 5.7% with the standard deviation bars representing the experimental variations obtained from repeating each experiment several times (Figure 10).
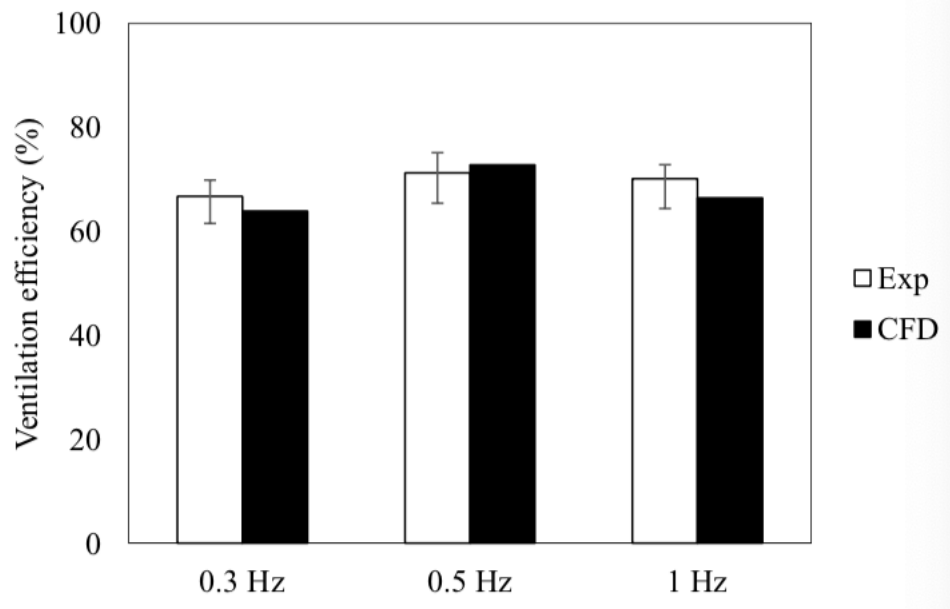
Figure 10 Ventilation efficiency ε$_V$ validation for an average flowrate of 3.5 L/s at frequencies: a) 0.3 Hz b) 0.5 Hz c) 1 Hz

b. Intermittent PV+CC

The validation of the CFD model was performed for a CC temperature of 16°C corresponding to a room temperature of 24±0.3°C. The PV was operated at an average flow rate of 3.5±0.25 L/s, a temperature of 21±0.2°C and three different operating frequencies (0.3 Hz, 0.5 Hz, 1 Hz). The validation is done based on values of vertical temperature gradients in the space in the vicinity of the occupant, segmental skin temperatures and ventilation effectiveness ε_v at the occupant BZ and surrounding microclimate for these three different frequencies.

The average values of vertical temperature gradients measured experimentally and predicted by the CFD model for the different simulation cases are summarized in Table 3 Average predicted and measured values of air temperature in the vicinity of the occupant for the different cases.. Measurements were taken at heights of 0.1 m and 1.1 m near the feet and head segments respectively. Air temperatures were also measured above the seated occupant at heights of 1.7 m corresponding to a standing occupant height, and 2 m, closer to the CC. According to Table 3 Average predicted and measured values of air temperature in the vicinity of the occupant for the different cases., increasing the PV jet frequency did not affect the temperatures at the heights of 0.1 m, 1.7 m and 2 m, except at 1.1 m where the PV jet is supplied in the occupant vicinity. When increasing the PV jet frequency from 0.3 Hz to 0.5 Hz and from 0.5 Hz to 1 Hz, the air temperature near the head at 1.1 m, decreased by 2.53% and 5.48% respectively. This is due to the increased rate of supply of PV fresh air, which provides

more cooling. Note that the maximum head-feet temperature difference was equal to 1.4°C at 1 Hz, lower than the maximum allowed of 2°C. Note that the vertical temperature gradient in the macroclimate between 0.1 m – 2 m was equal to 0.79°C/m. Similar gradients ranging between 0.71-0.77°C/m were also obtained in the work of Catalina et al.[11] at different CC temperatures. Good agreement was found between experimental and numerical values with a maximum relative error of 5.04% found at a height of 2 m.

Table 3 Average predicted and measured values of air temperature in the vicinity of the occupant for the different cases.

Height (m)	Intermittent PV/0.3 Hz		Intermittent PV/0.5 Hz		Intermittent PV/1 Hz	
	Exp±SD	CFD	Exp±SD	CFD	Exp±SD	CFD
0.1 (Feet)	24.2±0.3	24.5	24.2±0.3	24.5	24.2±0.3	24.5
1.1 (Head)	23.5±0.3	23.8	23.2±0.3	23.5	22.9±0.3	23.1
1.7	23.1±0.3	23.4	23.1±0.3	23.4	23.1±0.3	23.4
2	22.7±0.3	22.3	22.7±0.3	22.3	22.7±0.3	22.3

The average segmental skin temperatures predicted by the CFD model and measured experimentally are presented in It can be noted that with the increase of the PV jet frequency from 0.3 Hz to 1 Hz, the head segment temperature decreased from 31.6°C to 31°C respectively. This is due to the increase in the convective currents near the head and therefore heat losses from that segment; when increasing the PV jet frequency. Good agreement was found between numerical and experimental results with a maximum relative error of 4.53% for the abdomen segment. Note that the results in

Figure 11 Segmental surface temperature validation for an average flowrate of 3.5 L/s and 3 different frequencies., are only used to validate the CFD model. The considered CCPV operating conditions, which are not far off the typical range of operation, might not achieve optimal thermal comfort.
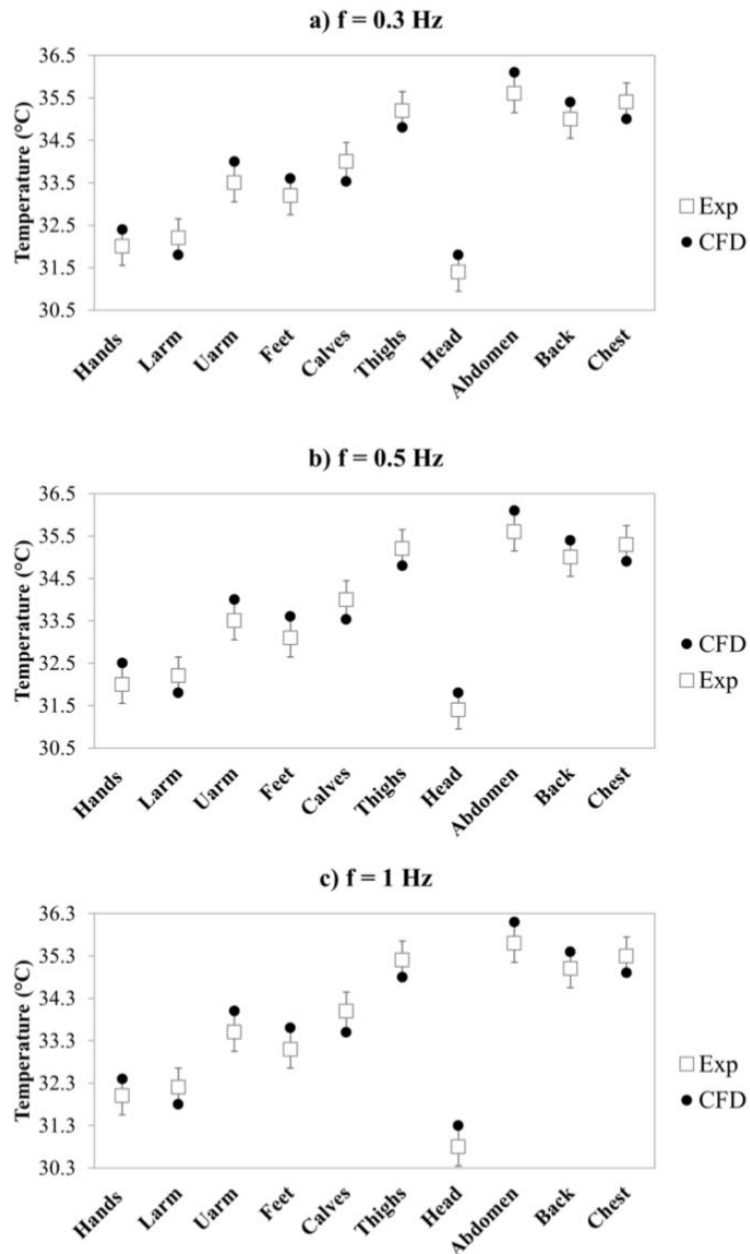
Figure 11 Segmental surface temperature validation for an average flowrate of 3.5 L/s and 3 different frequencies.

To investigate the ability of the CFD model in assessing IAQ, validation with experimental results was conducted based on average values of ventilation effectiveness index ε_v in the BZ ($\varepsilon_{v,BZ}$). The results are illustrated in Figure 12 for the three frequencies (0.3 Hz, 0.5 Hz and 1 Hz). When increasing the PV jet frequency, there are two competing physical phenomena: the increasing rate of supply of fresh air and the increasing turbulence and entrainment of pollutants. According to Figure 12, when increasing the PV jet frequency from 0.3 Hz to 0.5 Hz, ventilation effectiveness in the BZ increased from relatively low IAQ at 44% to satisfactory values of 53% due to the increased rate of supply of fresh air. However, when further increasing frequency to 1 Hz, ventilation effectiveness in the BZ deteriorated to 43% due to the turbulence overcoming the increased fresh air in the BZ. Note that turbulence increased by 15.1% and 22.3% when increasing frequency from 0.3 Hz to 0.5 Hz and from 0.5 Hz to 1 Hz. There was good agreement between measured and predicted results with a maximum relative error of 9.51% observed at a frequency of 1 Hz for $\varepsilon_{v,BZ}$. Therefore, assisting CC with intermittent PV can bring satisfactory IAQ if the PV is operated at 0.5 Hz. The obtained trend of ε_v is similar to the one obtained in the study of intermittent PV + MV.
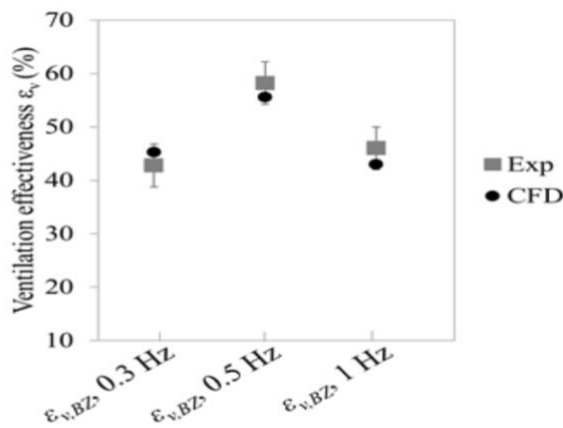
Figure 12 Illustration of the experimental and numerical results of ventilation effectiveness variation as a function of frequency

2. *Effect of fluctuating frequency, average flow rate, background temperature*

a. Intermittent PV + MV

    i. Thermal comfort

The effect of fluctuation frequency and average flowrate on thermal comfort was investigated. Table 4 and

Table 5 summarize the results for the overall thermal sensation (OTS) and overall thermal comfort (OTC) for different fluctuation frequencies and average flowrates. For a fixed average flowrate, when increasing frequency, the OTS decreases and OTC improves. This trend is observed for all flowrates. The decrease in OTS and improvement in OTC with higher frequencies is due to an increase in the convective currents near the head leading to lower head temperatures and higher rates of change. For instance, at an average flowrate of 3.5 L/s, the OTS decreases from 0.366 to 0.163 and the OTC increases from 0.325 (just comfortable) to 0.704 (comfortable) when the frequency increases from 0.3 Hz to 1 Hz. For this case, the average face skin temperature decreased from 34.28°C to 33.82°C and the average rate of change increased from 0.089°C/s to 0.296°C/s when the frequency increased from 0.3 Hz to 1 Hz.

In addition, when increasing the average flowrate, the OTS decreased for all frequencies. However, the OTC increased with flowrate just for the first two frequencies (0.3 Hz and 0.5 Hz). On the other hand, at a frequency of 1 Hz, the highest recorded OTC was obtained at 5 L/s. In fact, at a flowrate of 7.5 L/s, the increased convective air currents due to the combination of high frequency and flowrate led to overcooling of the head resulting in thermal draft (Table 4 and

Table 5).

Table 4 Overall thermal sensation at different wind frequencies and different average flowrates

	Ta=26°C, PV jet temperature = 22°C, RH=50%		
PV Flow Rate	3.5 L/s	5 L/s	7.5 L/s
Frequency (Hz)			
0.3 Hz	0.366	0.334	0.272
0.5 Hz	0.262	0.12	-0.226
1 Hz	0.163	0.1	-0.32

Table 5 Overall thermal comfort at different wind frequencies and different average flowrates

	Ta=26°C, PV jet temperature = 22°C, RH=50%		
PV Flow Rate	3.5 L/s	5 L/s	7.5 L/s
Frequency (Hz)			
0.3 Hz	0.325	0.334	0.341
0.5 Hz	0.418	0.4812	0.4966
1 Hz	0.704	1.2843	1.015

ii. Breathable air quality

It was shown that localized dynamic airflow gave good values of comfort. However, a transient PV fresh air profile might be challenging in providing good IAQ. In fact, transient flows create more turbulence than steady flows resulting in higher mixing between the PV jet and the surrounding air. In addition, when the flowrate reaches a minimum, not enough fresh air is diluting the contaminants in the BZ of the occupant.

Due to intermittent PV jet, the CO_2 concentration is transient in the BZ and fluctuates between a minimum and a maximum as can be seen in Figure 13. The CO_2

concentration profile is maximal when the minimum flowrate is supplied and is minimal when the maximal flowrate is delivered.
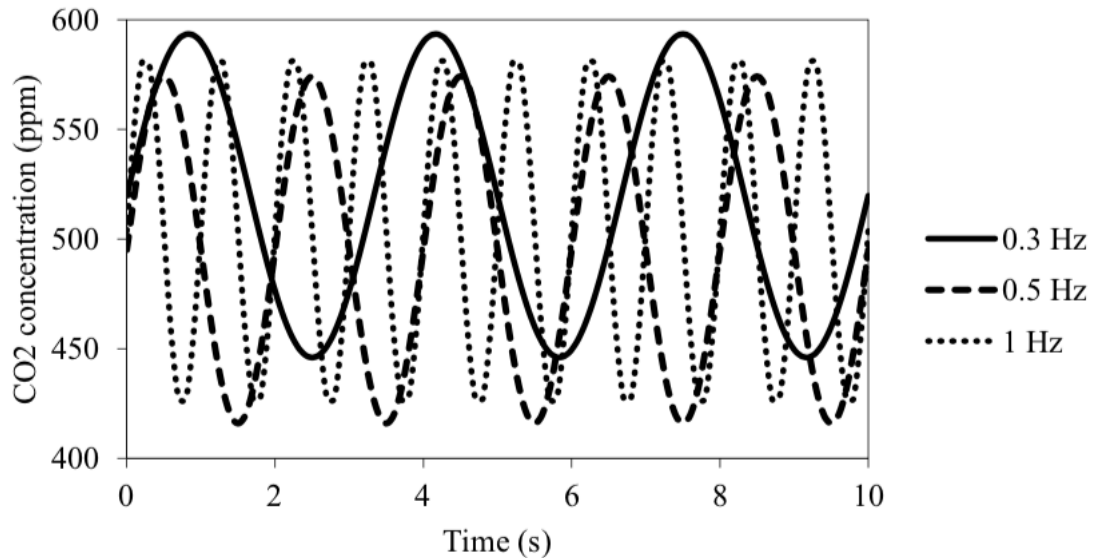
Figure 13 Fluctuation of CO_2 concentrations in the occupant BZ for 0.3 Hz, 0.5 Hz and 1 Hz for a fixed flowrate of 5 L/s

When increasing the frequency of an intermittent flow, the air is supplied at a faster rate and at the same time, turbulence is enhanced due to faster fluctuations. Therefore, there are two competing effects, which affect air quality: turbulence and rate of supply. Results show that when increasing frequency from 0.3 Hz to 0.5 Hz at a fixed average flowrate, the general CO_2 concentrations profile decreases. Consequently, minimum and maximum ventilation efficiencies ε_v increase (Table 6). Therefore, increasing the frequency of fresh air supply from 0.3 Hz to 0.5 Hz for all average flowrates was able to overcome the increasing turbulence effect in the occupant BZ which according to the simulations increased by a value of 13.53% for an average flowrate of 3.5 L/s. On the other hand, when further increasing frequency to 1 Hz, the general CO_2 concentrations profile increased and minimum and maximum ventilation

efficiencies ε_v decreased (Table 6). In this case, the turbulence effect overcame the positive impact of larger supply of fresh air. As a matter of fact, the turbulence intensity in the BZ increased by 25.93% when increasing the frequency from 0.5 Hz to 1 Hz at 3.5 L/s. This behavior was observed for all average flowrates.

When increasing the average flowrate at a fixed frequency, the [minimum and maximum] CO_2 concentrations decreased leading to higher ventilation efficiencies ε_v (Table 6). This is due to the increase quantity of fresh air reaching the BZ. This trend is observed for all frequencies. For instance, at 0.5 Hz, when increasing the average flowrate from 3.5 L/s to 7.5 L/s, the CO_2 concentrations decreased from [418.5, 597.5] ppm to [409.43, 501.93] ppm (Figure 13) and ventilation efficiencies ε_v increased from [21, 92.6] % to [59.23, 96.23] % (Table 6).

Table 6 Minimum and maximum ventilation efficiencies ε_V (%) at 3 frequencies and 3 average flowrates at background temperature of 26°C and a PV jet temperature of 22°C

	[MIN – MAX] $\epsilon_{v,BZ}(\%)$		
	3.5 l/s	5 l/s	7.5 l/s
0.3 Hz	[20.62, 76.84]	[22.6, 81.62]	[55.94, 85.43]
0.5 Hz	[21, 92.6]	[30.33, 93.63]	[59.23, 96.23]
1 Hz	[19.36, 84.1]	[26.45, 90.63]	[58.84, 94.89]

iii. Energy savings

To evaluate energy savings, the optimal case was compared to constant PV airflow. A constant flow PV system cannot simultaneously satisfy the same comfort and

air quality provided by the intermittent flow. Consequently, two sets of steady state simulations were performed to find

 (i) the constant flowrate that assured same OTC of 0.95 (comfortable) and

 (ii) the constant flowrate that provided the same average ventilation efficiency as the optimal intermittent flow.

For case (i), it was found that constant PV flowrate 9 L/s was able to provide the same OTC value of 0.95 (comfortable) as that of the intermittent PV at average flow rate of 7.5 L/s. Therefore, a higher constant PV flowrate was needed to provide the same level of comfort as the intermittent PV. In addition, it is expected that a flowrate of 9 L/s will be able to provide higher air quality than the intermittent PV. In fact, the ventilation efficiency recorded a value of 95.48%, which is much higher than the IAQ requirements and according to Melikov et al. [18], high values of ventilation efficiency (almost 100%) were obtained when operating with a constant PV flowrate of 10 L/s. However, satisfactory levels ($\varepsilon_v = 77\%$) were also achieved with an intermittent flow with the advantage of less energy cost. The optimized intermittent PV flow allowed reaching a compromise between thermal comfort, IAQ and energy cost.

For case (ii), it was found that a constant flowrate of 5.6 L/s was able to provide the same level of air quality ($\varepsilon_v = 77\%$) as the intermittent flow. The obtained flowrate is smaller than the average flowrate of the intermittent flow (7.5 L/s). This is expected since a constant flowrate delivers fresh air continuously in the BZ with minimal turbulence in the BZ and hence not the same amount of fresh air is needed to achieve acceptable levels of air quality. However, this constant flowrate was not able to provide the same level of comfort (OTC = 0.4, just comfortable) as that of the intermittent flow,

since the PV jet cannot penetrate the human thermal plume and cool the head as effectively as the higher jet velocities.

Thus, the intermittent PV flow was able to provide good comfort and good ventilation efficiency compared to a constant PV flow (9 L/s). In both cases, the fresh air is cooled by using the same chiller. To calculate the energy savings, the cooling capacity of each system as well as the fan power consumption for steady and transient operation were computed. The PV fan operating at steady state conditions with a constant flowrate of 9 L/s is considered as the reference case with a nominal power of 1.62 W. To calculate the PV fan power consumptions in the case of transient operation, the correlation of Keblawi et al. [16] was used:

$$P_{fan} = P_{ref} \left(\frac{\dot{m}_a}{\dot{m}_{ref}} \right)^3 \qquad (5)$$

Where P_{fan} is the fan power consumption and $\dot{m}_a$ is the mass flow rate of the fan, $P_{reference}$ and $\dot{m}_{ref}$ are the nominal power consumption and mass flowrate respectively considered for the steady state PV operation. For transient operation, the fan power was computed over a period according to the following equation:

$$P_{fan} = \frac{1}{T} \int_0^T P_{ref} \left(\frac{\dot{m}_a}{\dot{m}_{ref}} \right)^3 dt \qquad (6)$$

Where T is one period of oscillation. The obtained fan power consumption for transient operation at the optimal frequency might be slightly larger than the consumption for steady state operation.

The fan power consumption was calculated for transient operation for a frequency of 1 Hz and results showed that it is higher than the nominal fan power for steady state by 18.69%. As for the cooling capacity, results showed that the cooling capacity for transient condition decreased by 16.67% compared to steady state conditions. However, for a small nominal power of the fan of 1.62 W, the transient fan power consumption was 2 W with a small different of nearly 0.4 W. As for the cooling capacity, for a difference between outside temperature and supply temperature of 10°C at a relative humidity of 50 %, the transient PV operation spent 92 W while the steady state operation spent nearly 111 W. Therefore, the decrease in cooling capacity was more significant than the increase in fan power consumption between transient and steady state PV operation. Therefore, a transient PV system operating at an average flowrate of 7.5 L/s and a frequency of 1 Hz resulted in energy savings of 16.1 %.

   iv.   2.1.4 Conclusion

A validated transient 3D CFD model is integrated with a transient bio-heat model to select the optimal fluctuation frequency of a PV oscillating flow that can provide acceptable thermal comfort and good IAQ with the least energy consumption. This was done through variation of fluctuation frequency based on values used in indoor spaces, and through variation of the PV average flowrate. Energy analysis revealed that the intermittent PV system operating at 1 Hz for example recorded 16% energy savings compared to constant flow PV system providing same levels of comfort.

b.   Intermittent PV + CC

Note that in the case of intermittent PV+ CC, the average flow rate was not varied. In fact, in the intermittent PV + MV, the highest flow rate of 7.5 L/s was chosen

as operating flow rate due to its highest ventilation rates. Based on this conclusion, this flow rate was adopted as the operating flow rate in the case of intermittent PV coupled with CC.

    i.   Thermal comfort

The effect of standalone CC, steady PV and the intermittent PV operating frequency for two different CC/PV configurations; on thermal comfort was investigated. The results are showcased in Table 7**,** which illustrates the values of overall thermal sensation (OTS) and overall thermal comfort (OTC) for the different simulation cases (Table 2).

Table 7 Illustration of the values of OTS and OTC obtained for the different simulation cases.

	CC16/PV21 $T_{amb} = 24°C$, RH = 50 %		CC20 /PV23 $T_{amb} = 26°C$, RH = 50 %	
	OTS	OTC	OTS	OTC
Standalone CC	-0.051	0.140	0.324	0.071
Steady CCPV	-0.103	0.201	0.178	0.322
Intermittent PV/0.3 Hz	-0.155	0.115	0.136	0.386
Intermittent PV/0.5 Hz	-0.305	0.012	-0.188	0.578
Intermittent PV/1 Hz	-0.48	-0.13	-0.28	1.181

Operating under standalone CC and integrating the PV under steady or intermittent operation, yielded different effects on thermal comfort for the two CC temperatures. According to Table 7, both standalone CC systems configurations were able to provide good thermal comfort for the occupants due to the radiative heat exchanges between the ceiling and the occupant. Better comfort was obtained for CC16 compared to CC20, due to the cooler ambient conditions and higher radiative heat

losses (Figure 14 and Figure 15). In fact, the OTS/OTC values were -0.051 (slightly

cool) /0.14 (good comfort) and 0.324 (slightly warm)/0.071 (just comfortable) for CC16

and CC20 respectively.

When assisting the standalone CC system with a PV supplying continuous

airflow at 7.5 L/s, the OTS/OTC conditions improved by 50.5%/30.5% and 45.1%/78%

for CC16PV21 and CC20PV23 respectively (Table 7). In fact, supplying a high velocity

PV jet into the space introduces turbulence in the vicinity of the occupant. Therefore,

convective heat losses from the upper body segments (especially the head segment) are

added to the radiative heat losses due to the CC, which improves comfort conditions.

When integrating the steady PV, thermal comfort for CC20PV23 was 37.6% higher

than it was for CC16PV21 even though the occupant was slightly warmer (Table 7).

This is since CC16 already provided cool conditions while CC20 assured a warmer

environment. Thus, the introduction of the cool PV air to the occupant at warmer

conditions yielded warmth relief and hence, better comfort. This can be seen in Figure

16, which illustrates the contours of temperature around the occupant for CC16PV21

and CC20PV23.

When changing the PV operation from steady to intermittent, fluctuations are

introduced into the PV jet which results in an additional increase in turbulence and

hence, more convective heat losses near the occupant, that increase with frequency. In

fact, when increasing the PV frequency from 0.3 Hz to 0.5 Hz and from 0.5 Hz to 1 Hz;

turbulence intensities near the occupant increased by 15.1% and 14.6% respectively for

CC16PV21 and increased by 28.2% and 27.1% respectively for CC20PV23. This can

be seen in Figure 17, which illustrates the turbulence intensities around the occupant for

the CC20PV23 configuration for the three different frequencies (0.3 Hz, 0.5 Hz and 1 Hz).
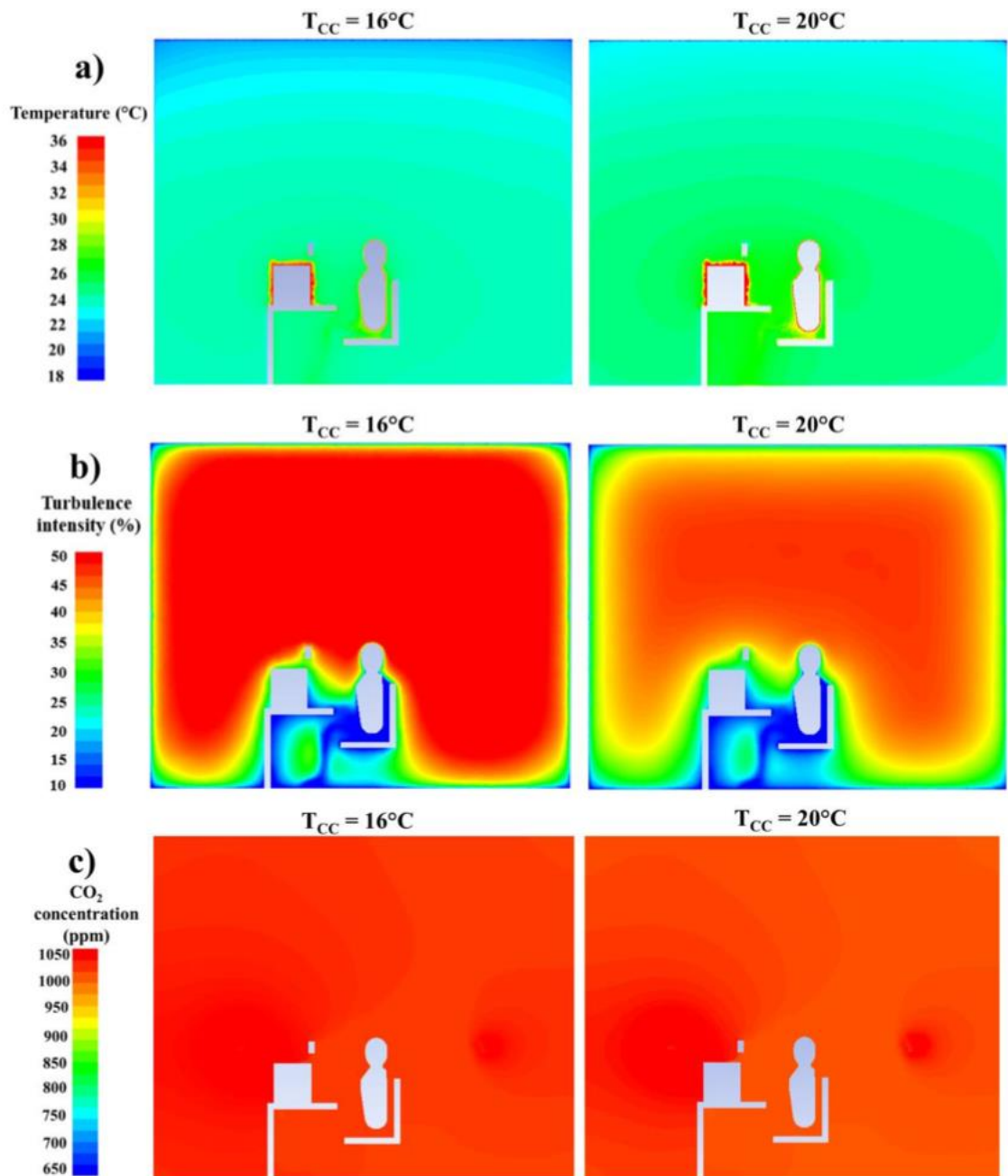
Figure 14 Illustration of the contours of: a) temperature, b) turbulence intensity (%), c) CO_2 concentration of CC16 and CC20.
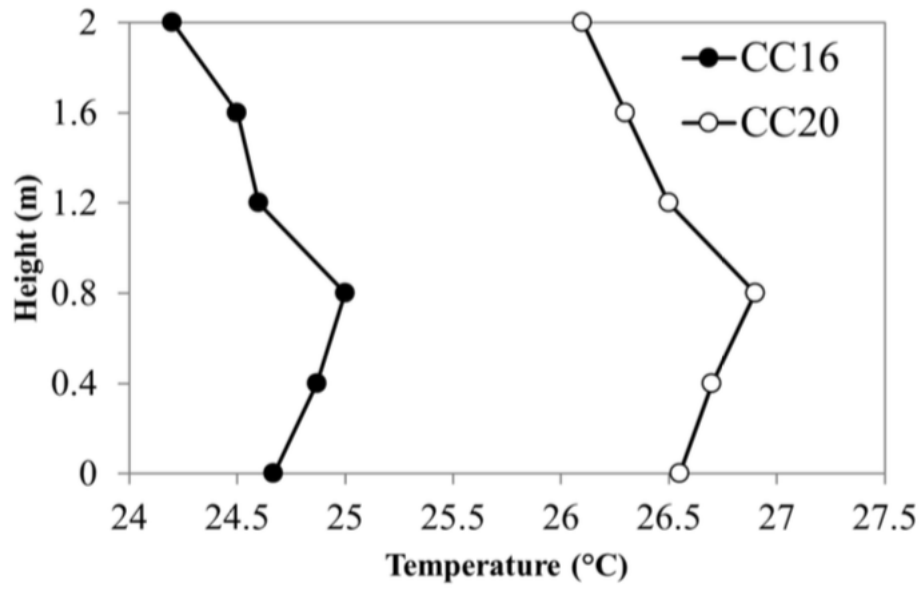
Figure 15 Illustration of the temperature variation with height for CC16 and CC20
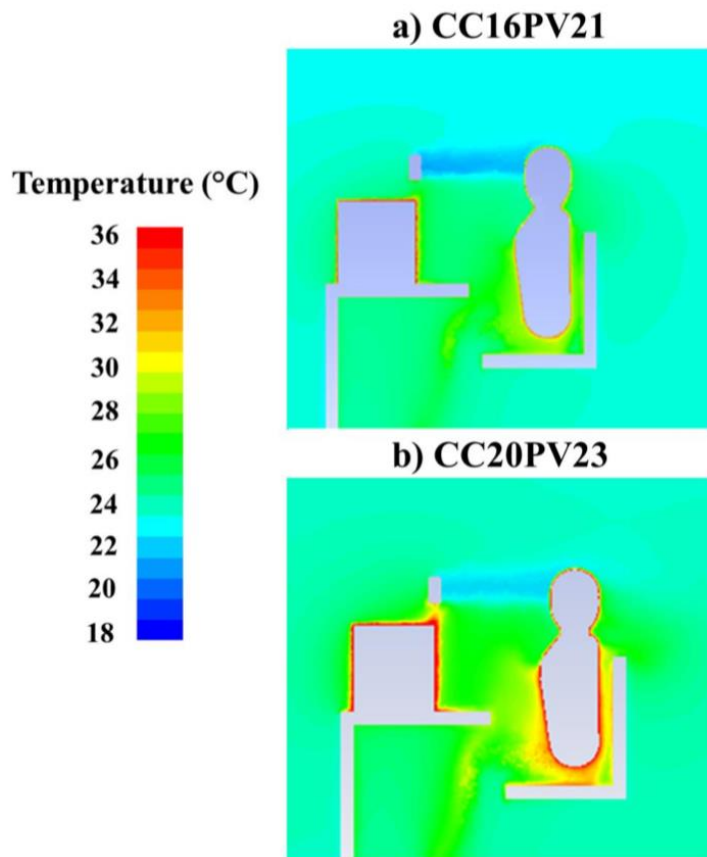
Figure 16 Illustration of the contours of temperature in the manikin cross sectional plane (y= 1.7 m), for: a) CC16PV21, b) CC20PV23.
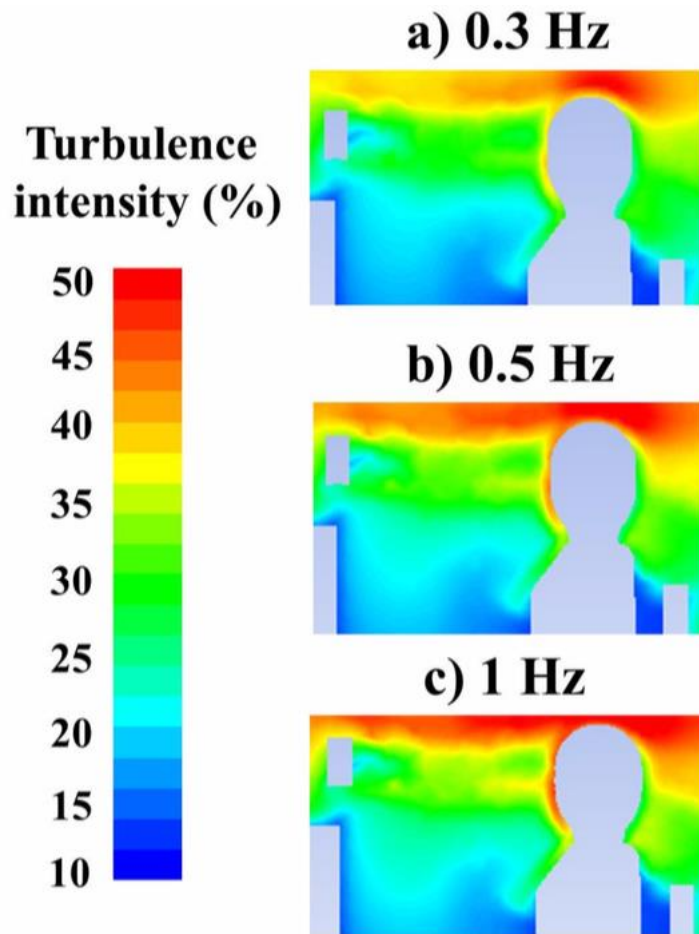
Figure 17 Illustration of the contours of turbulence intensity for the three different frequencies.

ii. Breathable air quality

The purpose of integrating the PV with the CC is also essential to assure good IAQ in the occupant BZ and surrounding microclimate since standalone CCs have a turbulent space and lack a fresh air source (Figure 14(b), (c)). Consequently, introducing clean fresh air towards the occupants through the addition of PV systems into workstations is crucial. To assess IAQ, the average ventilation effectiveness $\varepsilon_{v,BZ}$ (%) was calculated for the different CCPV configurations and results are shown in Table 8. According to Table 8, for all CCPV configurations and for steady and

intermittent PV operations, higher IAQ was obtained for CC20PV23 compared to CC16PV21. This is expected, since turbulence intensities at CC16 are 18% higher than CC20 (See Figure 14 **(b)**). For example, at a PV frequency of 1 Hz when lowering the ceiling temperature from 20°C to 16°C, $\varepsilon_{v,BZ}$(%) decreased by 8.33%. Therefore, PV gives the highest IAQ when assisting a CC having higher surface temperatures.

Table 8 Average ventilation effectiveness $\varepsilon_{v,BZ}$(%) values for the two CC/PV configurations, for a steady PV and intermittent PV at three different frequencies (0.3 Hz, 0.5 Hz and 1 Hz).

	Ventilation effectiveness ε_v (%)	
	CC16/PV21, T_{amb} = 24°C RH = 50 %	CC20/PV23, T_{amb} = 26°C RH = 50 %
	$\varepsilon_{v,BZ}$ (%)	$\varepsilon_{v,BZ}$ (%)
Steady PV	78.66	85.57
Intermittent PV/ 0.3 Hz	53.77	59.62
Intermittent PV/ 0.5 Hz	59.83	67.5
Intermittent PV/1 Hz	55.35	60

Operating the PV under continuous flow assured high IAQ in the BZ for both CCPV configurations due to the constant cleaning and dilution of contaminants [28]. High values of 78.66% and 85.57% were obtained for $\varepsilon_{v,BZ}$ (%) for CC16PV21 and CC20PV23 respectively (See Table 8). Intermittent CCPV can pose a bigger challenge in terms of supplying good breathable air quality compared to steady CCPV. As previously discussed, the fluctuations of the PV jet and increasing the frequency introduce additional turbulence to the already turbulent and polluted CC macroclimate.

Changing the PV operation from steady to intermittent at 0.3 Hz deteriorated IAQ for both CCPV configurations. According to Table 8, average $\varepsilon_{v,BZ}$ (%) decreased by 31.65% and 30.32% for CC16PV21 and CC20PV23 respectively. During

intermittent operation for both CCPV configurations, when increasing frequency from

0.3 Hz to 0.5 Hz, the average $\varepsilon_{v,BZ}(\%)$ increased by 10.12%. However, they decreased

by 11% respectively with a further increase in frequency to 1 Hz. When increasing

frequency from 0.3 Hz to 0.5 Hz, the increased rate of supply of fresh air surpassed the

increased turbulence. However, the opposite applies when increasing frequency from

0.5 Hz to 1 Hz. This can be seen in Figure 18, which illustrates the contours of average

CO_2 concentrations in the occupant vicinity for the CC16PV21 concentration at 0.3 Hz,

0.5 Hz and 1 Hz. Note that, similar to the steady PV operation; poor IAQ was obtained

in the surrounding microclimate compared to the BZ.
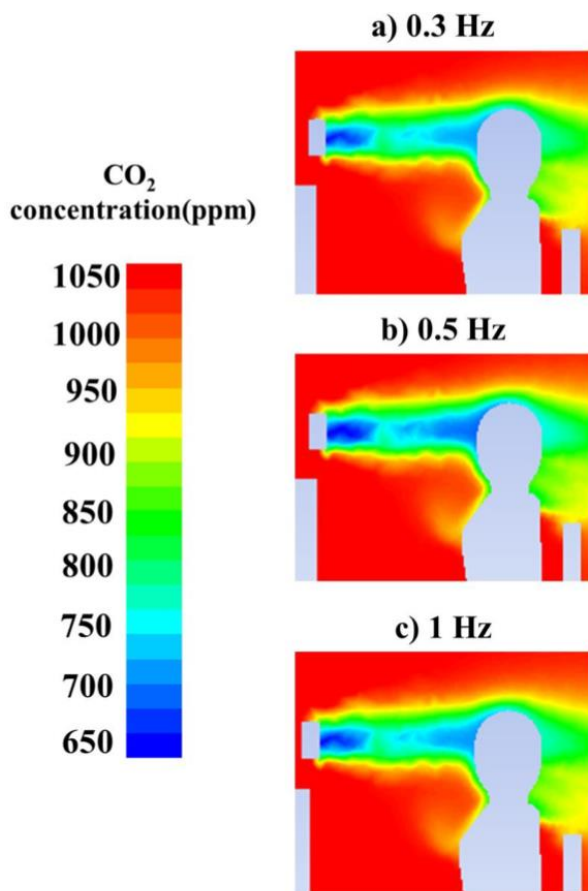
Figure 18 Illustration of the contours of average CO2 concentrations for CC16PV21 for the three different frequencies

iii. Energy savings

When varying the CC temperature and hence, the PV supply temperature in the steady CCPV system (Reference case 2), considerable energy savings can be achieved compared to a standalone CC system operating at 17°C (CC17: Reference case 1) for equivalent thermal comfort conditions (OTC = 0.25, see Table 7). Energy savings can also be achieved by an intermittent CCPV system compared to Reference case 2 for the same comfort as Reference case 1 (OTC = 0.25). To calculate energy savings, the heat load removal of the CC and the cooling capacity of PV system should be taken into consideration. The CC removes the heat load in the space by radiation and convection as seen in equation 7:

$$Q_{CC} = \sum_{s=1}^{l} \underbrace{h_r A(T_s - T_{CC})}_{radiant\ heat\ load\ removed} + \underbrace{h_c A(T_{amb} - T_{CC})}_{Convective\ heat\ load\ removed} \qquad (7)$$

where Q_{CC} is the heat load removed by the CC, h_r and h_C are the radiative and convective heat transfer coefficients (W/m^2.K) respectively, A is the CC surface area, T_{CC} and T_{amb} are the CC and ambient temperatures (K). T_s is the surface temperature, which exchanges radiative heat with the CC. These surfaces include the occupant, computer, walls etc. Note that s is the surface index and l is the number of radiating surfaces. As for the PV cooling capacity, it is given by equation 8:

$$Q_C = \dot{m} C_p \Delta T \qquad (8)$$

where Q_c is the cooling capacity in (W), $\dot{m}$ corresponds to the supplied PV mass flow rate (Kg/s) and ΔT is the temperature difference between the outside air (at 30°C) and the supplied PV air. Note that the PV fan power consumption for both PV operations (steady and intermittent) was also accounted for.

After several simulations, it is shown that, to obtain similar comfort (OTC = 0.25); as Reference case 1, the steady CCPV (Reference case 2) needs to be operated at a CC temperature of 18°C and a PV temperature of 22°C (CC18PV22). This corresponds to a total cooling capacity of 1117 W while the standalone CC16 had a cooling capacity of 1216 W. Therefore the steady CCPV (Reference case 2) was able to achieve energy savings of 8% compared to a standalone CC (Reference case 1). Moreover, to achieve similar comfort as Reference cases 1 and 2, the intermittent CCPV system needs to be operated at a CC temperature of 19°C and PV temperature of 22.5°C at a frequency of 0.5 Hz for example (CCPV). This corresponds to energy savings of 7.5% and 15% compared to References cases 2 and 1 respectively. The obtained energy savings are summarized in Table 9.

Table 9 Summary of energy savings obtained for reference cases 1 and 2

	Reference case I	Reference case II
Standalone CC17	-	-
Steady CC18PV22	8	-
Intermittent CC19PV22.5	15	7.5

iv. <u>Conclusion</u>

A transient 3D CFD model of an intermittent PV system coupled with a CC system for comfort enhancement, was developed and experimentally validated in a climatic chamber. A parametric study was conducted for different CCPV cases to find the compromise frequency between comfort and IAQ. The main conclusions from the case study are listed as follows:

- At low CC temperatures (16°C), the intermittent PV did not enhance comfort compared to steady PV. Consequently, it is better off to operate the PV under steady conditions for better comfort (OTC = 0.201) and better IAQ levels in the BZ and surrounding microclimate ($\varepsilon_{v,BZ}$ = 78.66% and $\varepsilon_{v,micro}$ = 35.33%).
- For higher and more conventional CC temperatures (20°C), the intermittent PV enhanced comfort compared to steady PV

An energy analysis was also performed to compute the energy savings that an intermittent CCPV can achieve compared to steady CCPV and standalone CC for similar comfort. It was found that:

- A steady PV at 22°C and 7.5 L/s assisting a CC at 18°C can achieve 8% energy savings compared to a standalone CC at 17°C.
- An intermittent PV at 22.5°C and 7.5 L/s coupled with a CC at 19°C can achieve 7.5% energy savings compared to a steady PV at 22°C and 7.5 L/s assisting a CC at 18°C. It can also achieve 15% energy savings compared to a standalone CC at 17°C.

CHAPTER II

PERSONALIZED VENTILATION: INHALATION EXPOSURE VS. CLOTHING-MEDIATED EXPOSURE

D. Introduction

1. *Background and context*

Many surveys and field studies conducted in office buildings have shown the direct correlation between decreased occupants' work performance and poor IAQ [51, 52]. Compromised IAQ in offices is attributed to the presence of contaminants, such as gaseous contaminants (volatile organic compounds, CO2, bio-effluents…) and more critically, aerosol particulate matter (PM) [53-55]. These contaminants could be cause of building related illnesses such as sick building syndrome (i.e. mucous membrane irritation, respiratory and skin symptoms, fatigue, headaches), asthma and possible viral infections, cardiovascular and respiratory diseases [56, 57].

2. *Sources of PM indoors*

PM can infiltrate into the building envelope from the outside environment or through the ventilation system. Particles of outdoor origin are sources from vehicular traffic or industrial pollution and are highly influenced by the ambient weather conditions [58]. However, with the increase in airtight buildings regulations, PM of indoor origin have emerged as a dominant determinant of IAQ. They can originate indoors from endogenous sources including occupants' respiratory activities (breathing [59], coughing [60], sneezing [61], smoking [62]). They can originate from exogenous sources such as office equipment emissions (i.e. laser printer machines emitting

ultrafine PM [63]) or emissions from cooking activities (i.e. cooking oils) [64], resuspension of particles from surfaces due to cleaning and vacuuming of particle-laden surfaces [65] or due to walking (i.e. dust particles, allergens) [66]. Depending on their properties and interaction with the room airflow, airborne particles can deposit on occupants' clothing.

Clothing exposure to contaminants is a topic of investigation that is gaining importance in the literature [67-69] as it was proven to be a mediator of different human exposure routes [70-73]. Notably, clothing that have picked up particles from the indoor environment can re-emit them indoors when occupants are engaged in various physical activities [74, 75]. They can also be released in other spaces during occupants' transition or when occupants handle their clothing. Hence, prolonged exposure of clothing items to indoor PM sources can lead to the deterioration of the inhaled air quality of the wearer and other residents [71]. The magnitude of PM deposition on worn garments is highly affected by the nature of the flow field in the vicinity of the occupant, PM source location, particle diameter, presence of electrostatic charges as well as the garment fit and form. Al Assaad et al. [67] studied the deposition of resuspended PM on upper body clothing. It was found that loose clothing altered the thermal plume and increased deposition compared to tight-fit clothes. While the study focused on the effect of clothing fit, it did not consider the effect of different ventilation designs or different sources of indoor PM.

3. *Personalized ventilation types*

Recent advances in ventilation design proposed the integration of PV systems. PV units have been installed in offices with the aim of providing occupants with high

breathable air quality by delivering a high momentum jet of cool clean air directly at their respective workspaces [18, 25, 76, 77]. PV units also allow the occupants control of the supply conditions (flow rate, temperature, and direction) according to their preferences. The efficiency of PV is a result of its interaction with the free convective and exhaled flows from the human body. This interaction is in large part, determined by the PV ATD. PV ATDs control the local air distribution and hence, play a major part in determining PV success. The following ATDs supply the air towards the breathing zone and have shown good performance in reducing inhalation exposure: computer mounted panels (CMP, horizontal jet), round movable panels (RMP, inclined downward jet) and vertical desk grills (VDG, inclined upward jet) [25]. Moreover, these ATDs are common in the building sector and have been used in office settings [78], air cabins [79], hospital wards [80] and different types of vehicles [81]. Despite them being a source of clean air, they still constitute a momentum source that impinges on the occupants' clothing and can entrain and deposit PM on them. Therefore, depending on the ATD and PM source location, PV has the possibility of contributing to clothing exposure and subsequent emissions. While the advantage of different PV ATDs on reducing inhalation exposure are well established [25], their secondary impacts on clothing contamination are still uncertain and to the authors' knowledge, is an issue that has yet to be addressed in the literature.

4. *Aims and research questions*

The aim of PART II of this work is to holistically investigate through computational fluid dynamics (CFD) modeling the effect of different PV ATDs (CMP, VDG and RMP) on direct inhalation exposure and indirect clothing-mediated exposure

due to typical indoor PM sources: furniture resuspension (S1), exogenous human exhalation of possible infectious PM from a standing occupant (S2) and endogenous exhalation of possible infectious PM from the PV user (S3). The aim is to compare the performance of the different PV ATDs at different operating flow rates to select the most versatile design, which allows for good breathable air quality and minimum clothing deposition. The results can also be used in developing an inclusive operation strategy for PV systems that takes into account all foreseeable exposure routes.

B. Methodology

1. System description

In this study, a typical office ($3.4 \times 3.4 \times 2.6$ m^3) was considered to be conditioned by a MV system, served by its own air handling unit (AHU). It supplied conditioned outdoor clean air from a rectangular grille diffuser (0.45×0.25 m^2) from the ceiling and exhausted it from a ceiling diffuser (0.45×0.25 m^2) (Figure 19). An occupant was stationed at a workspace performing sedentary office activities. The occupant's clothing apparel consisted of pants, shoes and a long-sleeved shirt. The ensemble was assumed to be tight-fitting since the effect of clothing form is not the direct interest of this work. The occupant was considered to breathe from his mouth. The breathing cycle was assumed to consist of a 3 s exhalation period and a 3 s inhalation period, varying according to a sinusoidal pattern [82]. The pulmonary ventilation rate was equal to 8.4 l/min with a respiration frequency of 10 cycles per minute corresponding to light physical activity level [83]. This corresponds to 0.84 liters per breathing cycle corresponding to instantaneous ventilation of 0.28 l/s. According to the experimental measurements of Xu et al. [39], the exhalation breath

temperature from the mouth ranged between 32°C and 36°C. An average exhalation

temperature of 34°C was selected in this work. Note that the exhalation flow has no

significant effect on the flow field. In fact, Xu et al. [39] reported that at a horizontal

distance of 3 cm from the mouth, the exhaled air velocities were equal to 0.4 m/s and

temperatures dropped to merely 24–26°C, leading to a negligible density difference

between the exhaled air and the surrounding air.

The occupant's workspace was conditioned by any of these three PV ATDs: CMP, VDG and RMP, since they provide the highest breathable air quality to the occupant's breathing zone (BZ) (Figure 19) [78]. Moreover, they are characterized by different directions (CMP: Horizontal, VDG: inclined upwards and RMP: inclined downwards) allowing to investigate distinct scenarios with different flow characteristics. All PV devices were served by their own AHU and ventilation rates varied from 5 to 10 l/s according to recommended guidelines [84, 85]. At these ventilation rates, smaller ATD outlet diameters can achieve better results [25]. The CMP and RMP had a circular outlet of diameter 10 cm, while the VDG had a small rectangular outlet (22×2 cm^2) integrated within the desk [25]. The position of the ATDs with respect to the occupant's BZ can be seen in Figure 19. In [25], the CMP and RMP had larger diameter of 18.5 cm, since ventilation rates reached 30 l/s and bigger outlets assured low supply velocities that will not cause local discomfort. To minimize the swirl effect of the PV fans, honeycomb flow straighteners were installed [49]. The occupant (100 W), lighting (100 W), laptop (50 W) and walls (62 W) contributed to the load to be removed from the office. The total air supply into the room was 43 l/s (generating velocities ranging from 0.06 to 0.1 m/s [67]) distributed between the PV and the MV system. Two representative PV flow rates were chosen to include the occupant's individual PV flow rate preference (low: 5 l/s and high: 10 l/s). For the

standalone MV system, the air was supplied at 18°C to guarantee a thermally comfortable environment at 24°C [86]. When operating the PV, the MV supply temperature was adjusted to ensure an ambient temperature of 26°C, since PV improves thermal comfort in warmer environments [49, 87]. The temperature difference between the ambient and the PV jet was fixed to 4°C to minimize temperature asymmetry between body segments [25]. The different ventilation cases are summarized in Table 10.
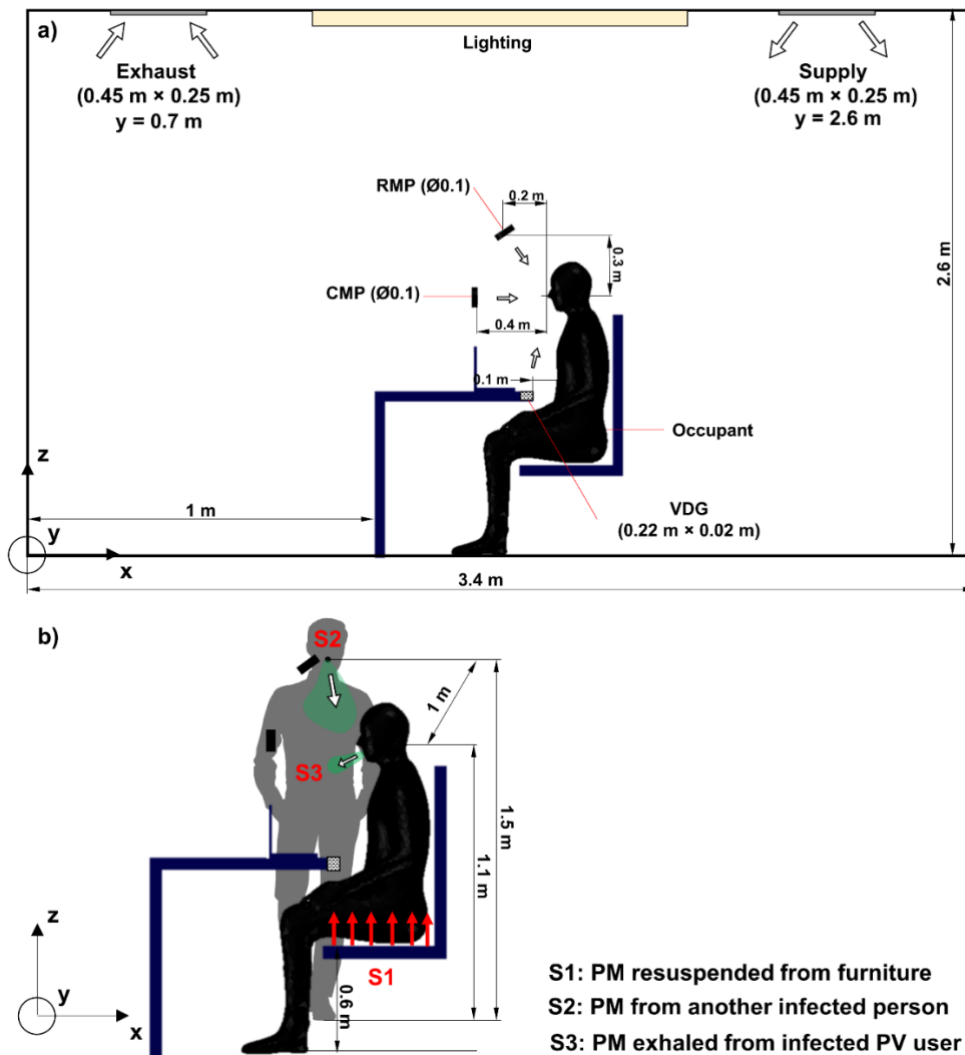
Figure 19 Schematic of: a) the office space conditioned by the MV + (CMP, VDG or RMP) and b) the different indoor PM sources

Table 10 Different ventilation cases

Ventilation cases	MV flow rate (l/s)	CMP flow rate (l/s)	VDG flow rate (l/s)	RMP flow rate (l/s)
No PV (Reference case)	43	-	-	-
CMP5	38	5	-	-
CMP10	33	10	-	-
VDG5	38	-	5	-
VDG10	33	-	10	-
RMP5	38	-	-	5
RMP10	33	-	-	10

g. Indoor PM sources

The first source denoted by **S1**, was due to PM resuspension from the occupant's chair seat cushion ($z = 0.5$ m). A seated occupant can trigger particles to resuspend from the floor due to his feet motion or from office furniture due to body motion (shift in body posture, fidgeting) [88, 89]. **S1** was chosen as it is closer to the occupant and can be easily entrained by the thermal plume (Figure 19 Schematic of: a) the office space conditioned by the MV + (CMP, VDG or RMP) and b) the different indoor PM sources). The particle diameter range of 1-10 µm (PM_{10}) was considered for **S1** as it is prevalent for resuspended particles indoors [67, 90]. The range of particles was divided into six size bins: 1-2 µm, 2-3 µm, 3-4 µm, 4-5 µm, 5-7.5 µm and 7.5-10 µm. The emission rates (kg/s) (Table 11) were identical to the ones considered in [67] and were assumed to be constant within each bin. They increased with coarser particle diameters due to higher resuspension rates [89].

The second source **S2** was considered to result from an infected occupant inside the room, standing midway between the PV and the seated occupant at a y-distance of 1 m ($z = 1.5$ m) (Figure 19 Schematic of: a) the office space conditioned by the MV + (CMP, VDG or RMP) and b) the different indoor PM sources). The standing occupant was considered to exhale particles in the positive *y*-direction (towards the seated occupant) (Figure 19 Schematic of: a) the office space conditioned by the MV + (CMP, VDG or RMP) and b) the different indoor PM sources). Emitted particles were considered to be emitted at the peak velocity of the exhaled flow of 1.46 m/s. **S2** was considered as a particle source only. In other words, the actual presence of the standing person and associated breathing function were not modeled. The particles emitted by **S2** can migrate towards the workstation and can be entrained by the PV jet. The third source **S3** was due to the breathing activities of an infected PV user (Figure 19 Schematic of: a) the office space conditioned by the MV + (CMP, VDG or RMP) and b) the different indoor PM sources). Exhaled particles are emitted in the negative x-direction c and followed the time-dependent velocity profile of exhaled air, which increases from zero to a peak of 1.46 m/s and decreases to zero again. Once emitted, they are directly affected by the PV jet momentum. **S2** and **S3** emitted particles in the diameter range 0.3-5 µm (PM_5). The range of particles were divided into six size bins: 0.3-0.5 µm, 0.5-1 µm, 1-2 µm, 2-3 µm, 3-4 µm and 4-5 µm. This is based on the work of Fabian et al. [91], who conducted experimental work to estimate the particle size distribution from infected breathing patients. The emission rates were taken as input into the CFD model from ref. [91] (Table 11). They increased with larger particles. Note that each source generated particles of density $\rho_p = 912$ kg/m^3 [48]

Table 11 Size-resolved particle emissions from each PM source

Particle diameter, d_p (µm)	**S1** Emission rate (kg/s)	**S2**, **S3** Emission rate (kg/s)
0.3-0.5	-	3.04×10^{-14}
0.5-1	-	1.43×10^{-13}
1-2	3×10^{-7}	1.04×10^{-12}
2-3	4×10^{-7}	3.66×10^{-12}
3-4	5×10^{-7}	7.40×10^{-12}
4-5	5.5×10^{-7}	1.12×10^{-11}
5-7.5	6×10^{-7}	-
7.5-10	7.5×10^{-7}	-

2. *CFD modeling*

This section will present the CFD model configuration, followed by the assessment indices for direct occupant exposure (i.e. inhalation intake fraction *iF*) and clothing contamination (i.e. deposition fraction index *DFr*). The overall IAQ of the office will be also assessed by measuring room average (RA) (µg/m^3) levels for each case. They will be used to evaluate and compare the performance of different PV ATDs in the presence of **S1**, **S2** and **S3**. The experimental methodology used for validation is presented next.

The flow field in the room involved complex physics due to the MV+PV system, the seated occupant constituting a heat source and the breathing function. To solve for the velocity, pressure, temperature and PM behavior, 3D CFD modeling was

adopted and the commercial software ANSYS Fluent v17.2 was used [40]. The occupant was represented by a computational thermal manikin acquired from CGtrader library for 3D models [92]. The manikin had a realistic surface area of 1.8 m^2. Note that the clothing ensemble here was modeled as a smooth surface and was part of the manikin geometry itself. This is since its surface roughness with the current PV airflow would not cause any shift in the boundary layer and would not affect PM deposition [93]. Since PM sources were considered, the CFD model was coupled with a DPM model that can predict particle trajectories in the domain (Figure 19 Schematic of: a) the office space conditioned by the MV + (CMP, VDG or RMP) and b) the different indoor PM sources).

To obtain an accurate solution, an appropriate mesh was implemented for the space (Figure 20). An unstructured grid with tetrahedral shaped elements was adopted. Face sizing of 2 cm and 4 cm were set for the MV diffusers and walls respectively. Face sizing of 1.5 cm was adopted for the manikin, CMP, VDG and RMP outlets, while face sizing of 5 mm and 1 cm were adopted at the nostrils and mouth respectively. Spheres of influence having an element size of 1.5 cm were created between each PV path and the BZ. Inflation layers were created around the manikin to solve for the thermal boundary layer, as this region affects PM deposition on clothes. The inflation was such that the dimensionless wall distance y^+ of the first grid point was approximately equal to 1 [87]. The generated grid had a maximum skewness of 0.89 and the final grid ensured a mesh independent solution with a maximum relative error of less than 5%. The relative error was defined based on the difference of average velocities between two consecutive meshes, in the manikin midplane ($y = 1.7$ m). The different mesh cases can be seen in Table 12.

Table 12 Grid independence test for five different mesh cases.

Face sizing Manikin/walls (cm)	Number of elements				Relative error (%)			
	No PV	CMP	VDG	RMP	No PV	CMP	VDG	RMP
Mesh 1: 2/10	536,616	601,703	629,773	616,578	-	-	-	-
Mesh 2: 2/8	607,908	681,643	713,220	699,069	21.5%	24.1%	22.5 %	25.0 %
Mesh 3: 1.5/7	801,948	904,036	940,800	919,828	14.5%	15.3%	17.4 %	16.5 %
Mesh 4: 1.5/5	1,063,479	1,192,503	1,247,746	1,219,929	6.7%	7.5%	6.5%	6.8%
Mesh 5: 1.5/4	1,396,216	1,565,582	1,638,107	1,601,576	4.0%	4.1%	4.5%	4.3%
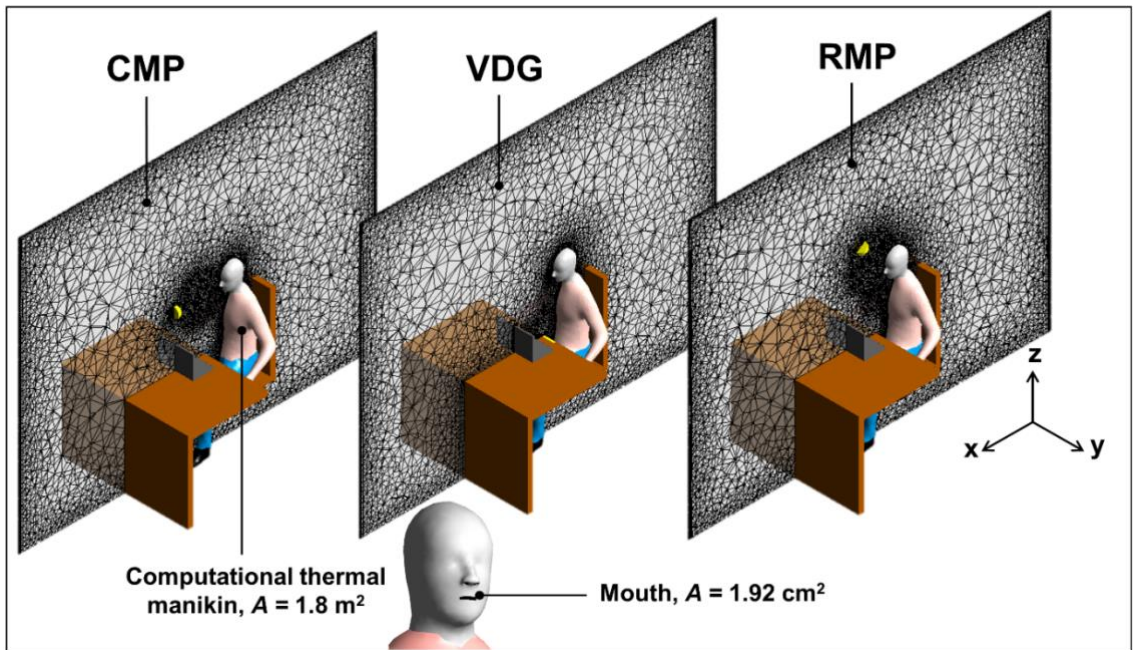
Figure 20 Illustration of the grids adopted for the different ventilation cases

a. Airflow modeling

Accurate prediction of the airflow is essential for robust tracking of particle movement. As a compromise between computational cost and accuracy, the RANS models were chosen. The Reynolds stress model (RSM) with linear pressure strain and enhanced wall functions was used. This model considers turbulence to be anisotropic near the wall, unlike the two equation RANS models which can lead to over prediction in particle deposition [94]. Hence, the RSM was chosen to model turbulence in this work due to its accuracy and reliability in predicting particle behavior, most specifically deposition.

To account for buoyancy driven flows, the Boussinesq approximation was used [95]. The momentum, energy, k, ε equations were discretized using the second order upwind scheme. As for pressure, the "PRESTO!" scheme was used since it accounts for pressure gradients at the boundaries. Due to the presence of time-dependence of the

human breathing, the solver was set to transient with the storage term discretized using a second order time stepping scheme with a time step δt of 0.05 s (< period of breathing cycle). This guaranteed capturing the smallest of transient changes in the flow without increasing computational cost. The pressure-velocity were coupled using the "PISO" algorithm-adequate for transient applications [40]. For a converged solution, several criteria were applied. The scaled residuals were lower than 10^{-8} for the energy equation and lower than 10^{-6} for the rest of the variables. Moreover, the net heat flux was 1% less than the total heat gained and mass balance was ensured in the space [96]. The CFD modeling methods are summarized in Table 13.

b. Particle tracking and intake fraction/deposition assessment

The CFD model was coupled with the unsteady DPM model in Fluent [40] to solve for particle behavior. Once the flow field in the space reached periodic conditions, **S1**, **S2** and **S3** were introduced into the space separately, to investigate the effect of source location. The DPM model tracks the particles using the Lagrangian approach by solving Newton's 2nd law on the particle. To guarantee the accuracy of the DPM model calculations, a higher order Runge-Kutta tracking scheme was used with an accuracy control having a tolerance of 10^{-5} and maximum time step refinements of 20. Maximum particle time steps of 10^6 were assigned with a step length factor of 5. The forces on the particles assigned in the DPM model were: Drag's law with spherical particles assumption, Saffman lift forces, pressure gradient forces and gravitational settling effects. Secondary forces such as Brownian forces and thermophoretic forces were not selected since they apply to submicron particles (< 0.1 μm) and large temperature gradients in the space. To predict turbulent particle dispersion, the discrete random walk

(DRW) model was used. The latter tracks particles by considering the interaction between particles and eddies.

To assess the effect of CMP, VDG and RMP on direct exposure, the inhalation intake fraction index seen in equation (9) was used [97]. It is defined as the ratio of the total mass inhaled over mass released into the space. According to equation (1), it is assumed that the emission of particles ER (kg/s) (Table 11) begins at time $t = 0$ s and spans continuously over a finite duration $\Delta t = 10$ min for **S1**, **S2**. As for **S3**, particles were generated over 10 minutes of breathing during exhalation ($\Delta t = 5$ min). In equation (1), exposure begins as soon as concentrations at the BZ rise above background level at a time t and finish when they decay to background values after a time T_e. The exposure time T_e differs depending on the ventilation case.

$$iF = \frac{M_{inhaled}}{M_{released}} = \frac{\int_t^{T_e} Q_{b,inh}(t) C_{BZ,inh}(t) dt}{ER\Delta t} \qquad (9)$$

The intake fraction is evaluated during inhalation having a rate of $Q_{b,inh}(t)$ (m³/s). The parameter $C_{BZ,inh}(t)$ (kg/m³) represents the transient particle mass concentration inhaled at the BZ, defined as a spherical control volume having a diameter of 2 cm and situated at a distance of 2.5 cm way from the mouth. $C_{BZ,inh}(t)$ follows a pre-defined trend. At a time t after the emissions event begins, $C_{BZ,inh}$ starts to increase and keeps increasing during Δt until reaching a peak value. After that, $C_{BZ,inh}$ decays to reach background values.

The DPM model tracks particles and terminates tracking when particles reach a boundary: the occupant's clothed segments (torso, arms, thighs, calves and feet). Deposition was monitored from the beginning of emissions at $t = 0$ s until particles no

longer deposit on the clothes. It was quantified using the cumulative deposited fraction index DFr seen in equation (10):

$$DFr = \frac{Number\ of\ particles\ deposited\ on\ the\ clothing}{Number\ of\ particles\ released\ at\ the\ source} \qquad (10)$$

This index is the ratio of the number of particles deposited on the clothed body over the number of particles initially released. To have more detailed information on deposition location, DFr was evaluated for the upper (torso and arms) and lower body (thighs, calves and feet). To grantee statistical accuracy, the number of particle trajectories for the PM sources was gradually increased from 10,000 to 200,000 to produce a convergent statistical sample with maximum relative error on DFr and iF less than 5% and compromise between computational cost and accuracy [96].

To assess the particle mass remainder in the space and further explain the fate of particles, the room average (RA) levels ($\mu g/m^3$) were measured at the exhaust [73]. Since, they follow a similar trend as $C_{BZ,inh}$, they were evaluated at their peak value.

c. CFD/DPM boundary conditions

A physical solution was determined by the proper assignment of the boundary conditions in the space. Both the MV and PV ATDs supply diffusers were set as velocity inlets having constant velocities, specified airflow temperatures, turbulence intensities (5%) and hydraulic diameters of 0.24 m and 0.01 m respectively. The exhaust was assigned as a pressure outlet with zero-gauge pressure, turbulence intensity (5%) and hydraulic diameter (0.36 m). Surfaces such as walls (62 W), ceiling lighting (100 W), and thermal manikin (100 W), laptop (50 W) were assigned as walls generating a heat flux adding to the room load. The different boundary conditions

(velocity, heat flux, turbulence intensity, temperature) were measured experimentally (instruments listed in Table 14) and used as input into the simulations.

The DPM model defines injection velocities independently from emission rates. The injection velocities should be adequately selected for each source: PM_{10} from **S1** were injected from the chair seat cushion using a surface DPM injection (Figure 19 Schematic of: a) the office space conditioned by the MV + (CMP, VDG or RMP) and b) the different indoor PM sources). They were injected at a minimal velocity of 0.15 m/s similar to velocities found in the thermal plume [98]. As for **S2**, PM_5 were injected using a cone injection having a base diameter of 1.5 cm equal to that of a circular mouth (1.92 cm^2)[82]. The injection velocity was equal to that of the exhaled air velocity profile. **S3** was injected similarly to **S2** at the seated occupant's mouth level during exhalation. The mean particle diameter in each size bin was injected at a time step of 0.005 s [99].

As for the DPM model boundary conditions, the walls, ceiling, manikin clothed and unclothed segments (head, chest, abdomen, thighs, calves, feet, back, arms, hands), floor, furniture and laptop were set as 'trap' boundary conditions. This means that particles that reach those boundaries get deposited and are no longer tracked by the DPM model. The exhaust was set as an 'escape' boundary condition to mean that particles reaching this boundary exit the domain and are also; no longer tracked by the DPM model. Other boundaries (MV and PV ATDs inlets) are set as 'reflect' so that the DPM keeps tracking their trajectories in the space. The CFD/DPM model boundary conditions were also summarized in Table 13.

Table 13 Summary of the CFD modeling methods and boundary conditions

Simulation solver	Transient
Turbulence model	RSM with linear pressure strain and enhanced wall functions
Pressure discretization scheme	PRESTO!
Momentum, energy, turbulence discretization scheme	Second order upwind
Pressure – velocity coupling	PISO algorithm
Convergence criteria	Continuity, momentum, turbulence residuals $< 10^{-5}$, energy residuals $< 10^{-6}$
DPM model	Unsteady particle tracking, one-way coupling, Runge-Kutta tracking scheme, tolerance of 10^{-5}, max. refinements of 20
CFD/DPM Boundary conditions	
MV, PV outlets	Velocity inlet, constant velocity, inlet temperature, turbulence intensity and hydraulic diameter, DPM: "Reflect"
Exhaust	Pressure outlet with zero-gauge pressure, turbulence intensity and hydraulic diameter, DPM: "Escape"
Nostrils	Velocity inlets, transient velocity (UDF), constant inlet temperature, turbulence intensity and hydraulic diameter, DPM: "Reflect"

Manikin, walls, lighting, laptop	Walls with constant heat flux input, DPM: "Trap"

3. Experimental methodology

To validate the numerical predictions, experiments were conducted in a climatic chamber equipped with the MV system and one PV ATD (CMP). **S1**, **S2** and **S3** were introduced to assess the effect of source location. The transient PM normalized concentrations $C^*(t)$ (normalized over the concentration at the source) were monitored near the clothed segments. The measured $C^*(t)$ were compared with CFD-predicted values. Experiments were conducted for the cases of No PV, CMP5 and CMP10 (

Table 10), for generation sources **S1**, **S2** and **S3**, resulting in 9 distinct

experiments. One ATD was chosen since the CMP velocities at the occupant location

are fairly common for the three ATDs as seen in section 3.2.

The chamber was a well-sealed chamber, with similar dimensions to the CFD

model (Figure 19 Schematic of: a) the office space conditioned by the MV + (CMP,

VDG or RMP) and b) the different indoor PM sources). It was thermally insulated (U-

value = 0.3 W/m^2.K,Table 13) but allowed for some heat dissipation (1.75 W/m^2)

contributing to the room load. It was occupied by the breathing thermal manikin

"Newton" manufactured by Northwestern measured technology. It was controlled with

"ThermDAC" software offering several control possibilities. The cycle, volume and

frequency of human breathing were replicated using Newton's breathing system (Figure

20). The exhaled air was not heated as previously explained [36]. The design and

operation of the MV, CMP for the different experimental cases was similar to that

described in section 2. Velocity and temperature inputs into the CFD model boundaries

were measured using SWEMA03 anemometers having a temperature measurement accuracy of ±0.1 °C and velocity measurements ranging between 0.05 m/s and 3 m/s with an accuracy of ±4%. As for the heat flux from the walls, it was measured using an OMEGA heat flux meter OS-652 model characterized by an accuracy of ±1% for heat flux measurement at ambient temperature range of -18 °C to 43 °C and a response time of 1 s. Note that flow field measurements in the space and CMP jet in the same climatic chamber were previously validated in [67, 95]. The list of measuring equipment used and their specifications are summarized in Table 14.

Figure 21 shows the point locations where **S1**, **S2** and **S3** were generated, as was described in Figure 19**,** using an aerosol particle generator (TSI model 3475), which generated highly monodisperse particles having a geometrical standard deviation < 1.15. The generated particles have a diameter of 1.5 μm (found in **S1**, **S2** and **S3**) and a density of 912 kg/m^3. The TSI particle generator emitted the particles at a velocity of 1.3 m/s and a rate of 4 l/min. The tubes were made from silicon and their length was reduced to minimize deposition inside the tube. It was operated for a duration Δt of 10 minutes for **S1** and **S2** and 5 min for **S3**. Note that for the validation only, the DPM injection properties and rates were modified to mimic the experimental injections. The real-time evolution of PM mass concentrations $C^*(t)$ was measured at 1-minute intervals using an optical particle sizer (TSI model 3330) at a rate of 0.017 L/s having a relative error of 5% (Figure 21). Silicon Tubes of small diameter and minimal length were connected to two measurement locations: **M1** and **M2**. **M1** was located on the lower body level, 2 cm above the thigh segment and **M2** was located on the upper body level, 2 cm in front of the chest segment. Their exact locations are shown in Figure 21. Measurements of $C^*(t)$ were conducted for a duration of 70 min after the emissions

events were completed to follow the decay period. CFD model predictions of particle mass concentrations were monitored for the same duration at the same locations (**M1** and **M2**), normalized with respect to the concentration at the source and subsequently compared to the experimental value of $C^*(t)$.
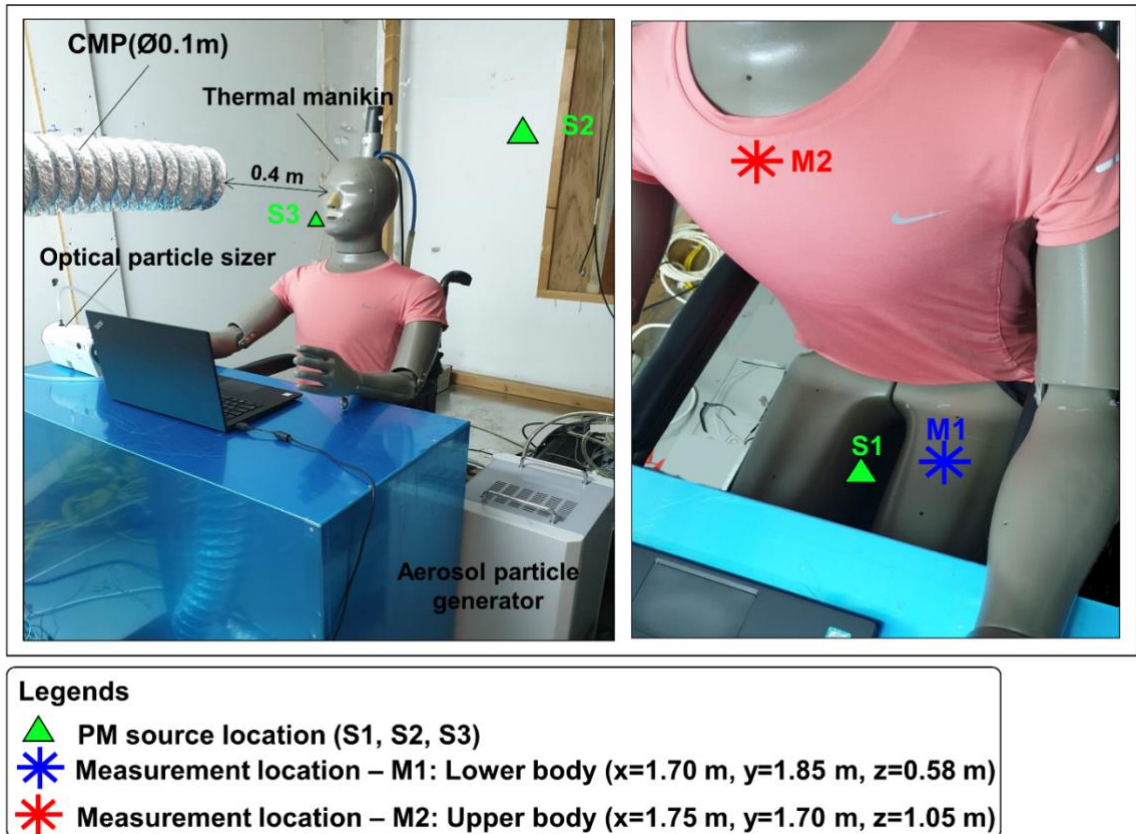
Figure 21 The experimental setup, including the three PM sources, and measurement locations

Table 14 Different measuring instruments used in the experiments and their specs

Instrument used	Specifications

SWEMA03 hot wire anemometer	Temperature measurement 10-40°C, with accuracy of ±0.1 °C and velocity measurements 0.05-3 m/s with an accuracy of ±4%, response time < 0.2 seconds, sampling frequency: Max 100 Hz
TSI hot wire anemometry	Velocity measurement from cm/s to 100 m/s, turbulence intensity (%), high frequency response (100 kHz), accuracy ±3%.
OMEGA heat flux meter OS-652 model	Heat flux measurement characterized at ambient temperature range of -18 °C to 43 °C characterized by an accuracy of ±1% and a response time of 1 s
Aerosol particle generator (TSI model 3475)	Generates highly monodisperse particles having a geometrical standard deviation < 1.15, density of 912 kg/m^3, at a velocity of 1.3 m/s and a rate of 4 l/min
Optical particle sizer (TSI model 3330)	Measures the real-time evolution of particle mass/number concentrations from 0.3-10 μm, at a rate of 0.017 l/s and accuracy of 5%

a. Experimental protocol

The experiment was initiated by turning on the MV in the room as well as the lights and the thermal manikin. Before the injection start, the room air was filtered from particles using a MI air purifier, which filters over 99% of particles sized 0.3 μm and larger using HEPA filters [100]. After 5 hours of running the experiment, the flow field in the room reached quasi steady state conditions. The optical sizer was turned on to

measure background concentration initially for a duration of 5 minutes. After that, the particle generator was turned on for 10 minutes and the optical sizer measured the real-time PM concentrations at **M1** and **M2** (Figure 21). Since the sizer measures at one location, each experiment was conducted twice: once to measure at **M1** and the second time to measure at **M2**. To avoid the effect of particle resuspension, the floor and room furniture were cleaned prior to experiments. Between each experimental run, the room air was filtered using the MI air purifier. Each experiment was repeated 5 times to ensure repeatability of the findings. The predicted PM concentrations by the DPM model for validation were incremented with the background PM mass concentration. This is since no initial concentration was present in the CFD model as is case in reality.

C. Results and discussions

The validation results of the CFD model will be presented for the case of No PV, CMP5 and CMP10 for **S1**, **S2** and **S3**. This will be followed by the results of *iF (‰)*, *DFr* and also room average (RA) levels (μg/m^3) for the different ventilation cases.

1. Experimental validation

Figure 22, Figure 23 and Figure 24 present the real-time evolution of PM normalized mass concentration $C^*(t)$ for **S1**, **S2** and **S3**, measured and predicted at **M1** and **M2**. For all three sources and ventilation cases (No PV, CMP5 and CMP10). According to these figures, both experimental measurements and numerical predictions were able to capture the increasing/decreasing trend of $C^*(t)$ with good agreement between measured and predicted and maximum relative errors ranging between 4.2% and 15.4%. The experimental error bars represent the standard deviation from the mean

of the experimental findings due to the repetition of measurements and due to the precision of the optical particle sizer.

For **S1** (Figure 22), $C^*(t)$ reached its maximum peak value (C_p^*) for the case of No PV (Figure 22**(a)**). C_p^* for **M1** and **M2** decreased by an average of 31% and 7% when operating CMP5 (0.64 m/s) (Figure 22**(b)**), and CMP10 (1.27 m/s) (Figure 22**(c)**), respectively. The decrease was more apparent near upper body segments directly influenced by the CMP jet. CMP5 dilutes particle concentrations reducing C_p^* (Figure 22**(b)**). However, at CMP10, the jet pushed particles transported by the plume from the chair level, towards the upper body, concentrating them in that area. This explains the increase in $C^*(t)$ compared to CMP5. The variation of C_p^* between ventilation cases can be indicative of deposition rates on the body. In that aspect, it is expected that operating a CMP decreases deposition on clothing due to **S1**, with CMP5 outperforming CMP10. The decay was longest for the case of No PV (60 min, Figure 22**(a)**), CMP5 (50 min, Figure 22**(b)**) and CMP10 (45 min, Figure 22**(c)**). This is since higher velocities have a faster effect on particles.
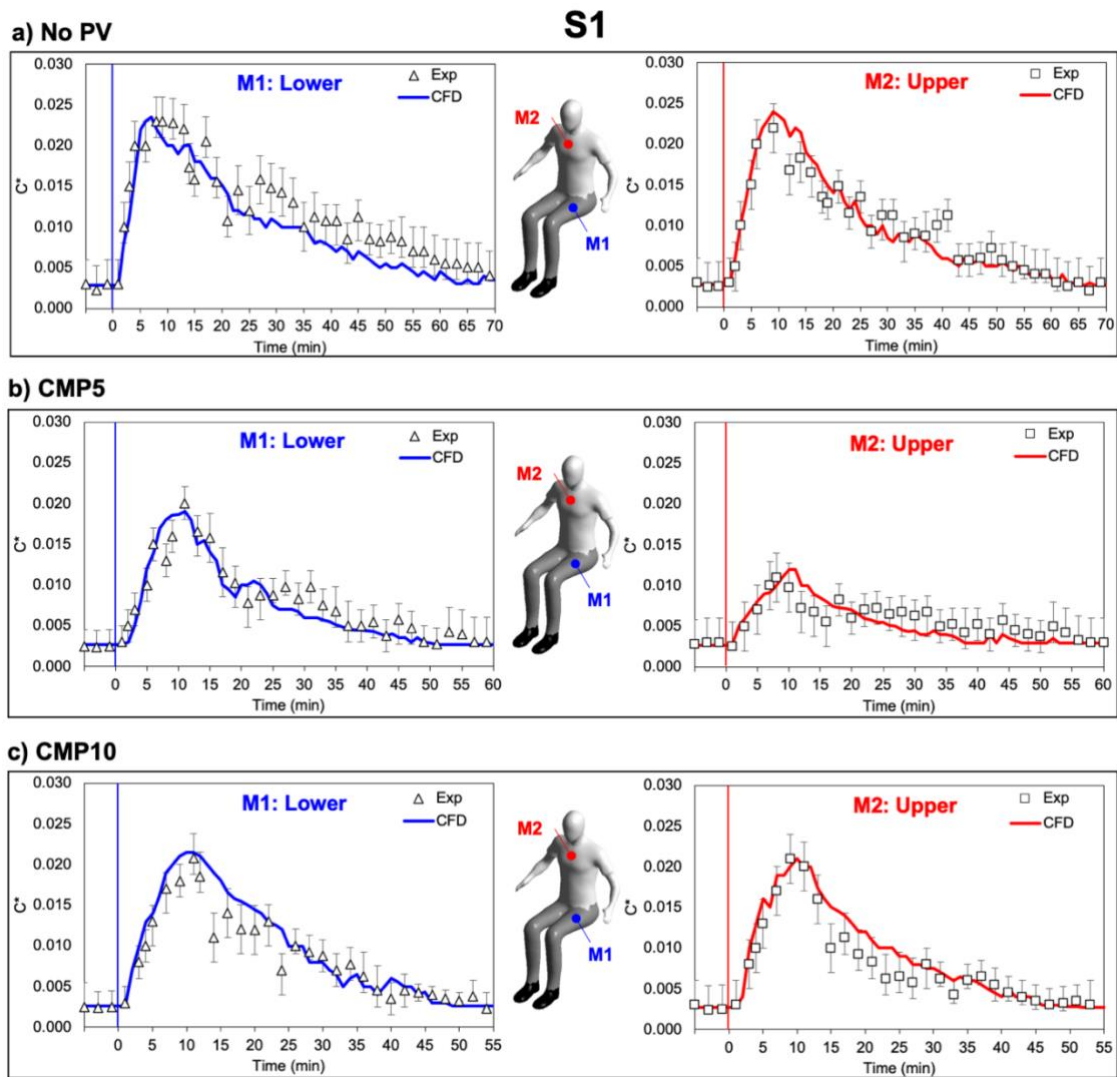
Figure 22 Comparison of measured vs predicted real-time PM normalized concentration C*(t) at **M1** and **M2** for **S1**

For **S2** (Figure 23), C_p^* was at its highest for the case of No PV (Figure 23**(a)**). It decreased for **M1** and **M2** by an average of 13% and 18% when operating CMP5 (0.64 m/s) (Figure 23**(b)**), and CMP10 (1.27 m/s) (Figure 23**(c)**), respectively. The decrease was also more distinct near the upper body. CMP5 diluted particle concentrations reducing C_p^* (Figure 23**(b)**). This dilution effect increased with higher flow rates since particles were not present in the direct vicinity of the jet path as was the case for **S1**. Thus, it is expected that operating a CMP decreases deposition of

exogenous exhaled particles on clothing with CMP10 outperforming CMP5. Similarly to **S1**, the decay was the longest for the case of No PV (60 min, Figure 23**(a)**), CMP5 (49 min, Figure 23**(b)**) and CMP10 (44 min, Figure 23**(c)**).
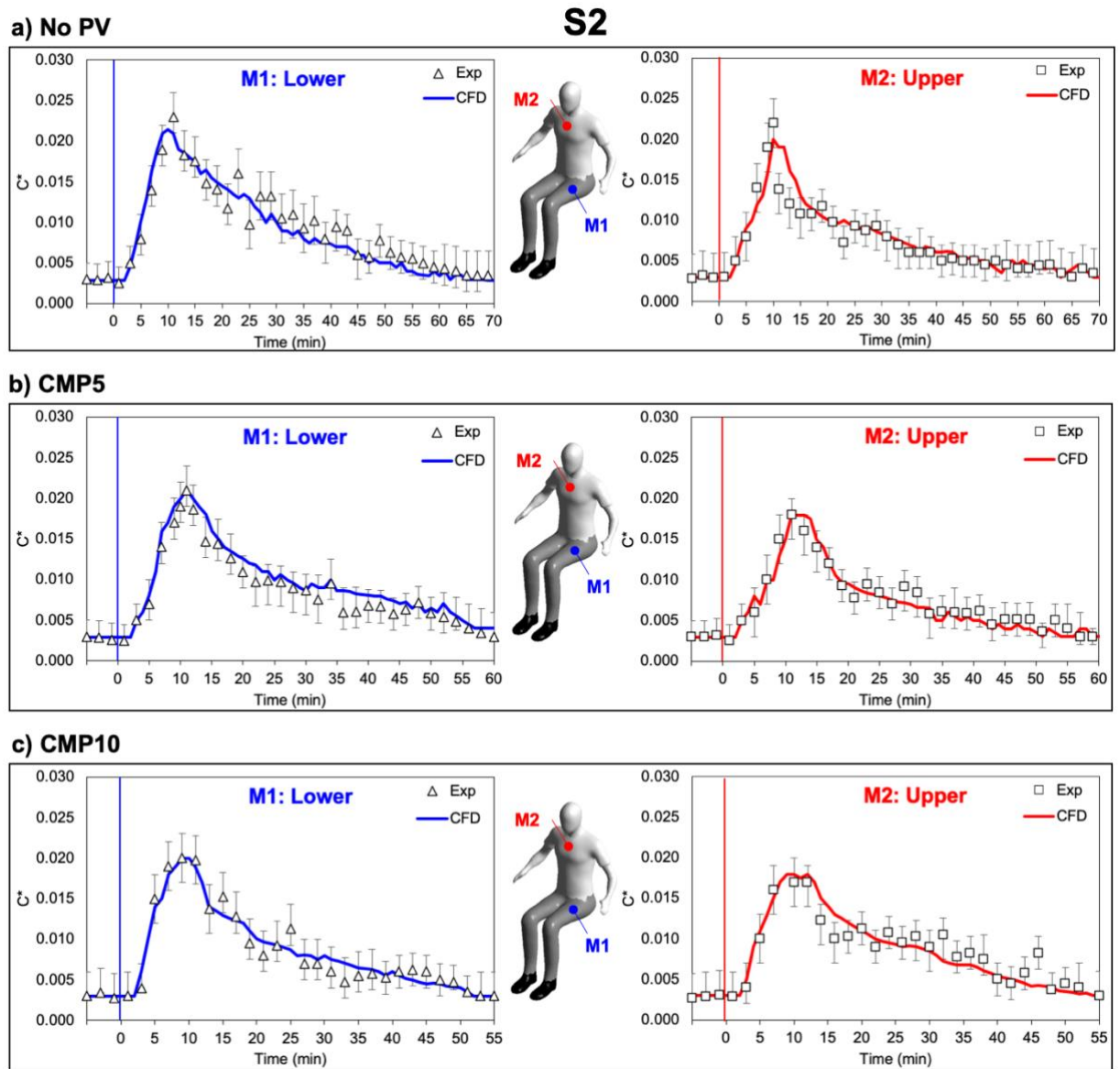
Figure 23 Comparison of measured vs predicted real-time PM normalized concentration C*(t) at **M1** and **M2** for **S2**

For **S3** (Figure 24), C_p^* was at its highest for the case of No PV (Figure 24**(a)**), decreased by an average of 17% and 13% when operating CMP5 (0.64 m/s) (Figure

24(**b**)), and CMP10 (1.27 m/s) (Figure 24(**c**)), respectively. The decrease was also more distinct near the upper body. CMP5 diluted particle concentrations reducing C_p^* (Figure 24(**b**)). However, CMP10 pushed exhaled particles down elevating their concentration near **M2**. Thus, it is expected that operating a CMP decreased deposition of endogenous exhaled particles on clothing with CMP5 outperforming CMP10. Similarly to **S1**, the decay was longest for the case of No PV (60 min, Figure 24(**a**)), CMP5 (49 min, Figure 24(**b**)) and CMP10 (44 min, Figure 24(**c**)).

To further support these claims, the decreasing slope of $C^*(t)$ was analyzed, as researchers showed that there is a proportionality between the slope and particle deposition on the surface in question [101]. The evolution of the decreasing slope with the ventilation case can be mostly observed on upper segments as they are directly in the jet path (measurement point M2). The slope was highest for the case of No PV, followed by CMP10 and CMP5. For example, for source **S1**, it was equal to 0.032 (No PV), 0.028 (CMP10) and 0.025 (CMP5) (Figure 22). This goes to show, that operating CMP can decrease deposition compared to No PV with lower flow rates (5 l/s) performing better than 10 l/s. Moreover, the decreasing slopes between lower (M1) and upper segments (M2) for the injected particle diameter of 1.5 μm, are nearly of equal magnitude [102]. Thus, the CFD model is also reliable in predicting particle deposition on clothing and its dependence on particle diameter and surface orientation.
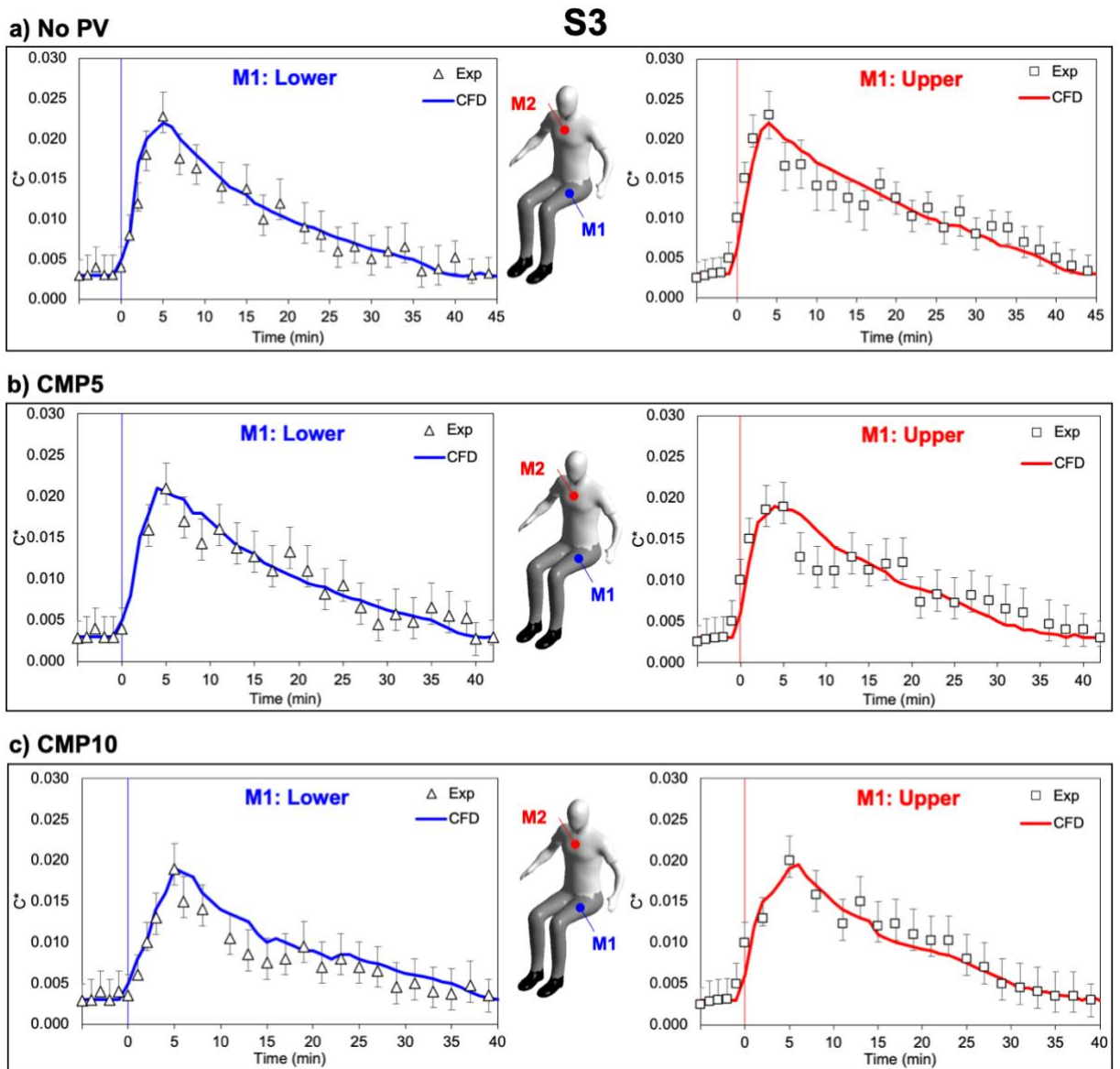
Figure 24 Comparison of measured vs predicted real-time PM normalized concentration C*(t) at the upper (chest) and lower (thighs) body for contamination source **S3**

2. *Intake and deposition fraction: Comparison of PV ATDs, impact of source location*

Figure 25 presents the results of cumulative *iF* (‰), RA ($\mu g/m^3$) and cumulative *DFr* disaggregated into upper and lower body deposition, due to **S1**, **S2** and **S3**, for the different ventilation cases compared to the reference case of No PV. Figure

26 to Figure 29 illustrate the corresponding contours of velocity and total particle mass concentration at the manikin midplane ($y = 1.7$ m) for the ventilation cases of No PV, CMP, VDG, and RMP respectively.

a. Reference case: No PV

The space was quiescent allowing for the occupant's thermal plume to develop at maximum velocities of 0.3 m/s above the head level (Figure 26) [103]. The plume was largely responsible for the transport of PM towards the BZ and their deposition on the clothing. Moreover, it transported PM to the rest of the space increasing RA levels. This is an accordance with the observations of Rim et al. [103], which stated that in spaces with incomplete mixing, the thermal plume establishment leads to airflow stratification and non-uniform concentration patterns.

Results show that significant intake fractions were recorded for the case of No PV (Figure 25**(a)**). Values were highest for **S3** since it corresponds to the fraction of re-inhaled exhaled air, which is inherently large in the absence of PV. This was followed by **S1** and **S2** since particles from **S1** were closer to the BZ and transported by the plume upwards, while **S2** was further away. This decreasing trend also applied to the rest of the ventilation cases. This was also observed in [103], where the thermal plume played a significant role in transporting contaminants from a source beneath the occupant, increasing occupant exposure to four times the background levels.

Deposition from **S1** was the highest with 6% of particles deposited equally on the upper (3%) and lower body (3%) (Figure 25**(a),** Figure 26**(a)**). This is since particles were emitted beneath the occupant and entrained by the free convective flow upwards, covering the lower and upper body segments [103]. Deposition was second highest for **S3**. 0.7% of exhaled particles deposited on the upper body since it was closer to the

mouth, while 0.4% deposited on the lower body (Figure 26(**c**)). Deposition was the

lowest from **S2**, with 0.3% and 0.1% depositing on the upper and lower body

respectively (Figure 26(**b**)). Deposition from **S2** and **S3** was due to particles migrating

towards the occupant, where they were entrained by the plume and deposited on

clothing.
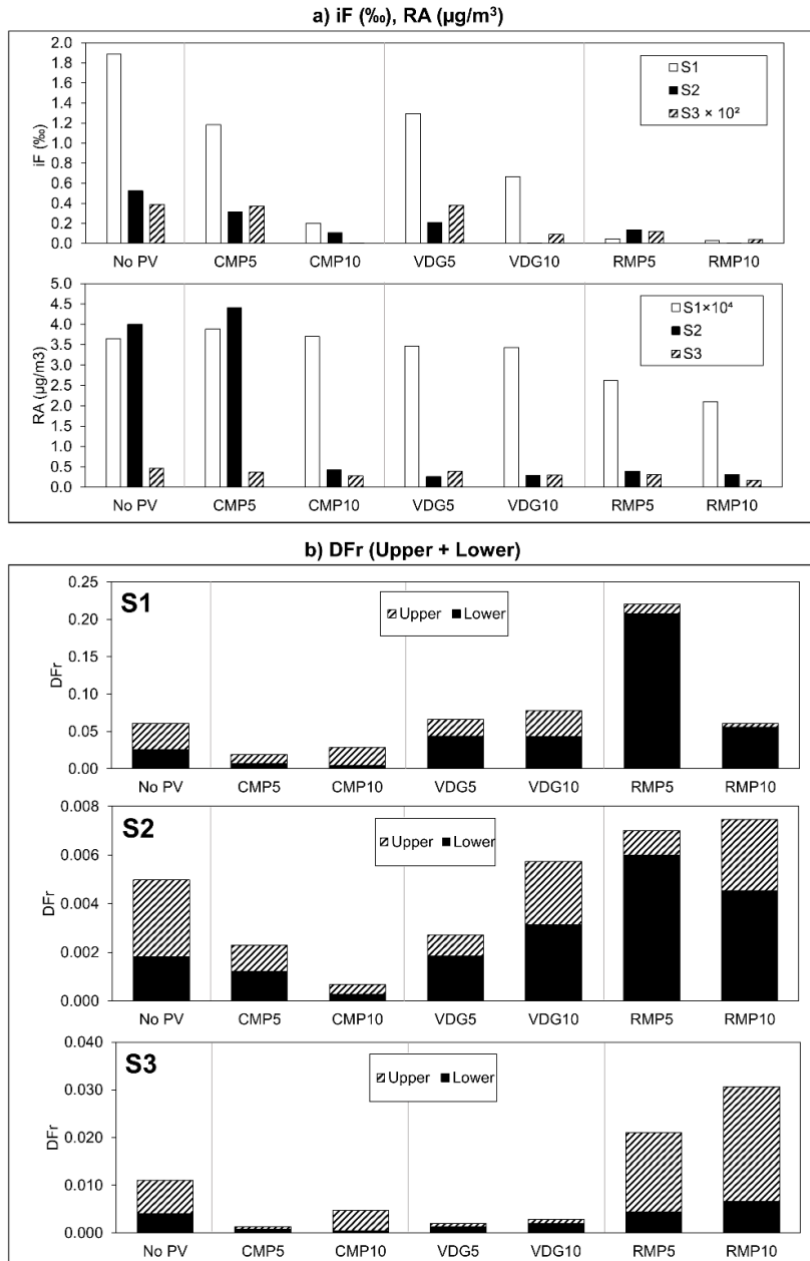
Figure 25 Illustration of: a) cumulative iF (‰), RA ($\mu g/m^3$) and b) cumulative DFr disaggregated into upper and lower body deposition due to the three PM sources **S1**, **S2** and **S3**, evaluated for the different ventilation cases

Figure 26 Contours of velocity and cumulative PM mass concentration at the manikin midplane (y = 1.7 m) and the manikin's clothed segments for the case of No PV, evaluated for: a) **S1**, b) **S2** and c) **S3** (t = 20 min)

The CMP supplies air horizontally towards the BZ. At low flow rates, the thermal plume still persists. At high flow rates, the plume deteriorates and the jet develops behind the occupant (Figure 27) as also seen in [104]. With the addition of CMP, both inhalation exposure and clothing contamination due to **S1**, **S2** and **S3** were reduced (Figure 25). The rate of decrease, was dependent on the CMP flow rate and PM source location. Compared to No PV, operating CMP5 (0.64 m/s) reduced inhalation exposure to **S1**, **S2** and **S3** by 37%, 39.4% and 4% respectively (Figure 27). The lowest reduction was noted for **S3** since the momentum of the contaminated exhaled air competed with the CMP jet momentum at the mouth level (Figure 27**, CMP5 (c)**). As for RA levels, compared to No PV, they slightly increased for **S1**, **S2** (Figure 25 **(a)**). This is since the CMP5 jet did not fully degenerate the thermal plume but rather dispersed it in the upper space levels, which increased RA by around 5 to 10% (Figure 26**(a, b)**, Figure 27 **CMP5 (a, b)**). The dispersion of contaminants emitted from lower levels due to the CMP jet at low flow rates can also be seen in [105]. As for **S3**, RA levels decreased by 21.7% compared to No PV, since the CMP jet reduced the amount of total PM_{10} transported by the plume into the rest of the space (Figure 26**(c)**, Figure 27**(c)**). CMP10 (1.27 m/s) further reduced inhalation exposure by 83%, 68.4% for **S1** and **S2**, and to negligible values for **S3** (Figure 27**, CMP10**). This is a typical outcome of integrating PV systems in offices [18]. For **S1**, RA levels reduced compared to that of No PV, due to significant additional fresh air supply from CMP10, overcoming the side effects of particle transport and dispersion due to the degenerated plume (Figure 27**, CMP10(a)**). RA levels reduced for **S2** and **S3** by 90% and 40% respectively

compared to No PV (Figure 25**(a),** Figure 27**, CMP10 (b, c)**) due to the dilution effect and since **S2** and **S3** were more localized than **S1**.

Compared to No PV, CMP5 reduced total DFr due to **S1**, **S2** and **S3** by 68%, 55% and 88% respectively (Figure 27, **CMP5**). Reduction rate was equal for both upper and body segments (Figure 25**(b)**) since CMP5 cleared particles away from all the clothing uniformly. In the case of **S1** and **S2**, they dispersed to the rest of the space, further explaining the witnessed increase in RA (Figure 27**, CMP5 (a, b)**). In the case of **S3**, exhaled particles stagnated in high concentrations in the region between the occupant and the desk. The smaller remainder dispersed in the space, explaining the reduction of RA (Figure 27**, CMP5(c)**). For CMP10, DFr decreased compared to No PV, by 53%, 87% and 57% respectively (Figure 27**, CMP5**). Deposition due to **S2** reduced further, as CMP10 kept on dispersing particles away from the body. The increase in DFr due to **S1** and **S3**, compared to CMP5, was due to a rise in PM_{10} deposition on the upper body, despite a reduction in lower body deposition (Figure 25**(b)**). Having high momentum, CMP10 resulted in a dumping effect, pushing particles (entrained by the plume from **S1** or exhaled from **S3**) downwards, where they deposit on the upper body and particularly the chest (Figure 27**, CMP10 (a, c)**)

Hence, the CMP performs well in reducing inhalation exposure and clothing contamination compared to an office equipped with standalone MV. Moreover, they can reduce RA levels. However, at high flow rates (10 l/s), the effectiveness of CMP in reducing deposition on clothing is slightly compromised compared to low flow rates (5 l/s), especially when the particle sources are in the direct path of action of the jet peripheries.
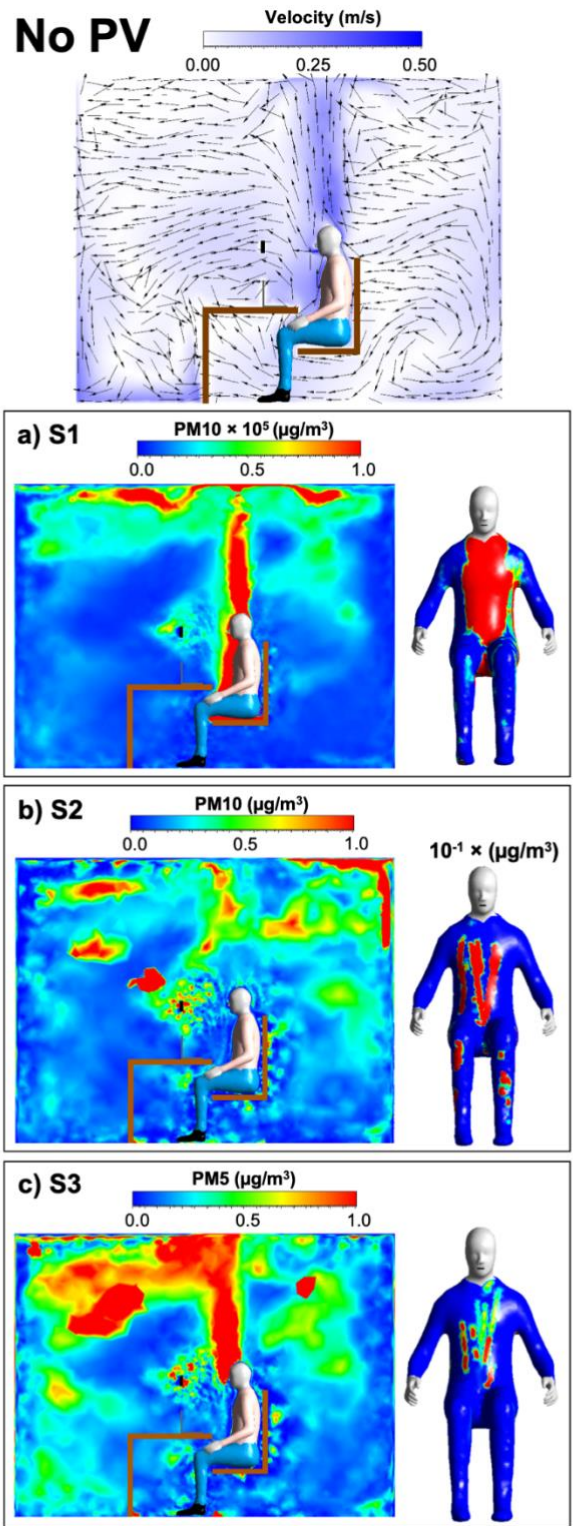
Figure 27 Contours of velocity and cumulative PM mass concentration at the manikin midplane (y = 1.7 m) and the manikin's clothed segments for the case of CMP, evaluated for: a) **S1**, b) **S2** and c) **S3** (t = 20 min)

PV ATD 2: VDG

The VDG supplied air upwards at an inclination angle of 15° towards the occupant's

BZ. Hence, the VDG interacted similarly to the thermal plume, with higher velocities

and additional fresh air (Figure 28). Cermak et al. [78] also stated that the upward

airflow of the VDG can assist the thermal plume to remove contaminants from the

occupied zone. Compared to the case of No PV, VDG5 (1.3 m/s) reduced inhalation

exposure due to **S1**, **S2** and **S3** by 32%, 60% and 4% respectively (Figure 25**(a)**). RA

due to **S1**, **S2** and **S3** decreased compared to No PV, by 6%, 94% and 18% (Figure

25**(a)**). This is since the VDG5 jet that continues its trajectory in the upper space

consists of fresh air. The results of Cermak et al. [78] also showed that the use of VDG

could reduce contaminants' concentration in the upper space level. Dilution was highest

for **S2**, followed by **S3** and **S1**. Note that for **S1** and **S3**, VDG5 concentrated particles in

specific locations in the space instead of dispersing them like the case of No PV (Figure

28, **VDG5**). At VDG10 (2.2 m/s), inhalation exposures due to **S1**, **S2** and **S3** further

reduced by 50%, 98% and 76% respectively. RA for VDG10 decreased slightly

compared to VDG5 by 9% due to additional fresh air supply.

Compared to No PV, VDG5 did not affect *DFr* for **S1**. The only difference was that

upper to lower body deposition ratios fluctuated slightly (Figure 25**(b)**). Upper body

DFr decreased while lower body *DFr* increased, since VDG5 impinged on the upper

body, consistently clearing the region from particles (Figure 28**, VDG5 (a)**). However,

similar to CMP10, VDG5 re-directed particles downwards to deposit them on lower

segments. VDG5 caused a reduction in *DFr* due to **S2** and **S3** by 46% and 82% (Figure

25**(b)**). This is in accordance with the observations of Cermak et al. [78], who noted that

VDG can concentrate contaminants emitted at low level in the lower zones near the

occupant desk. For **S2**, the reduction is noted on the upper segments (Figure 28**, VDG5 (b)**). As for **S3**, the reduction was uniform over the entire body since the exhaled air was fully diverted upwards by VDG5 (Figure 28**, VDG5 (c)**). As for VDG10, compared to No PV, *DFr* due to **S1** and **S2**, increased by 23% and 13% respectively. The increase was noticeable for both upper and lower body segments since VDG10-having a longer core region, does not impinge on the upper body as is the case for VDG5 (Figure 25**(b)**). All particles were re-directed downwards, where they deposit on both upper and lower segments (Figure 28**, VDG10 (a, b)**). The only decrease in *DFr* was due to **S3** since VDG10 blows away exhaled particles upwards quicker than VDG5 (Figure 28**, VDG10 (c)**).

Hence, the VDG performed well in reducing inhalation exposure and clothing contamination compared to an office equipped with standalone MV. Moreover, they can reduce RA levels. However, at high flow rates (10 l/s), the VDG was not effective in reducing deposition on clothing as VDG operated at 5 l/s, when the particle sources were in the direct path of action of the jet peripheries.
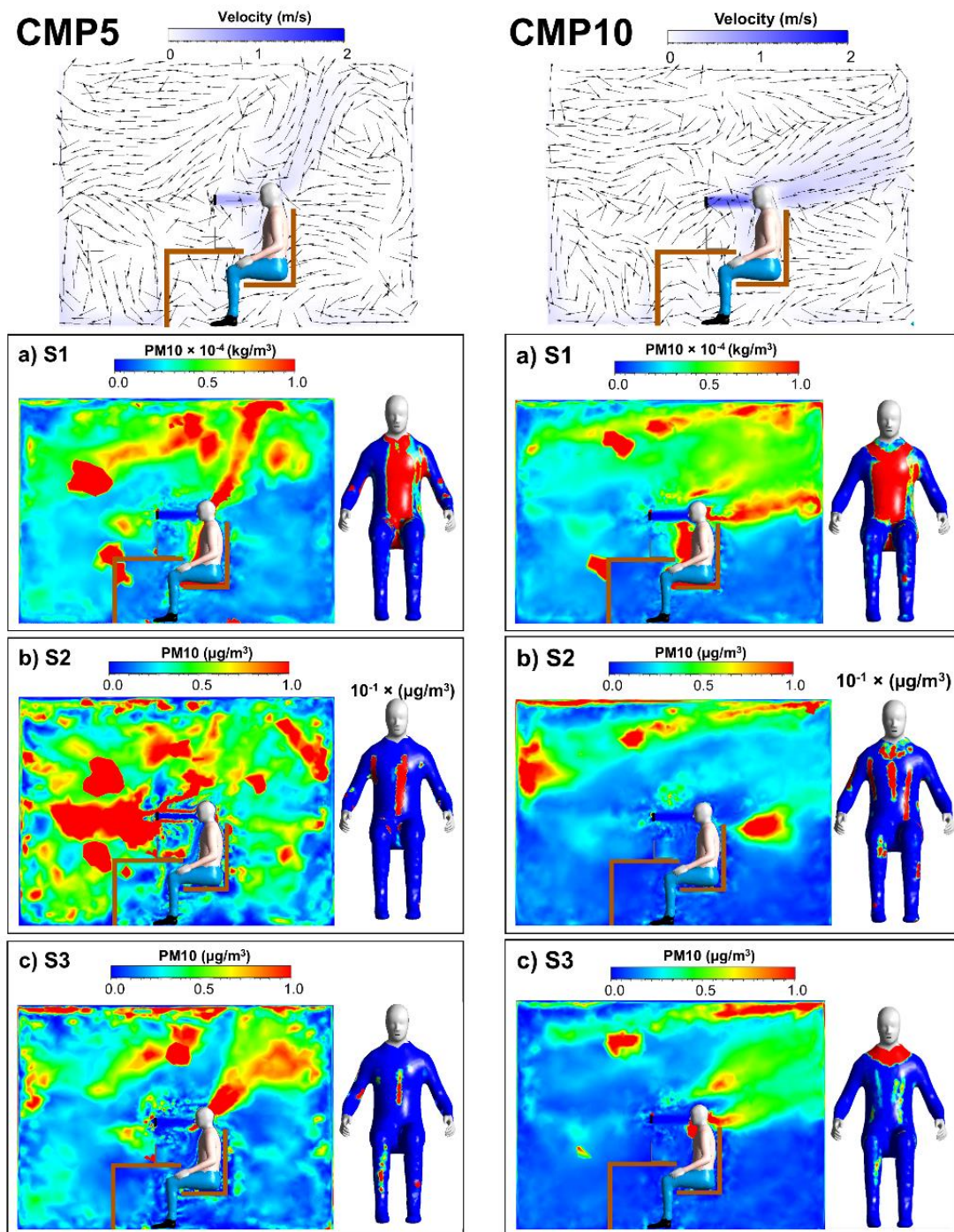
Figure 28 Contours of velocity and cumulative PM mass concentration at the manikin

midplane (y = 1.7 m) and the manikin's clothed segments for the case of VDG,

evaluated for: a) **S1**, b) **S2** and c) **S3** (t = 20 min)

c. PV ATD 3: RMP

The RMP supplies air downwards at an inclination angle of 20° towards the

occupant's BZ. After impinging, it spreads downwards covering the occupant's chest

and abdomen (Figure 29). Compared to No PV, RMP5 (0.64 m/s) reduced inhalation

exposure due to **S1**, **S2** and **S3** by 98%, 74.3% and 70% respectively (Figure 25**(a)**). RA

due to **S1**, **S2** and **S3** decreased the most compared to No PV, by 29%, 90% and 35%

respectively (Figure 25**(a)**). This is since the RMP pushes most of the particles towards

the lower volume of the space, and in some cases (**S2**) towards the room peripheries

(Figure 29**, RMP5**). At RMP10 (1.27 m/s), inhalation exposures due to **S1**, **S2** and **S3**

further reduced by 36%, 99% and 65% respectively. RA levels for RMP10 further

decreased compared to RMP5 by 20% due to **S1** and **S2** and by 40% due to **S3** since

RMP10 has stronger momentum (Figure 29**, RMP10**). This was also observed in the

study of Cermak et al. [78], where an RMP was direct at a polluting manikin. In their

case, the RMP also pushed pollutants downwards where they spread out in horizontal

layer in the lower space. This was possible due to the large temperature gradients

preventing any upward vertical air movements. This downward pushing effect was

more pronounced at higher flow rates as well. The RMP might thus result in some

disadvantageous repercussions on clothing contamination as will be explained next.

Compared to No PV, RMP5 increased *DFr* due to **S1**, **S2** and **S3** by 73%, 29%

and 45% respectively (Figure 25**(b)**). For **S1** and **S2**, the increase in deposition is mostly

on the lower body while deposition reduces for the upper body. As particles from **S1**

travel upwards or particles from **S2** migrate towards the occupant, they reach a certain

height at the lower abdomen, where RMP5 pushes them downward and deposits them

on the lower body (Figure 29**, RMP5 (a, b)**). Deposition on the upper body was reduced

since RMP5 impinges on the chest and upper abdomen and is constantly cleaning the area (Figure 29**, RMP5 (a, b)**). For **S3**, it was evident that the RMP5 pushed the exhaled particles to deposit on the upper body, and mostly notably the chest as was the case with CMP (Figure 25**(b)**, Figure 29**, RMP5 (c)**). The increase in deposition further explains why RMP caused the largest reduction in RA between the three PV ATDs. As for RMP10, *DFr* due to **S1** did not vary compared to No PV. However, the ratio between upper and lower body deposition shifted. Deposition on the lower body increased while that on the upper body decreased. RMP10 was able to impinge even on lower body segments. Hence, particles emitted from **S1**, did not get the chance to rise upwards and remained near the chair, where they eventually deposit on the thighs' peripheries and calves (Figure 29**, RMP10 (a)**). *DFr* due to **S2** and **S3** kept on increasing by 32.4% and 65% respectively. For **S2**, the increase was noted on the upper body. This is since RMP10 does not impinge on as wide of a surface as RMP5 (Figure 29**, RMP10 (b)**). This allowed particles from **S2** to deposit on the shoulders and sleeves. As for **S3**, the RMP10 pushed more exhaled particles towards, not only the chest as RMP5, but also towards the abdomen, increasing deposition there (Figure 29**, RMP10 (c)**). This further explains also the drastic reduction in RA levels for both **S2** and **S3**.

Hence, the RMP performed well in reducing inhalation exposure compared to office equipped with standalone MV and reduced RA levels. However, when it comes to clothing contamination, the RMP drastically increased it for many possible indoor sources of PM and at any operating flow rate.
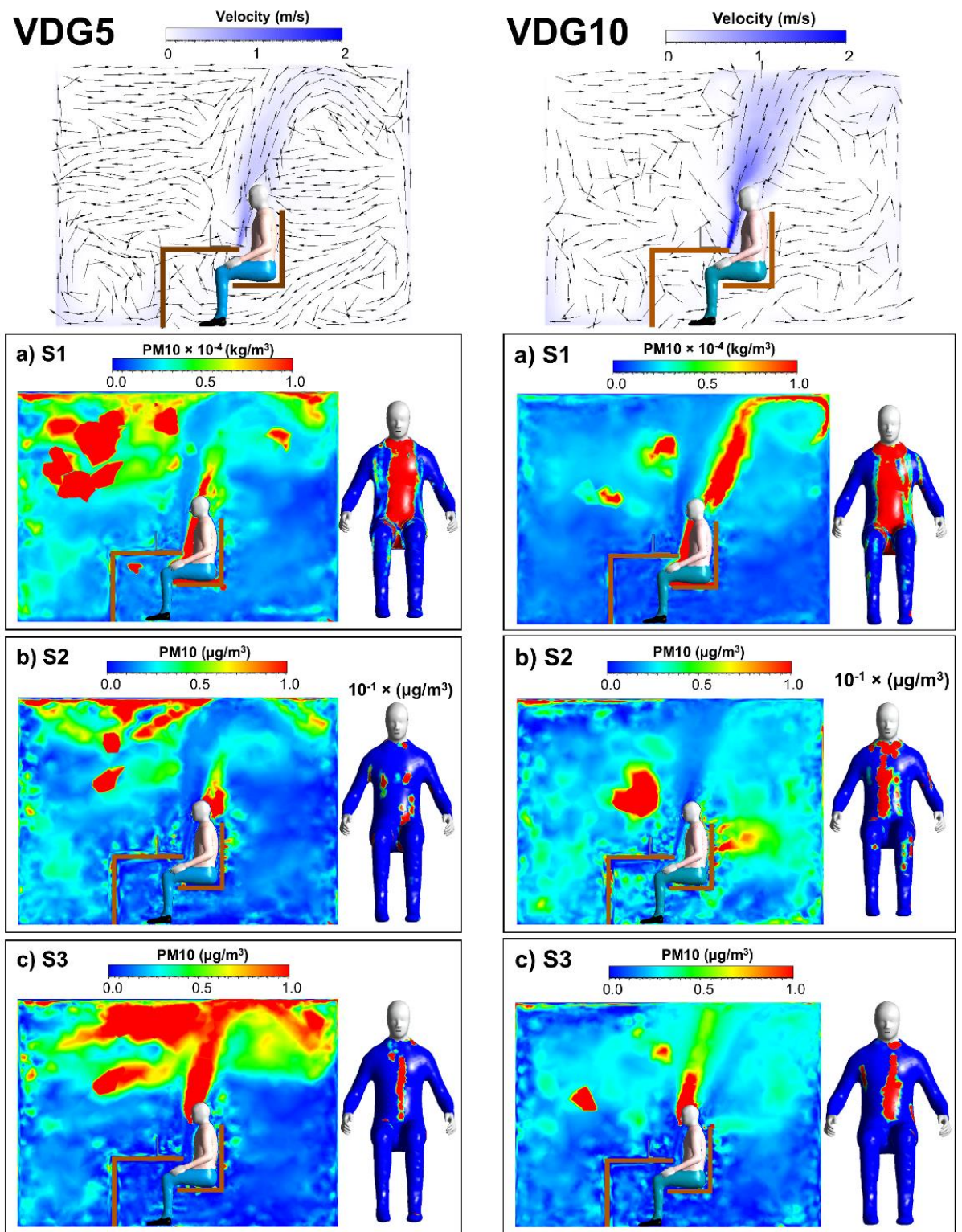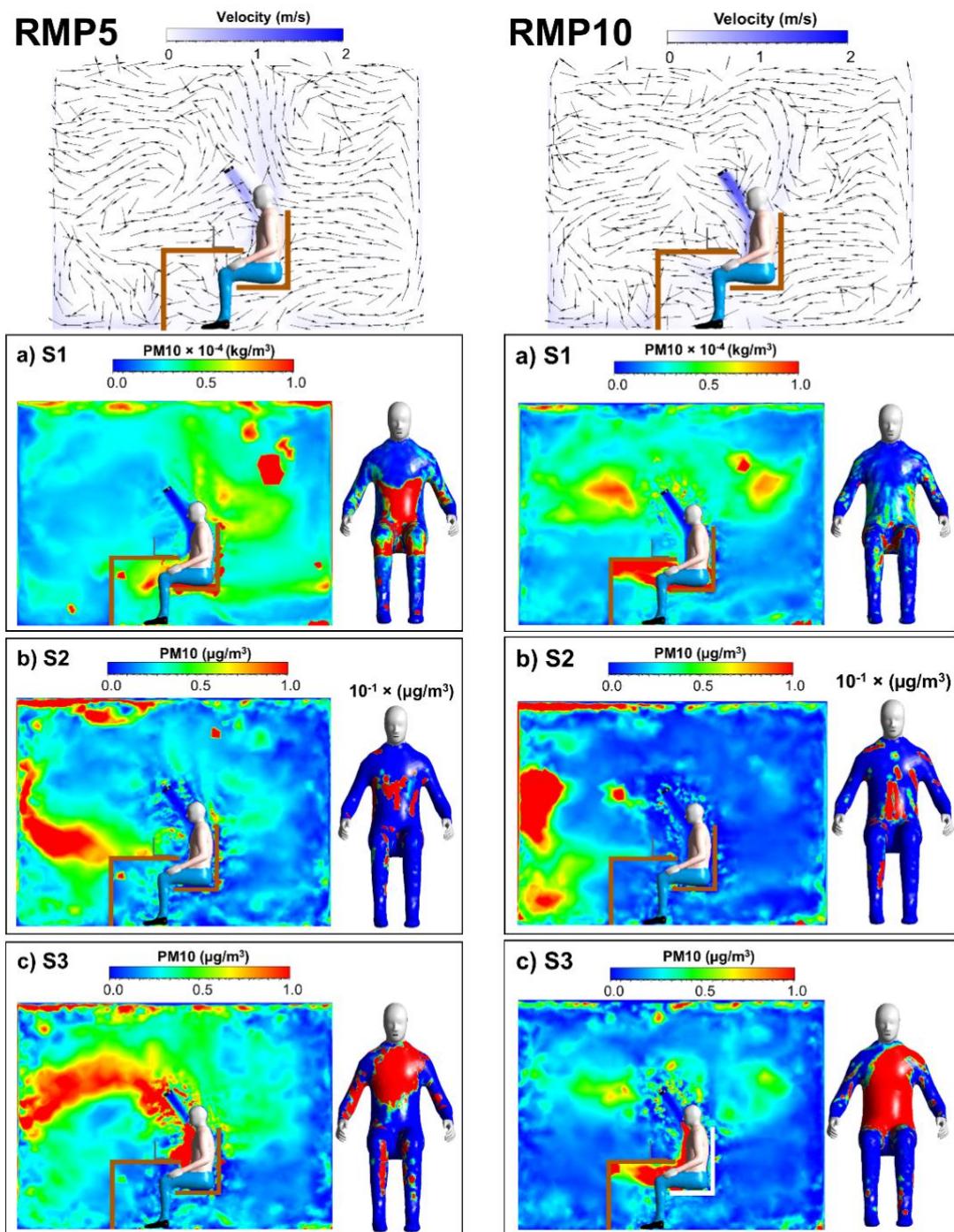
Figure 29 Contours of velocity and cumulative PM mass concentration at the manikin midplane (y = 1.7 m) and the manikin's clothed segments for the case of RMP, evaluated for: a) **S1**, b) **S2** and c) **S3** (t = 20 min)

3. *Comparison of the three PV ATDs and recommendations*

Based on the previous results, the three PV ATDs, each had their advantages and shortcomings when it came to protecting occupants from direct exposure (due to direct inhalation) or exposure to subsequent particle release due to clothing contamination (clothing-mediated exposure) and to reducing RA levels in the office:

- The CMP reduced both inhalation exposures, and clothing contamination compared to standalone MV, at all operating flow rates and also reduced RA levels.

- For most PM sources, VDG outperformed CMP by 6% in terms of reducing direct exposure as was obtained in [25]. However, CMP outperformed VDG in protecting occupants from **S1** (low-height source), since the vertical upwards direction and the short core region of the VDG jet can help entrain particles to the BZ. The VDG also outperformed the CMP in reducing RA by 38% for all possible sources. However, its operation should be limited to low flow rates so that it can compete with the CMP in controlling clothing contamination.

- RMP outperformed both CMP and VDG, in reducing direct exposure by 27% and 30% and reduced RA levels by 55% and 17% respectively. Note that in [25], RMP did not perform better than VDG since its downward jet had lower supply velocities and did not reach the BZ as effectively due to its larger outlet diameter. Despite effectively decreasing *iF*, RMP increased clothing contamination drastically at all operating flow rates.

Taking both *iF* and *DFr* into account, CMP and VDG perform better than RMP. However, VDG operation should be limited to low flow rates since higher ones start increasing deposition. No limitation on CMP operation is needed since clothing

103

contamination was always lower than standalone MV at any CMP flow rate. This does not restrict the occupants' ability in adjusting the PV operating conditions to suit their personal preferences. Hence, among the three PV ATDs, the CMP performed best followed by the VDG and RMP.

D. Conclusion

In this work, a 3D CFD model was developed to evaluate the performance of different PV ATDs (CMP, VDG and RMP) in terms of their ability to reduce inhalation exposure (iF) and clothing contamination (DFr) due to typical indoor sources of PM. The model was successfully validated in a climatic chamber equipped with the CMP and the considered sources. The main conclusions of this work are listed as follows:

- The CMP, VDG and RMP effectively enhanced breathable air quality. The RMP had lowest iF (and IAQ) followed by VDG and CMP.

- CMP had the highest reduction in DFr compared to standalone MV followed by the VDG when it supplies preferably lower flow rates. However, this limits its operation and is not favorable for iF.

- The RMP had the worst effect on DFr at low and high flow rates. It drastically increased DFr compared to standalone MV due to its downward flushing effect.

- As a compromise between iF, DFr and keeping the advantage of PV individual control, the best PV ATD would be the CMP. It still reduces iF to trivial values, while also reducing clothing contamination and improving overall IAQ at all possible operating conditions.

1. Limitations and future work

Knowledge gained so far on PV integration in occupied spaces, focused on its abilities in enhancing breathable air quality and thermal comfort. The developed CFD model here, allowed to gain a more holistic view on the performance of PV devices. While they are always able to enhance breathable air quality, their effect on clothing contamination highly depends on their design and operating flow rate and should not be ignored. Note that the current model only allows to predict clothing contamination. However, further modeling and experimental work is needed to estimate the actual released fraction of these deposited particles from clothing and their effect on occupants' exposure. Nonetheless, the current modeling method could be applied to develop design and operation strategies for PV in various types of spaces and indoor layouts, where different background ventilation systems might be encountered.

REFERENCES

[1]   P. J. Franklin, "Indoor air quality and respiratory health of children," *Paediatric respiratory reviews,* vol. 8, no. 4, pp. 281-286, 2007.

[2]   M. Arif, M. Katafygiotou, A. Mazroei, A. Kaushik, and E. Elsarrag, "Impact of indoor environmental quality on occupant well-being and comfort: A review of the literature," *International Journal of Sustainable Built Environment,* vol. 5, no. 1, pp. 1-11, 2016.

[3]   EPA. "Climate Change Indicators: Atmospheric Concentrations of Greenhouse Gases." https://www.epa.gov/climate-indicators/climate-change-indicators-atmospheric-concentrations-greenhouse-gases (accessed.

[4]   P. Wargocki and D. P. Wyon, "The effects of outdoor air supply rate and supply air filter condition in classrooms on the performance of schoolwork by children (RP-1257)," *Hvac&r Research,* vol. 13, no. 2, pp. 165-191, 2007.

[5]   B. Tashtoush, M. Molhim, and M. Al-Rousan, "Dynamic model of an HVAC system for control analysis," *Energy,* vol. 30, no. 10, pp. 1729-1745, 2005.

[6]   B. Yu, Z. Hu, M. Liu, H. Yang, Q. Kong, and Y. Liu, "Review of research on air-conditioning systems and indoor air quality control for human health," *International journal of refrigeration,* vol. 32, no. 1, pp. 3-20, 2009.

[7]   G. A. Florides, S. A. Tassou, S. A. Kalogirou, and L. Wrobel, "Review of solar and low energy cooling technologies for buildings," *Renewable and Sustainable Energy Reviews,* vol. 6, no. 6, pp. 557-572, 2002.

[8]   R. D. Watson, *Radiant heating and cooling handbook*. McGraw-Hill Education, 2002.

[9]   C. Karmann, S. Schiavon, and F. Bauman, "Thermal comfort in buildings using radiant vs. all-air systems: A critical literature review," *Building and Environment,* vol. 111, pp. 123-131, 2017.

[10]   D. Saelens, W. Parys, and R. Baetens, "Energy and comfort performance of thermally activated building systems including occupant behavior," *Building and environment,* vol. 46, no. 4, pp. 835-848, 2011.

[11]   T. Catalina, J. Virgone, and F. Kuznik, "Evaluation of thermal comfort using combined CFD and experimentation study in a test room equipped with a cooling ceiling," *Building and environment,* vol. 44, no. 8, pp. 1740-1750, 2009.

[12]   A. Gramez and F. Boubenider, "Acoustic comfort evaluation for a conference room: A case study," *Applied acoustics,* vol. 118, pp. 39-49, 2017.

[13]   S. A. Mumma, "Chilled ceilings in parallel with dedicated outdoor air systems: Addressing the concerns of condensation, capacity, and cost," *Ashrae Transactions,* vol. 108, p. 220, 2002.

[14]   K.-N. Rhee, B. W. Olesen, and K. W. Kim, "Ten questions about radiant heating and cooling systems," *Building and Environment,* vol. 112, pp. 367-381, 2017.

[15]   J. Martin, P. Demokritou, S. Woskie, and D. Bello, "Indoor air quality in photocopy centers, nanoparticle exposures at photocopy workstations, and the need for exposure controls," *Annals of work exposures and health,* vol. 61, no. 1, pp. 110-122, 2017.

[16]   A. Keblawi, N. Ghaddar, and K. Ghali, "Model-based optimal supervisory control of chilled ceiling displacement ventilation system," *Energy and Buildings,* vol. 43, no. 6, pp. 1359-1370, 2011.

[17] H. Maula, V. Hongisto, V. Naatula, A. Haapakangas, and H. Koskela, "The effect of low ventilation rate with elevated bioeffluent concentration on work performance, perceived indoor air quality, and health symptoms," *Indoor Air,* vol. 27, no. 6, pp. 1141-1153, 2017.

[18] A. K. Melikov, "Personalized ventilation," *Indoor air,* vol. 14, pp. 157-167, 2004.

[19] F. Kalmár, "An indoor environment evaluation by gender and age using an advanced personalized ventilation system," *Building Services Engineering Research and Technology,* vol. 38, no. 5, pp. 505-521, 2017.

[20] C. Xu, P. V. Nielsen, L. Liu, R. L. Jensen, and G. Gong, "Impacts of airflow interactions with thermal boundary layer on performance of personalized ventilation," *Building and Environment,* vol. 135, pp. 31-41, 2018.

[21] E. Z. Conceição, C. I. Santiago, M. Lúcio, and H. B. Awbi, "Predicting the air quality, thermal comfort and draught risk for a virtual classroom with desk-type personalized ventilation systems," *Buildings,* vol. 8, no. 2, p. 35, 2018.

[22] H. Zhang, E. Arens, and Y. Zhai, "A review of the corrective power of personal comfort systems in non-neutral ambient environments," *Building and Environment,* vol. 91, pp. 15-41, 2015.

[23] W. Chakroun, N. Ghaddar, and K. Ghali, "Chilled ceiling and displacement ventilation aided with personalized evaporative cooler," *Energy and buildings,* vol. 43, no. 11, pp. 3250-3257, 2011.

[24] M. Veselý and W. Zeiler, "Personalized conditioning and its impact on thermal comfort and energy performance–A review," *Renewable and Sustainable Energy Reviews,* vol. 34, pp. 401-408, 2014.

[25] A. K. Melikov, R. Cermak, and M. Majer, "Personalized ventilation: evaluation of different air terminal devices," *Energy and buildings,* vol. 34, no. 8, pp. 829-836, 2002.

[26] A. Makhoul, K. Ghali, and N. Ghaddar, "Desk fans for the control of the convection flow around occupants using ceiling mounted personalized ventilation," *Building and Environment,* vol. 59, pp. 336-348, 2013.

[27] C. Habchi, K. Ghali, N. Ghaddar, and A. Shihadeh, "Chair fan-enhanced displacement ventilation for high IAQ: effects on particle inhalation and stratification height," *Building and Environment,* vol. 84, pp. 68-79, 2015.

[28] A. Lipczynska, J. Kaczmarczyk, and A. K. Melikov, "Thermal environment and air quality in office with personalized ventilation combined with chilled ceiling," *Building and Environment,* vol. 92, pp. 603-614, 2015.

[29] A. Uğursal and C. H. Culp, "The effect of temperature, metabolic rate and dynamic localized airflow on thermal comfort," *Applied energy,* vol. 111, pp. 64-73, 2013.

[30] S. Tanabe and K. Kimura, "Effects of air temperature, humidity, and air movement on thermal comfort under hot and humid conditions," American Society of Heating, Refrigerating and Air-Conditioning Engineers …, 0001-2505, 1994.

[31] A. Kabanshi, H. Wigö, and M. Sandberg, "Experimental evaluation of an intermittent air supply system–Part 1: thermal comfort and ventilation efficiency measurements," *Building and Environment,* vol. 95, pp. 240-250, 2016.

[32] K. Ghali, N. Ghaddar, and M. Bizri, "The influence of wind on outdoor thermal comfort in the city of Beirut: a theoretical and field study," *HVAC&R Research,* vol. 17, no. 5, pp. 813-828, 2011.

[33] G. Zhou, A. K. Melikov, and P. O. Fanger, "Impact of equivalent frequency on the sensation of draught," in *Roomvent-8th International Conference on Air Distribution in Rooms: Individually Controlled Environment*, 2002, pp. 297-300.

[34] J. Kaczmarczyk, A. Melikov, and D. Sliva, "Effect of warm air supplied facially on occupants' comfort," *Building and Environment,* vol. 45, no. 4, pp. 848-855, 2010.

[35] V. Kulkarni, N. Sahoo, and S. D. Chavan, "Simulation of honeycomb–screen combinations for turbulence management in a subsonic wind tunnel," *Journal of wind engineering and industrial aerodynamics,* vol. 99, no. 1, pp. 37-45, 2011.

[36] Y. Zhu, Q. Ouyang, B. Cao, X. Zhou, and J. Yu, "Dynamic thermal environment and thermal comfort," *Indoor air,* vol. 26, no. 1, pp. 125-137, 2016.

[37] P. Fanger, "Discomfort due to air velocities in spaces," in *Proc. of Meeting of Commission B1, B2, E1, of Instit. Refrig.*, 1977, vol. 4, pp. 289-296.

[38] L. Huang, Q. Ouyang, and Y. Zhu, "Perceptible airflow fluctuation frequency and human thermal response," *Building and Environment,* vol. 54, pp. 14-19, 2012.

[39] C. Xu, P. Nielsen, G. Gong, L. Liu, and R. Jensen, "Measuring the exhaled breath of a manikin and human subjects," *Indoor Air,* vol. 25, no. 2, pp. 188-197, 2015.

[40] A. Fluent, "Ansys fluent," *Academic Research. Release,* vol. 14, 2015.

[41] W. Abou Hweij, N. Ghaddar, K. Ghali, and C. Habchi, "Optimized performance of displacement ventilation aided with chair fans for comfort and indoor air quality," *Energy and Buildings,* vol. 127, pp. 907-919, 2016.

[42] Y. Liu, H. Li, and G. Feng, "Simulation of inhalable aerosol particle distribution generated from cooking by Eulerian approach with RNG k–epsilon turbulence model and pollution exposure in a residential kitchen space," in *Building Simulation*, 2017, vol. 10, no. 1: Springer, pp. 135-144.

[43] C. D. Hodgman, R. Weast, and S. Selby, "Handbook of Chemistry and Physics, 39," *Aufl. Cleveland, Ohio (USA): Chem. Rubber Publ. Co,* 1954.

[44] M. Al-Othmani, N. Ghaddar, and K. Ghali, "A multi-segmented human bioheat model for transient and asymmetric radiative environments," *International Journal of Heat and Mass Transfer,* vol. 51, no. 23-24, pp. 5522-5533, 2008.

[45] H. Zhang, E. Arens, C. Huizenga, and T. Han, "Thermal sensation and comfort models for non-uniform and transient environments, part II: Local comfort of individual body parts," *Building and Environment,* vol. 45, no. 2, pp. 389-398, 2010.

[46] H. Zhang, E. Arens, C. Huizenga, and T. Han, "Thermal sensation and comfort models for non-uniform and transient environments, part III: Whole-body sensation and comfort," *Building and Environment,* vol. 45, no. 2, pp. 399-410, 2010.

[47] H. Zhang, E. Arens, C. Huizenga, and T. Han, "Thermal sensation and comfort models for non-uniform and transient environments: Part I: Local sensation of individual body parts," *Building and Environment,* vol. 45, no. 2, pp. 380-388, 2010.

[48]   D. Al Assaad, C. Habchi, K. Ghali, and N. Ghaddar, "Effectiveness of intermittent personalized ventilation in protecting occupant from indoor particles," *Building and Environment,* vol. 128, pp. 22-32, 2018.

[49]   D. Al Assaad, K. Ghali, N. Ghaddar, and C. Habchi, "Mixing ventilation coupled with personalized sinusoidal ventilation: Optimal frequency and flow rate for acceptable air quality," *Energy and Buildings,* vol. 154, pp. 569-580, 2017.

[50]   "Newton thermal manikin - Thermal manikin designed for clothing and environmental testing." https://thermetrics.com/products/manikin/newton-thermal-manikin/ (accessed.

[51]   S. Muhič and V. Butala, "The influence of indoor environment in office buildings on their occupants: expected–unexpected," *Building and Environment,* vol. 39, no. 3, pp. 289-296, 2004.

[52]   O. Seppanen and W. J. Fisk, "Association of ventilation system type with SBS symptoms in office workers," 2001.

[53]   EPA. "Health and environment effects of particulate matter " https://www.epa.gov/pm-pollution/health-and-environmental-effects-particulate-matter-pm (accessed.

[54]   C. A. Pope III *et al.*, "Heart rate variability associated with particulate air pollution," *American heart journal,* vol. 138, no. 5, pp. 890-899, 1999.

[55]   J. Schwartz, D. W. Dockery, and L. M. Neas, "Is daily mortality associated specifically with fine particles?," *Journal of the Air & Waste Management Association,* vol. 46, no. 10, pp. 927-939, 1996.

[56] C. A. Pope III *et al.*, "Cardiovascular mortality and long-term exposure to particulate air pollution: epidemiological evidence of general pathophysiological pathways of disease," *Circulation,* vol. 109, no. 1, pp. 71-77, 2004.

[57] C. A. Redlich, J. Sparer, and M. R. Cullen, "Sick-building syndrome," *The Lancet,* vol. 349, no. 9057, pp. 1013-1016, 1997.

[58] E. Diapouli, A. Chaloulakou, and P. Koutrakis, "Estimating the concentration of indoor particles of outdoor origin: A review," *Journal of the Air & Waste Management Association,* vol. 63, no. 10, pp. 1113-1129, 2013.

[59] R. S. Papineni and F. S. Rosenthal, "The size distribution of droplets in the exhaled breath of healthy human subjects," *Journal of Aerosol Medicine,* vol. 10, no. 2, pp. 105-116, 1997.

[60] S. Yang, G. W. Lee, C.-M. Chen, C.-C. Wu, and K.-P. Yu, "The size and concentration of droplets generated by coughing in human subjects," *Journal of Aerosol Medicine,* vol. 20, no. 4, pp. 484-494, 2007.

[61] L. Bourouiba, E. Dehandschoewercker, and J. W. Bush, "Violent expiratory events: on coughing and sneezing," *Journal of Fluid Mechanics,* vol. 745, pp. 537-563, 2014.

[62] T. Hussein *et al.*, "Particle size characterization and emission rates during indoor activities in a house," *Atmospheric Environment,* vol. 40, no. 23, pp. 4285-4307, 2006.

[63] M. Scungio, T. Vitanza, L. Stabile, G. Buonanno, and L. Morawska, "Characterization of particle emission from laser printers," *Science of the Total Environment,* vol. 586, pp. 623-630, 2017.

[64] Q. Zhang, R. H. Gangupomu, D. Ramirez, and Y. Zhu, "Measurement of ultrafine particles and other air pollutants emitted by cooking activities," *International Journal of Environmental Research and Public Health,* vol. 7, no. 4, pp. 1744-1759, 2010.

[65] R. L. Corsi, J. A. Siegel, and C. Chiang, "Particle resuspension during the use of vacuum cleaners on residential carpet," *Journal of Occupational and Environmental Hygiene,* vol. 5, no. 4, pp. 232-238, 2008.

[66] J. Qian, J. Peccia, and A. R. Ferro, "Walking-induced particle resuspension in indoor environments," *Atmospheric Environment,* vol. 89, pp. 464-481, 2014.

[67] D. Al Assaad, K. Ghali, N. Ghaddar, and E. Shammas, "Modeling of indoor particulate matter deposition to occupant typical wrinkled shirt surface," *Building and Environment,* p. 106965, 2020.

[68] B. M. Alexander and C. S. Baxter, "Flame-retardant contamination of firefighter personal protective clothing–a potential health risk for firefighters," *Journal of occupational and environmental hygiene,* vol. 13, no. 9, pp. D148-D155, 2016.

[69] G. C. Morrison *et al.*, "Role of clothing in both accelerating and impeding dermal absorption of airborne SVOCs," *Journal of Exposure Science & Environmental Epidemiology,* vol. 26, no. 1, pp. 113-118, 2016.

[70] M. Gong, C. J. Weschler, and Y. Zhang, "Impact of clothing on dermal exposure to phthalates: observations and insights from sampling both skin and clothing," *Environmental Science & Technology,* vol. 50, no. 8, pp. 4350-4357, 2016.

[71] M. Gorman Ng *et al.*, "The relationship between inadvertent ingestion and dermal exposure pathways: a new integrated conceptual model and a database of

dermal and oral transfer efficiencies," *Annals of occupational hygiene,* vol. 56, no. 9, pp. 1000-1012, 2012.

[72] D. Licina, G. C. Morrison, G. Bekö, C. J. Weschler, and W. W. Nazaroff, "Clothing-mediated exposures to chemicals and particles," *Environmental science & technology,* vol. 53, no. 10, pp. 5559-5575, 2019.

[73] D. Licina, Y. Tian, and W. W. Nazaroff, "Emission rates and the personal cloud effect associated with particle release from the perihuman environment," *Indoor air,* vol. 27, no. 4, pp. 791-802, 2017.

[74] A. McDonagh and M. Byrne, "A study of the size distribution of aerosol particles resuspended from clothing surfaces," *Journal of aerosol science,* vol. 75, pp. 94-103, 2014.

[75] R. You, W. Cui, C. Chen, and B. Zhao, "Measuring the short-term emission rates of particles in the "personal cloud" with different clothes and activity intensities in a sealed chamber," *Aerosol and Air Quality Research,* vol. 13, no. 3, pp. 911-921, 2012.

[76] R. De Dear and G. S. Brager, "Developing an adaptive model of thermal comfort and preference," 1998.

[77] D. Li, C. C. Menassa, and V. R. Kamat, "Personalized human comfort in indoor building environments under diverse conditioning modes," *Building and Environment,* vol. 126, pp. 304-317, 2017.

[78] R. Cermak, A. K. Melikov, L. Forejt, and O. Kovar, "Performance of personalized ventilation in conjunction with mixing and displacement ventilation," *Hvac&R Research,* vol. 12, no. 2, pp. 295-311, 2006.

[79]   N. Gao and J. Niu, "Personalized ventilation for commercial aircraft cabins," *Journal of aircraft,* vol. 45, no. 2, pp. 508-512, 2008.

[80]   P. V. Nielsen, M. Polak, H. Jiang, Y. Li, and H. Qian, "Protection against cross infection in hospital beds with integrated personalized ventilation," *Indoor air,* pp. 17-22, 2008.

[81]   A. Melikov, T. Ivanova, and G. Stefanova, "Seat headrest-incorporated personalized ventilation: Thermal comfort and inhaled air quality," *Building and Environment,* vol. 47, pp. 100-108, 2012.

[82]   E. Katramiz, D. Al Assaad, N. Ghaddar, and K. Ghali, "The effect of human breathing on the effectiveness of intermittent personalized ventilation coupled with mixing ventilation," *Building and Environment,* p. 106755, 2020.

[83]   D. Huang, "Physical diagnostics," ed: China Commerce Publishing Co Beijing, 1977.

[84]   C. CEN, "Ventilation for buildings: Design criteria for the indoor environment," *Brussels, European Committee for Standardization,* 1998.

[85]   A. Standard, "Standard 62-1989," *Ventilation for acceptable indoor air quality,* vol. 41, p. 51, 1989.

[86]   A. Standard, "Standard 55-2004," *Thermal environmental conditions for human occupancy,* vol. 3, 2004.

[87]   D. Al Assaad, K. Ghali, and N. Ghaddar, "Effectiveness of intermittent personalized ventilation assisting a chilled ceiling for enhanced thermal comfort and acceptable indoor air quality," *Building and Environment,* vol. 144, pp. 9-22, 2018.

[88] B. E. Boor, M. P. Spilak, R. L. Corsi, and A. Novoselac, "Characterizing particle resuspension from mattresses: chamber study," *Indoor Air,* vol. 25, no. 4, pp. 441-456, 2015.

[89] A. Benabed, K. Limam, B. Janssens, and W. Bosschaerts, "Human foot tapping-induced particle resuspension in indoor environments: Flooring hardness effect," *Indoor and Built Environment,* vol. 29, no. 2, pp. 230-239, 2020.

[90] J. Qian, A. R. Ferro, and K. R. Fowler, "Estimating the resuspension rate and residence time of indoor particles," *Journal of the Air & Waste Management Association,* vol. 58, no. 4, pp. 502-516, 2008.

[91] P. Fabian *et al.*, "Influenza virus in human exhaled breath: an observational study," *PloS one,* vol. 3, no. 7, p. e2691, 2008.

[92] C. Trader, "Cg trader," *URL http://www. cgtrader. com,* vol. 4.

[93] B. Zhao and J. Wu, "Particle deposition in indoor environments: analysis of influencing factors," *Journal of hazardous materials,* vol. 147, no. 1-2, pp. 439-448, 2007.

[94] N. Gao, J. Niu, Q. He, T. Zhu, and J. Wu, "Using RANS turbulence models and Lagrangian approach to predict particle deposition in turbulent channel flows," *Building and Environment,* vol. 48, pp. 206-214, 2012.

[95] D. Al Assaad, K. Ghali, and N. Ghaddar, "Effect of flow disturbance induced by walking on the performance of personalized ventilation coupled with mixing ventilation," *Building and Environment,* vol. 160, p. 106217, 2019.

[96] C. Habchi, W. Chakroun, S. Alotaibi, K. Ghali, and N. Ghaddar, "Effect of shifts from occupant design position on performance of ceiling personalized

ventilation assisted with desk fan or chair fans," *Energy and Buildings,* vol. 117, pp. 20-32, 2016.

[97] W. W. Nazaroff, "Inhalation intake fraction of pollutants from episodic indoor emissions," *Building and Environment,* vol. 43, no. 3, pp. 269-277, 2008.

[98] D. Licina, J. Pantelic, A. Melikov, C. Sekhar, and K. W. Tham, "Experimental investigation of the human convective boundary layer in a quiescent indoor environment," *Building and Environment,* vol. 75, pp. 79-91, 2014.

[99] D. Al Assaad, K. Ghali, and N. Ghaddar, "Particles dispersion due to human prostration cycle and ventilation system in a prayer room," *Building and Environment,* vol. 150, pp. 44-59, 2019.

[100] M. a. purifier. https://www.mi.com/global/air/ (accessed.

[101] Y. Wang, X. Fan, A. Li, L. Shang, and H. Wang, "Deposition of fine particles on vertical textile surfaces: A small-scale chamber study," *Building and Environment,* vol. 135, pp. 308-317, 2018.

[102] N. Gao and J. Niu, "Modeling particle dispersion and deposition in indoor environments," *Atmospheric environment,* vol. 41, no. 18, pp. 3862-3876, 2007.

[103] D. Rim and A. Novoselac, "Transport of particulate and gaseous pollutants in the vicinity of a human body," *Building and Environment,* vol. 44, no. 9, pp. 1840-1849, 2009.

[104] H. Alsaad and C. Voelker, "Performance assessment of a ductless personalized ventilation system using a validated CFD model," *Journal of Building Performance Simulation,* vol. 11, no. 6, pp. 689-704, 2018.

[105] H. Alsaad and C. Voelker, "Could the ductless personalized ventilation be an alternative to the regular ducted personalized ventilation?," *Indoor air,* 2020.